Aus dem Institut für Virologie

des Fachbereichs Veterinärmedizin

der Freien Universität Berlin

Structural, enzymological and functional studies on the binding of fatty acids to the haemagglutinin and the M2 membrane protein of the influenza virus

Inaugural-Dissertation

zur Erlangung des Grades eines

Doctor of Philosophy (PhD) in Biomedical

Sciences

an der Freien Universität Berlin

vorgelegt von

Xiaorong Meng

aus Hebei, Volksrepublik China

Berlin 2023

Journal-Nr.: 4423

Gedruckt mit Genehmigung

des Fachbereichs Veterinärmedizin

der Freien Universität Berlin

Dekan:	Univ.-Prof. Dr. Uwe Rösler
Erster Gutachter:	PD Dr. Michael Veit
Zweiter Gutachter:	Prof. Dr. Benedikt Kaufer
Dritter Gutachter:	PD Dr. Soroush Sharbati

Deskriptoren (nach CAB-Thesaurus):
Influenza A virus, influenza B virus, respiratory diseases, palmitoleic acid, hemagglutinin, surface proteins

Tag der Promotion: 21.09.2023

Table of contents

List of Figures

Table

Abbreviations

ABE	Acyl-biotin exchange
Acyl-RAC	acyl resin-assisted capture
AH	Amphipathic helix
APT	Acyl protein thioesterases
CRD	Cysteine-rich domain
cRNA	Complimentary RNA
CT	Cytoplasmic tail
Endo H	Endoglycosidase H
ER	Endoplasmic reticulum
FP	Fusion peptide
HA	Haemagglutinin
HEF	Hemagglutinin Esterase Fusion
IAV	Influenza A virus
IBV	Influenza B virus
ICV	Influenza C virus
IDV	Influenza D virus
IFITM	Interferon-induced transmembrane
NA	Neuraminidase
NEP	Nuclear export protein
NP	Nucleoprotein
NS1	Non-structural protein 1
PA	Polymerase Acidic Protein
PB1	Polymerase Basic Protein 1
PB2	Polymerase Basic Protein 2
PNGase F	Peptide N-glycosidase F
RdRp	RNA-dependent RNA polymerase
SA	Sialic acid
ssRNA(-)	Segmented negative-sense single-stranded
TMD	Transmembrane domain
vRNA	Viral RNA
vRNP	Viral ribonucleoprotein
VSV	Vesicular Stomatitis virus

Amino acids used in this paper

A/Ala	Alanine
C/Cys	Cysteine
D/Asp	Aspartic acid
E/Glu	Glutamic acid
F/Phe	Phenylalanine
G/Gly	Glycine
H/His	Histidine
I/ Ile	Isoleucine
K/Lys	Lysine
L/Leu	Leucine
N/Asn	Asparagine
R/Arg	Arginine
S/Ser	Serine
T/Thr	Threonine
W/Trp	Tryptophan
Y/Tyr	Tyrosine

1. Introduction

1.1 Influenza virus

Influenza viruses are the major respiratory viruses, that cause annual epidemics and occasional pandemics. They cause high mortality and morbidity around the world. Influenza viruses belong to the family Orthomyxoviridae and have a segmented, negative-sense, single-stranded RNA (ssRNA(-)) genome. Influenza viruses consists of four genera, distinguished on the antigenic differences between their matrix proteins (M) and nucleoproteins (NP), which include influenza A virus (IAV), Influenza B virus (IBV), Influenza C virus (ICV) and Influenza D virus (IDV). IAV and IBV have 8 genomic segments(1). Only seven genomic segments exit in ICV and IDV, as the hemagglutinin–esterase fusion (HEF) protein replaces the hemagglutinin (HA) and the neuraminidase (NA) (2).

Influenza A viruses have a wide range of hosts and are classified into 18 HA subtypes (H1–H18) and 11 NA subtypes (N1–N11) based on the antigenicity of the glycoproteins HA and NA. The waterfowl is the main animal reservoir of IAVs. Avian influenza viruses can cross species barriers thereby establishing new lineages in a wide variety of hosts(3). H17N10 and H18N11 subtypes only have been found in bats (4) (5). So far, bat influenza viruses have not been observed to cross into other species(3). All four genera can infect humans but only influenza A virus has been responsible for pandemics. The influenza B viruses have limited number of hosts, causing disease mainly in humans with few reports of animals (2). IBVs are classified into two antigenically distinct lineages, B/Victoria-like and B/Yamagata-like viruses. The two lineages were found to co-circulate(6). Influenza C virus mainly infects children where it causes mild respiratory disease. Humans are the main reservoir of ICVs, but the virus also infects pigs. The latest member in Orthomyxoviridae are IDVs which were isolated from pigs in 2011, but its main reservoir are cattle(7).

Antigenic variation of influenza virus comes in two forms: antigenic drift and antigenic shift. Antigenic shift is found only with IAV and results from the replacement of the HA and NA and also other genes from different subtypes. Antigenic shifts often have severe outcomes leading to a new strain emerging and a pandemic occurring. Antigenic drift involves the mutations within the antibody-binding sites in the HA and NA and causes seasonal infections. Antigenic drift can occur in both IAV and IBV, but the pattern may be different for the different viruses. Antigenic drift can overcome pre-existing immunity in humans and escape from neutralizing antibodies(8). Antigenic drift and antigenic shift cause the rapid antigenic evolution in hemagglutinin (HA) of

the influenza A virus. These lead to changes in the antigenic properties of the virus, affecting the effectiveness of existing vaccines(9).

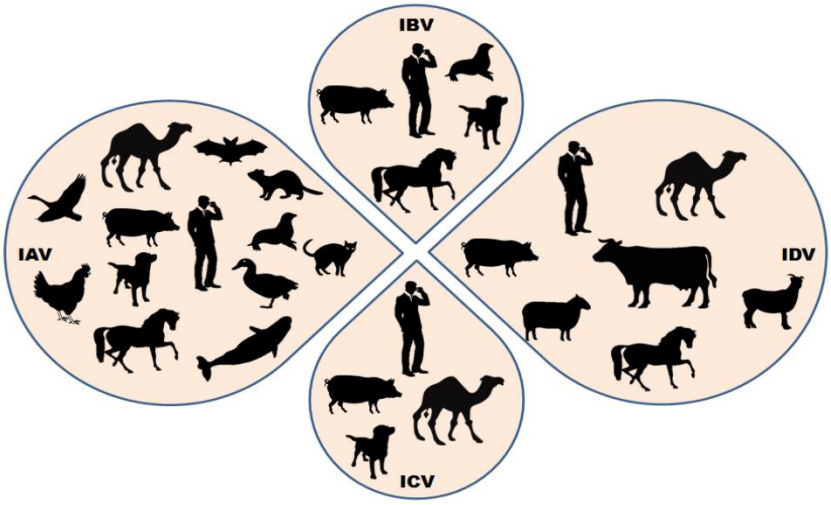

Figure 1. The summary of the host range of influenza viruses

The figure obtained from (2) with permission

1.1.1 Virus Structure and genome

The influenza virion is pleiomorphic, forming spherical or filamentous virions. The average diameter of spherical virions is 80-100 nm. The filamentous virions have a similar diameter but the length can reach up to 20 μm. Three transmembrane proteins HA, NA, and M2 are inserted into the viral lipid envelope which is derived from the host plasma membrane. HA is a homo-trimer and the most abundant protein (~80%) on a lipid envelope. HA is synthesized as a precursor protein, called HA0 which can be cleaved into the HA1 subunit, which is responsible for receptor binding and the HA2 subunit which contains the fusion peptide and hence is important to membrane fusion. The second most abundant envelope protein is NA, which forms a homo-tetramer. The function of the NA is to cleave sialic acid from the viral receptor and helps to release the virion at the end of the virus life cycle. M2 is an integral membrane homo-tetramer and functions as a proton channel, but is present in low copy numbers (16 - 20 M2 molecules) in each virion. Inside the virus and under the viral envelope there is a M1 protein layer which connects the envelope with the viral ribonucleoproteins (vRNPs)(10). vRNPs (in Figure 2A) are the core of the virus containing the negative stranded vRNAs, which are wrapped around the nucleoprotein (NP) along with minor amounts of nuclear export protein (NEP) and

RNA-dependent RNA polymerase (RdRp) which include PB1, PB2 and PA. RdRP is important to viral transcription and replication. Each NP monomer interacts with around 20 nucleotides of the vRNA and is important for the structural organization and stabilization of the RNP(11–13).

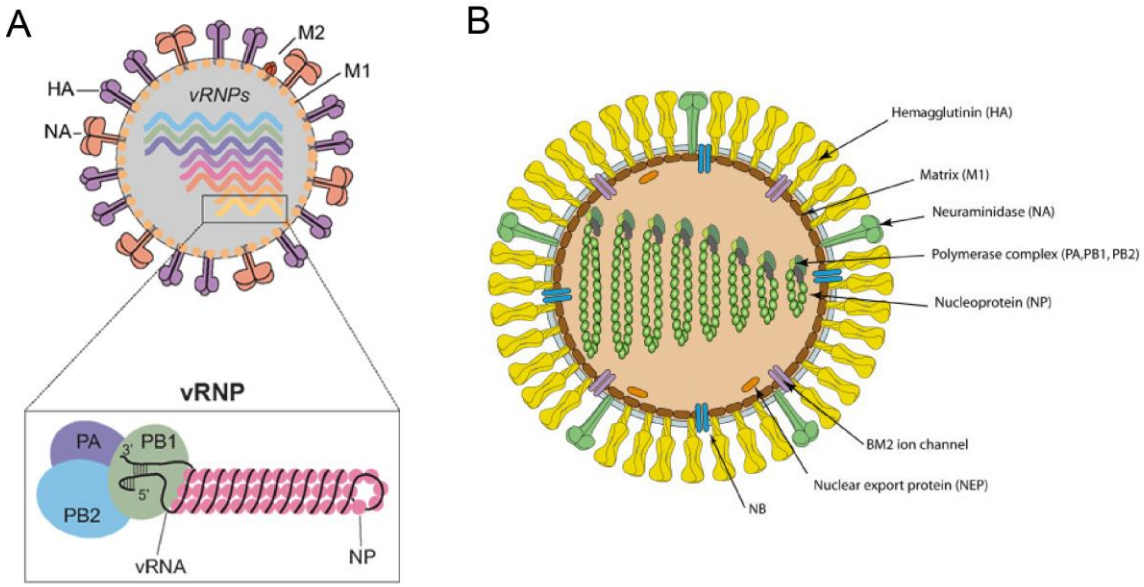

Figure 2. Scheme of an influenza A and influenza B virus particle

(A) Scheme of influenza A virus and vRNP. The structural proteins HA, NA, and M2 are inserted in the lipid envelope, under the viral envelope there is an M1 protein layer, and inside the virus particle, there are eight viral ribonucleoproteins (vRNPs). vRNPs are the core of the virus containing the negative-stranded vRNAs, which are wrapped around multiple nucleoproteins (NP) along with minor amounts of nuclear export protein (NEP) and RNA-dependent RNA polymerase (RdRp) which include PB1, PB2, and PA. The figure obtained from (14) with permission.

(B) Schematic of influenza B virus. The viral envelope includes HA, NA, BM2 and NB. The figure obtained from viralzone https://viralzone.expasy.org/80?outline=all_by_species with permission.

Figure 2 shows a scheme of the influenza A and influenza B virus. Compared to influenza A virus, influenza B virus encodes two unique proteins called NB and BM2. RNA segment 6 of IBV encodes NA and NB. NB is a type III integral membrane protein and is found incorporated into the virion(15). NB is conserved among influenza B viruses but the function of NB remains unclear. One group found that the NB protein is not important for IBV replication in cell culture by deleting the NB in the viral genome, but the NB knockout virus promotes growth in mice (16).

BM2 is encoded by RNA segment 7(17). Like M2 from the influenza A virus, BM2 is a pH-activated proton channel(18) but the two proteins share little sequence homology. BM2 has a

similar function as M2 of influenza A virus and plays an important role in virus growth. Adamantane drugs were found to inhibit the M2 from the influenza A virus, but not BM2(19).

1.1.2 The life cycle of the influenza virus

The life cycle starts with the virus entry, glycoprotein HA first binds to the sialic acid-containing receptor on the cell membrane and triggers receptor-mediated endocytosis. The virus is transported into the cell within the endocytic vesicle, which fuses with the endosome. It has a low pH and triggers a conformational change in HA protein. The N-terminal fusion peptide of HA2 is exposed and inserts itself into the endosomal membrane, which causes the fusion of the viral and endosome membrane(20). The M2 ion channel function is also activated by the low pH in the endosome, and transports protons into the interior of the virus which dissociates the vRNPs from M1 proteins. The vRNPs are released into the cytoplasm of the host cells and are transported into the nucleus through the importin-α–importin-β nuclear import pathway, by recognition of the nuclear localization sequences (NLSs) on NP(21, 22). In the nucleus, the viral RNA-dependent RNA polymerase (RdRp) complex initiates the transcription and replication of the vRNAs. The cRNAs are produced by an unprimed replication. During the viral infection, mRNA synthesis was found to occur before cRNA and vRNA transcription. mRNA transcripts are much more abundant and efficient because the viral mRNA generation is primed which increases the initiation efficiency(23). The replication of the vRNAs involves two steps: first transcription of complimentary RNA (cRNA) from vRNA, then transcription of new vRNAs using the cRNAs as templates (from cRNA to vRNA).

The protein synthesis of the virus is dependent on the translational machinery of the host. So viral mRNAs need to be transported to the cytoplasm for translation. The translation happens in host ribosomes and later the structural proteins are translocating into the ER and transported to the Golgi for further modification and finally transported to the plasma membrane for virus assembly. The NS1 protein is important to suppress the production of host mRNAs. NS1 also inhibits the innate and adaptive immunity of the host by suppressing synthesis of interferon-β mRNAs. The newly synthesized NP, PA, PB1, and PB2 proteins are imported into the nucleus and form new vRNPs with the newly synthesized vRNAs.

The new vRNPs are transported to the cytoplasm, mediated by a M1–NS2 complex that is bound to the vRNPs. It has been found that the C-terminus of NS2 is essential for M1 binding and affect the nuclear export of progeny vRNPs(24). NS2 can target to the vRNPs by interacting with the CRM1 protein and exports the vRNPs through the CRM1 nuclear export pathway to the

cytoplasm(25–27). The vRNPs are transported to the cell membrane for virus assembly and later release from the host cells. The virus release is highly dependent on the sialidase activity of NA. By removing sialic acid residues, NA prevents HA binding to the surface of the cell, which already has been infected (14, 28, 29).

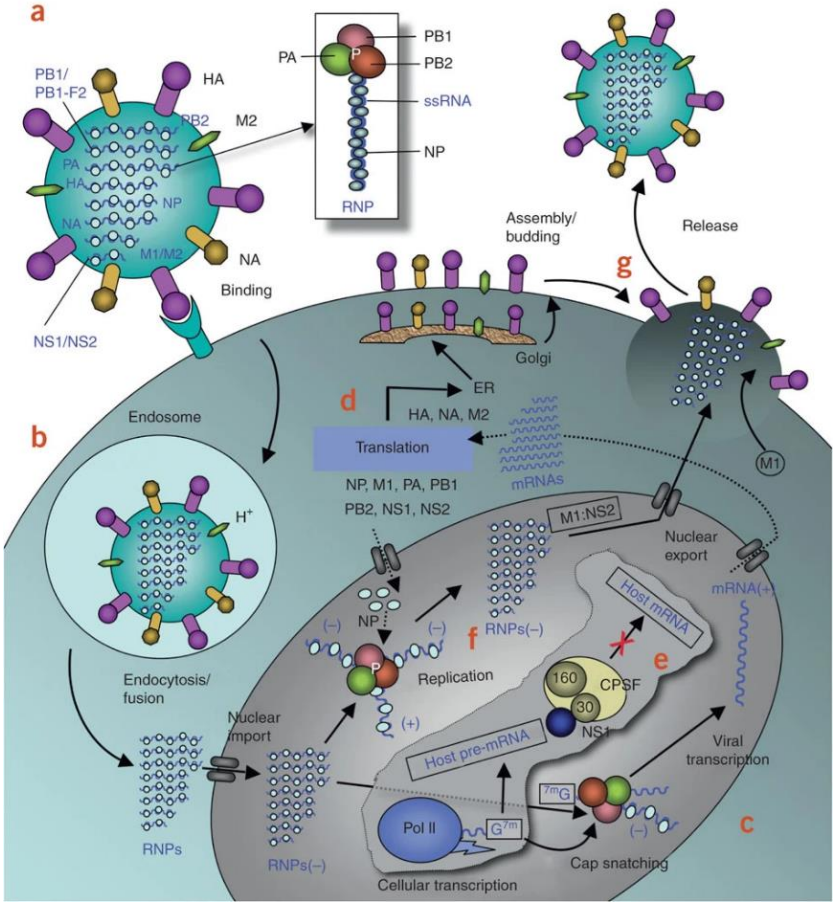

Figure 3. The virus particle and the virus life cycle

(a) shows the structure of the virus particle. Influenza A and B have a lipid envelope where HA, NA, and M2 are integrated. The influenza virus recognizes sialic acid-containing receptors on the cell membrane and the virus is transported into the cell in an endocytic vesicle. **(b)** The low pH in the endosome induces a conformational change of HA, which causes the fusion of the viral and endosomal membrane thereby releasing the eight vRNP segments. **(c)** vRNPs are transported into the nucleus and initiate the transcription and replication of the vRNAs. **(d)** After transcription, the viral mRNAs are transported to the cytoplasm, where they are translated. The structural proteins HA, NA, and M2 are later transported into the ER and Golgi for further modification, and finally transported to the plasma membrane. **(e)** non-structural protein NS1 plays an important role in suppressing the host mRNAs production. **(f)** The newly synthesized NP, PA, PB1 and PB2 proteins are imported into the nucleus and form the new vRNPs with vRNAs. The new vRNPs are transported to the cytoplasm, through an M1–NS2 complex that binds to the vRNPs and then to the plasma membrane. **(g)** indicates the assembly and budding of an influenza virus particle. The figure is obtained from**(29)** with permission**.**

1.2 Hemagglutinin (HA)

1.2.1 Structure and function of HA

Hemagglutinin (HA) is a type I integral membrane protein which forms a homotrimer. Each HA monomer contains a large glycosylated ectodomain, followed by a transmembrane (TM) domain (25-27 aa) and a short cytoplasmic tail (CT,10-11aa)(30). HA is synthesized in the ER as the precursor protein HA0, which is co-translationally N-glycosylated and post-translationally S-acylated (described in more detail below). In order to be activatable HA0 must be cleaved into the HA1 and HA2 by host proteases. Cleavage is essential for virus infectivity and hence the proteases responsible for cleavage are important targets for therapeutic intervention. HA1 contains the sialic acid (SA) binding site responsible for receptor binding and HA2 has the fusion peptide that is important to membrane fusion. The cleavage occurs in HA either at a monobasic or a multibasic cleavage site(31). Multibasic cleavage sites contain multiple arginines and/or lysines, which are found in highly pathogenic avian influenza viruses (HPAIV). The site is cleaved by the ubiquitous cellular protease furin which locates in the trans-Golgi network. (32). Human influenza viruses and low pathogenic avian have a monobasic cleavage site(31)(33).

Even though the HA of influenza A and B viruses has little homology in the genome sequence, both proteins share a similar fold(34–36). Each HA subunit of influenza B/Hong Kong/8/73 (B/HK) and influenza B/Yamanashi/98 (37) contains seven disulfide bridges. Each monomer contains a fusion domain, which includes the HA2 subunit and the N-terminal and C-terminal parts of the HA1 subunit. It is important for the membrane fusion step in virus infection(38). The hydrophobic fusion peptide at the N-terminus of the HA2 is the most highly conserved region in HA(20). The HA1 subunit has a receptor-binding site (RBS)(39).

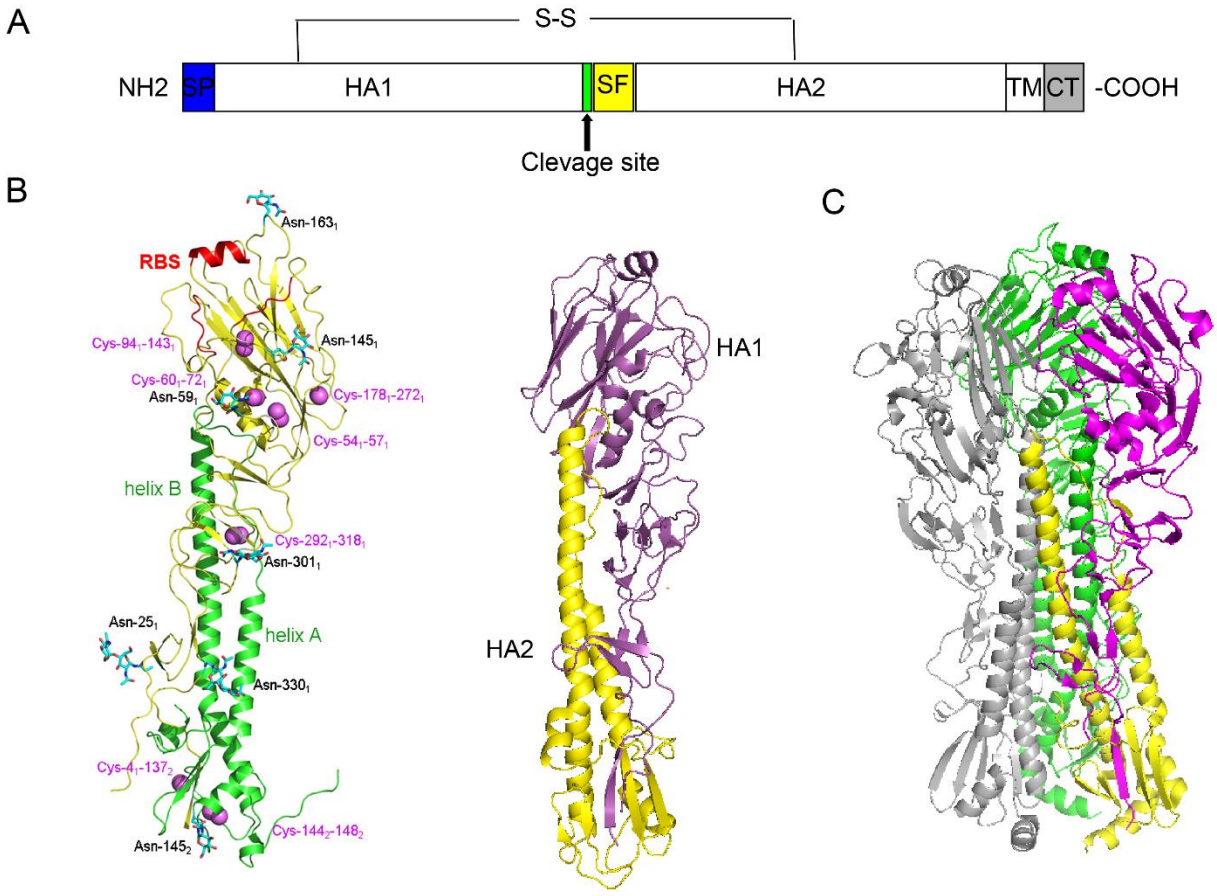

Figure 4. The structure of HA of the influenza A and influenza B virus

(A) The scheme of an HA0 monomer, it contains two subunits HA1 and HA2 which are linked by a disulfide bond. HA1 contains a cleaved signal peptide (SP). HA2 has the fusion peptide (FP), a transmembrane (TM) domain, and a short cytoplasmic tail (CT) with 10-11 amino acids.

(B) The monomer of influenza B/Yamanashi/98 is shown on the left. Yellow represents the HA1 subunit, while green represents HA2, which has two helices, helix A and helix B. The receptor-binding site (RBS) is highlighted in red. Disulfide bonds are in purple and seven sugar residues are in ball-and-stick models. The figure is obtained from(37) with permission. The monomer of influenza B/Hong Kong/8/73 (PDB: 3BT6) was shown on the right, with the HA1 portion highlighted in magenta and the HA2 portion highlighted in yellow.

(C) The trimer of HA of influenza A virus (PDB: 4LXV). Two of the monomers from the HA trimer are highlighted in grey and green, whereas the subunits that make up the third monomer, HA1 were highlighted in magenta and HA2 in yellow.

HA proteins are important to determine host tropism by binding to host cell receptors that contain terminal α-2,6-linked or α-2,3-linked sialic acid residues (α-2,6-SAs or α-2,3-SAs). It was shown that HAs from avian IAVs bind mainly to receptors with α-2,3-SAs which are enriched in human lower respiratory tract (LRT) and in the intestine of birds. By contrast, HA from human-adapted IAVs prefer α-2,6-SAs, which are expressed in bronchial epithelial cells in the upper respiratory

tract (URT) of humans. The terminal sialic acid residues α-2,3-SAs was found to have a “linear” presentation and α-2,6-SAs shows a more “bent” presentation(14, 40). The swine trachea has receptors with both α-2,3-SAs and α-2,6-SAs moieties that allow it to bind to both avian and human viruses. It was therefore proposed that pigs are the ‘mixing vessel’ in which the reassortment of avian and human viruses can occur(41). It may generate a new virus and causes the pandemic (42).

HAs of most influenza B viruses have a binding pocket that is capable of binding receptors with both α-2,3-SAs and α-2,6-SAs(43). HA of IBVs tends to lose its glycosylation site Asn194 when grows in embryonated chicken eggs(44). Further research found that Asn-194 in HA of human-adapted influenza B virus severely interferes with the binding of α-2,3-SAs(45). The loss of the Asn194 of HA discernible impact on binding to the human receptor analog LSTc, but the affinity for the avian analog LSTa increases (46).

1.2.2 Glycosylation of HA

HA and NA of influenza A and B viruses have several Asn-X-Ser/Thr motifs, potential sites for N-linked glycosylation, the modification occurs on the Asn residue where an oligosaccharide chain is attached through a N-glycosidic linkage(47). No O-linked glycosylation in HA and NA has been reported(48).The gain or loss of glycosylation sites during virus evolution in HA and NA can have severe effects on its biological properties, host specificity, and also the function of the protein(49)(50), such as receptor binding attenuation(51) and preventing the cleavage of HA0(52). The glycosylation of HA takes place in the protein secretory pathway (ER and Golgi) of eukaryotic cells(53) (54).

Oligosaccharyltransferase is the central enzyme of the N-glycosylation modification, which starts in the ER(55). HA is later transported to the Golgi for further modification of the carbohydrates. After HA was modified by α-mannosidase II, it becomes resistant to digestion by the bacterial enzyme Endoglycosidase H (Endo H)(47). This is used as a tool to determine transport of a glycoprotein to the medial-Golgi, since α-mannosidase II is located in this compartment (56). But the modification can be removed by Peptide N-glycosidase F (PNGase F).

Brefeldin A is a fungal metabolite, which has dramatic effects on the secretory pathway in mammalian cells. It’s also widely used to inhibit protein transportation at an early step in the secretory pathway. Immunofluorescence experiments and electron microscopic observations after treatment of cells with BFA showed that the block occurred in a pre-Golgi compartment, and thus proteins are retained in the ER(57)(58).

1.3 M2 of influenza A virus

1.3.1 The structure of M2

M2 is a type III transmembrane protein with a single transmembrane part. M2 protein of influenza A viruses form a homo-tetrameric proton channel. Each monomer consists of 97 amino acids, the N-terminal domain is from the amino acids 1 to 25, followed by the transmembrane domain (TM) which contains the residue 26 to 43 and the cytoplasmic tail (CT) including the residue 44 to 97 (59).

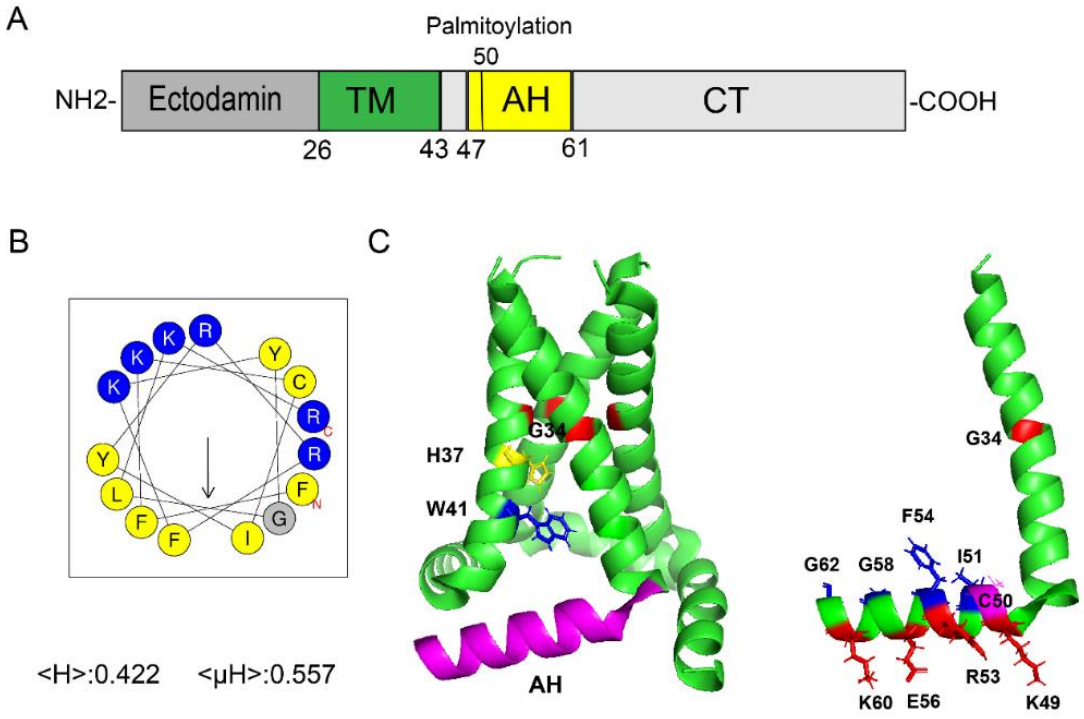

Figure 5. Scheme and NMR structure of M2 of influenza A virus

(A) The scheme of M2 monomer, each monomer contains a short ectodomain domain, a transmembrane domain (TM), and a long cytoplasmic tail (CT) which contains one amphiphilic helix (AH) at the beginning of the CT. Cysteine at position 50(C50) is modified by palmitoylation.

(B) The helical wheel plots of AH of M2. Positively charged amino acids are in blue, and hydrophobic amino acids are in yellow. The arrow points to the hydrophobic face. The length of the arrow corresponds to the hydrophobic moment <μH>. The picture was made by Heliquest (https://heliquest.ipmc.cnrs.fr/) using the amino acids from 47 to 61 of M2 (Gene bank: ACF54600.1).

(C) NMR structure of the TM and AH of M2. The tetramer of M2 shows on the left, the AH was highlighted in magenta, and G34 is in red. H37 and W41 are important for proton function and are highlighted in yellow and blue, respectively. On the right is the monomer of M2, the hydrophobic side was highlighted in blue and the polar side was in red. Palmitoylation Cysteine is in magentas. The structure was labeled using Pymol and the structure is from PDB(2L0J).

Two conserved cysteines at positions 17 and 19 of the ectodomain form an intermolecular disulfide bond. A highly conserved Glycine (G34) in the middle of the transmembrane region causes a slight kink in the helix. Important for my work is a membrane-near amphipathic helix (AH residue 47-61) in the CT part, which is palmitoylated at one cysteine (residue 50) at its beginning (60). The C-terminus contains an M1 binding site (residue 71 to 73) (61).

1.3.2 Amphipathic helix (AH) of M2

The residue 47-61 of M2 from influenza A virus forms an amphipathic helix (AH), a secondary structure motif commonly used by proteins to mediate reversible binding to membranes. An amphipathic helix has two faces with opposite features: a side with hydrophobic amino acids which can insert between the lipid acyl chains of a membrane and a face with polar residues that could interact with the polar headgroup of lipids. The bioinformatics tool Heliquest facilitate the identification of AHs. Using Heliquest we can predict an amphiphilic helix and calculate various parameters. Two values(<μH> (hydrophobic moment) and <H> (hydrophobicity) indicate the character of the helix. The hydrophobic moment is a measure of the amphiphilicity of a helix. The hydrophobicity shows the avidity of the helix for lipids/membranes(71). In the helical wheel plot for AH of M2(Figure 5B), the hydrophobic amino acids are in yellow, and the positive amino acids are in blue. The arrow points to the hydrophobic side, and the length corresponds to the hydrophobic moment. AH of M2 protein not only promotes membrane curvature but also facilitates the virus budding at the final stage. The four amphipathic helices in the M2 also stabilize the tetramer(62). The AH of M2 binds cholesterol and is important for viral filament formation, and also stabilizes the viral filaments (72).

AHs are present in many cellular and viral proteins and they are important for various biological processes. AHs bind membranes weakly and the insertion into the membrane regulates bilayer physical properties (65). Proteins with AHs also mediate membrane fission by insertion of the helix into the lipid bilayer. This causes membrane curvature supporting the fission reaction (66). AHs in several proteins promote the targeting to intracellular membranes where they are involved in protein-lipid interaction and protein-protein interaction. AHs deform lipid bilayers (like Pex11), change the membrane curvature (like ALPS and M2), and recognize specific lipids (67).

1.3.3 The function of M2 from influenza A virus

Proton channel

M2 plays an essential role in virus entry, and in virus assembly, and budding. At the early stage of virus infection when virus particles are present in the acidic endosome the M2 proton channel opens and mediates proton influx into the virus particles which triggers the dissociation of the vRNPs from M1. His37 and Trp41, the two most conserved amino acids in the M2 protein are essential for the function of the proton channel(63). His 37 is the pH sensor and Trp41 is the gate that opens and closes the channel(64). Another function of the M2 protein is to prevent the conformational changes of cleaved HA protein during protein transport by maintaining the neutral pH in the trans-Golgi network(65). This is especially important for HA proteins (H5 and H7 subtypes) that contain a polybasic cleavage site, which is cleaved in all cell types in the trans Golgi-network, but also for some HA subtypes (H1N1) that contain a monobasic cleavage site(66)

Assembly and Budding

The cytoplasmic tail (residues 70–77) of M2 is essential to recruit the M1 protein to the plasma membrane to facilitate virus assembly(61). Mutations in and deletion of the cytoplasmic tail of the M2 protein also inhibits virus budding(67). Both spherical and filamentous strains of influenza virus require the M2 protein for membrane scission at the virus budding stage, the mutations of M2 results in a scission-defective morphology(67, 68). It has been found that M2 mediates the final steps of viral budding, bypassing host ESCRT proteins(69).

1.4 S-acylation, a hydrophobic modification of proteins

Protein S-acylation is a posttranslational modification and refers to long chain fatty acid attachment to cysteine residues of a target protein via a thioester linkage. It is also known as S-palmitoylation since most proteins are modified with this 16-carbon fatty acid. DHHCs, the enzymes required for fatty acid transfer also have the ability to efficiently transfer other fatty acids like myristate (C14) and stearate (C18). It has been predicted that around 10% of the human proteome is modified by palmitoylation(70). The S-acylation modification can be removed by thioesterases. It has been found that depalmitoylation is catalyzed by four thioesterases including APT1, APT2, PPT1 and PPT2(71)(72).

1.4.1 Function of S-acylation

S-acylation regulates many important biological processes including ion transport, protein function, protein trafficking, cell signaling, protein stability, protein localization, neuronal plasticity, and immune response. Palmitoylation as a lipid modification provides a membrane anchor to proteins that would otherwise interact only weakly with membranes(73). But S-acylation is more than just a membrane anchor since it also occurs in transmembrane proteins. It has been found that S-palmitoylation is a signal to protein sorting. In mammalian cells, some transmembrane proteins like G protein-coupled receptors use palmitoylation for efficient protein sorting(74). S-palmitoylation also acts as a sorting signal to accelerate the anterograde transport at the Golgi(75). So far over 2000 proteins have been predicted to be palmitoylated which takes around 12% of the human proteins(76). In addition, pathogens like envelope viruses use the S-palmitoylation machinery of host cells to promote infection such as the influenza virus and SARS-CoV-2(77).

1.4.2 S-acylated proteins in influenza virus

I. S-acylation of influenza A virus proteins

There are three S-acylated amino acids in the **HA** of Influenza A virus, which are highly conserved (78). Two of them are located in the short cytoplasmic tail and modified by palmitates (C16:0). One is at the end of the transmembrane part and is modified by stearate (C18:0) (77, 79, 80) (See figure 6). S-acylation of HA of IAV is essential for virus growth. For the subtype H1(H1N1) virus, after removing one or two of the S-acylation sites at the cytoplasmic tail, no viable virus could be rescued using reverse genetic systems. The stearate modification has only a small effect on the virus growth(81). The S-acylation in the H3 subtype(H3N2) of influenza A virus was found important to virus assembly(82). For the H7N1 subtype, the virus can be rescued after removing one of the S-acylation sites at the CT but the virus growth was greatly affected. Especially the third S-acylation site reduced the growth rates in cell culture. The viruses with double or triple mutations of the H7N1 virus could not be rescued(83). S-palmitoylation is catalyzed by acyltransferases also called DHHC proteins, which are described below. DHHC2, 8, 15, and 20 are important to the HA of influenza A virus acylation for both avian influenza (H7N1) and human WSN virus (H1N1)(84).

The proton channel **M2** of influenza A virus contains one palmitoylated cysteine located at the beginning of the amphiphilic helix(60). However, this cysteine at position 50 is not completely conserved in all strains of influenza A viruses(85)(86). In line with that, S-acylation of M2 is not

essential for virus growth(87). The S-acylation in M2 protein is not required for its targeting to the hemagglutinin-defined budozone (88).The modification also does not impact the ion channel function of the M2 protein(89). M2 of influenza A virus also uses DHHC2, 8, 15, and 20 as acylating enzymes, but how DHHCs recognize the M2 protein remains unknown(84).

II. S-acylation of influenza B virus proteins

Hemagglutinin of the Influenza B virus contains two S-acylated cysteines at the cytoplasmic tail which are modified by palmitates (77, 79, 80). We have limited information related to the function of S-palmitoylation in influenza B virus. HA-catalyzed membrane fusion was significantly affected by removing one modification sites, but not two modification sites in HA protein (B/Kanagawa/73 strain). (90).Unlike influenza A virus, the role of acylation in the HA of influenza B virus has not been investigated using recombinant viruses. DHHC 2, 8, 15, and 20 have been identified to be involved in the S-acylation of HA from influenza A virus, but the same enzymes had little effect on acylation of influenza B virus (84). Identifying the responsible enzymes for acylation HA from influenza B virus is important but hasn't been investigated.

NB protein is palmitoylated on cysteine 49. The palmitoylation of NB is crucial for its transport to the plasma membrane. The overall virus growth was unaffected by the removing palmitoylation site of the NB, although the virus growth was slowed down in the early time periods(91).

III. S-acylation of influenza C virus proteins

Only one S-acylated cysteine exits at the end of TM part in **HEF** protein of the Influenza C virus and predominantly contains stearate (78). After removing the acylation site, the membrane fusion activity of HEF was only slightly reduced and the mutation has only a modest effect on virus growth (92).

CM2, the proton channel of Influenza C virus is acylated at residue 65. Protein synthesis and transport were not affected in a mutant lacking the modification site. S-acylation of CM2 of Influenza C virus is also dispensable for virus replication in vitro(93).

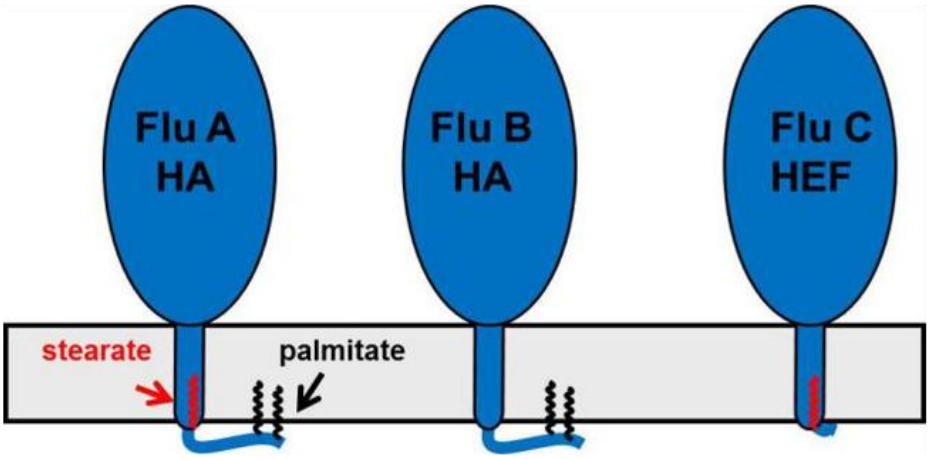

Figure 6. The acylation sites and the fatty acyl chains in HA and HEF proteins.

Three acylation sites exit in HA of the influenza A virus, one at the end of the transmembrane domain (TMD) which is modified by stearate, and two located in the cytoplasmic tail which are modified by palmitates. HA of the influenza B virus contains two acylation sites at the cytoplasmic tail which are modified by palmitates. HEF protein has one acylation site at the end of the TMD and is modified by stearate.

1.4.3 Structure and function of S-acyltransferases DHHC enzymes

S-palmitoylation is catalyzed by acyltransferases, also called DHHC proteins due to the presence of the conserved Asp–His–His–Cys (DHHC) motif, the catalytic center of the enzyme which is embed in a cysteine-rich domain (CRD). Twenty-three DHHCs from DHHC1 to DHHC 24 (DHHC 10 is missing) exist in human cells (94). The majority of DHHC proteins localize to the Golgi, a small number remains in the endoplasmic reticulum (ER) or is targeted to the plasma membrane, but cell type specific differences have been described (95)(75)(96).Acyl chain transfer occurs via a two-step ping-pong mechanism: first, the fatty acid is transferred from the lipid donor acyl-CoA to the cysteine residue of the DHHC motif (autoacylation reaction) followed by the acyl group being transferred from the enzyme to the protein substrate (97).

The publication of the experimentally determined 3D-structures of hDHHC20 (Figure 7B) and zebrafish DHHC15 facilitates the understanding of DHHC enzymes. Four transmembrane (TM) helices of hDHHC20 form a tepee-like structure and the catalytic DHHC motif within the highly conserved cysteine-rich domain (CRD) is located between TM2 and TM3. The CRD binds two zinc (Zn^{2+}) ions which is important to structural stability but does not directly participate in catalysis. The four TM helices form a hydrophobic cavity where (in the autoacylated form of a DHHC protein) the acyl chain is inserted.

The N-terminus of DHHCs located at the cytoplasmic face also contains conserved motifs such as the TTXE motif (Thr240-Thr-X-Glu243). It is essential for enzymatic activity since the fatty acid transfer is drastically reduced in an AAXE mutant. An amphipathic helix(a′2) exits at the C-terminus of the DHHCs which is conserved within many DHHCs.

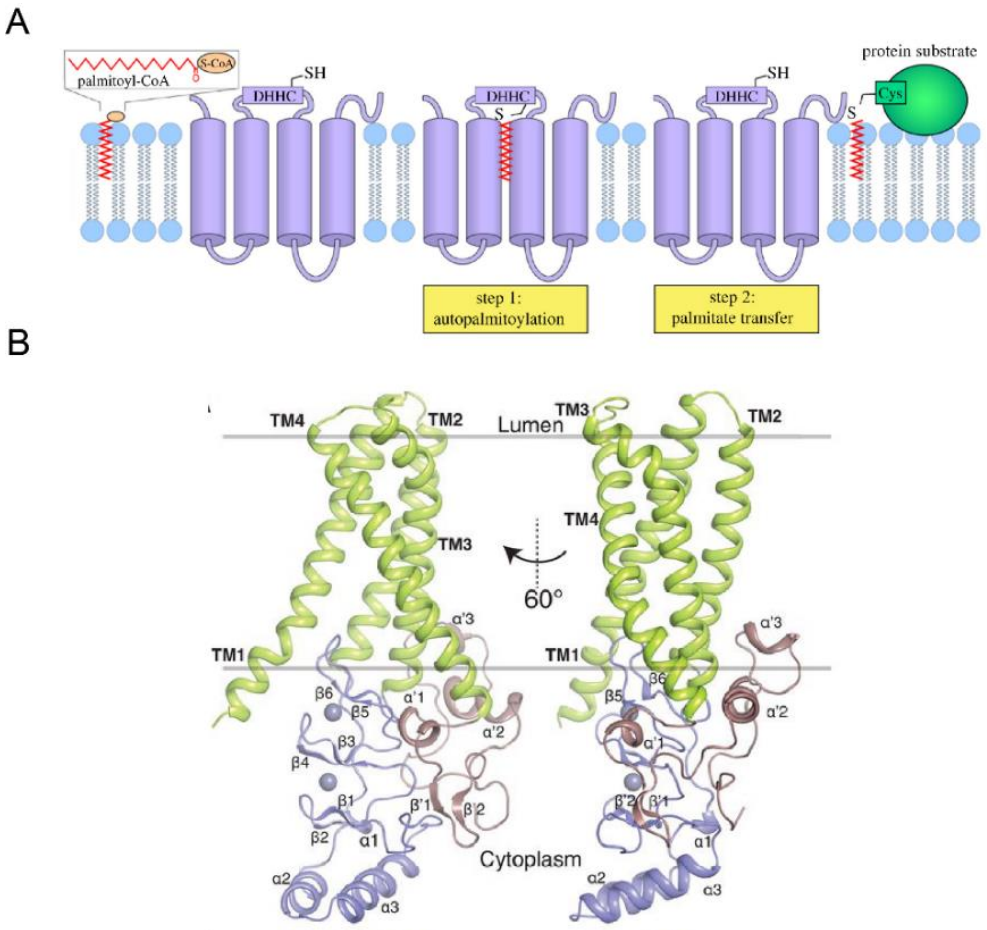

Figure 7. The structure of DHHCs

(A) The two steps mechanism of fatty acid transfer catalyzed by DHHCs. First is the DHHCs autoacylation reaction followed by the second step, the acyl group is transferred to the substrate.

(B) Structure of human DHHC 20, the four transmembrane (TM) helices are in green and form a tepee-like structure, and the catalytic center embedded in the cysteine-rich domain in blue, is located between TM2 and TM3. The two spheres indicate the Zn2+ ions. The four TM forms a hydrophobic cavity where the acyl chain is inserted. The C-terminal domain is brown, where an amphipathic helix(a′2) exits and is conserved within many DHHCs. hDHHC20 (PDB: 6BMN). Figure (A) is obtained from(98) and figure (B) is from(99) with permission.

Experimental structures are available only for hDHHC20 and DHHC15 of zebrafish. But the neural network-based Alphafold system was developed and won the 14th Critical Assessment of protein Structure Prediction (CASP14), which demonstrates the accuracy and the outperformance of this method (100). The Alpha fold protein structure database (https://alphafold.ebi.ac.uk/) now has over 200 million predicted protein structures, including all the DHHCs in humans(101).

1.4.4 The protein substrate specificity of DHHCs

Unlike other modifications, for example N-glycosylation, S-palmitoylation is not determined by a specific sequence motif(102). The majority of cellular proteins can be acylated by several, but not each, of the twenty-three DHHC proteins. For example, DHHC20 and 9 participate in acylation of the spike protein of SARS-CoV-2 (103).This indicates that the enzymes show distinct, partially overlapping substrate specificities(104, 105). The molecular mechanism by which the protein substrates are recognized and enzyme catalysis is initiated is poorly understood. Several DHHCs contain N- or C-terminal interaction domains, such as ankyrin repeats (106), PDZ-binding motifs (107) , Src-homology 3 (SH3) domain(108, 109) and SH2 domains with which they recruit (mainly intrinsically hydrophilic) substrates. Only one structure of such a complex is known, namely for an N-terminal ankyrin domain of DHHC17 bound to a peptide from the substrate SNAP 25(110).

How transmembrane proteins are recognized by DHHC enzymes is essentially unknown(98, 111, 112)However, there is increasing evidence that in various cellular proteins an amphiphilic helix, often located near a transmembrane region, serves as a recognition feature for DHHC20, but no molecular structural information is available for any of these helices(113–116).

1.4.5 The lipid substrate specificity of DHHCs

The crystal structure of DHHC20 delivered a model of how the specificity of DHHCs for palmitate and stearate might be encoded. The residues in the ceiling of the hydrophobic cavity where the acyl chain is inserted are essential for the fatty acyl chain selectivity. At the narrow end of the cavity of DHHC20, Ser 29 on TM1 forms a hydrogen bond with Tyr 181 on TM3, which effectively closes the hydrophobic groove. Ser 29 and Tyr 181 are not conserved between various DHHC proteins; but most DHHCs contain either two bulky residues, one bulky and one small or two small amino acids at the homologues position. It was hypothesized that the presence of certain amino acids (large or small) determines the lipid binding specificity of a DHHC enzyme. This model has been so far confirmed by experiments. The preference for

stearoyl-CoA (C18) of DHHC20 increases after changing Tyr181 to Ala (a small amino acid) and the mutation Ser29 to Phe (a bulky hydrophobic residue) increases the preference for the shorter acyl chain of palmitate (100). Likewise, DHHC3 and DHHC7 are closely related enzymes but showed different abilities to use C18:0 acyl-CoA as a substrate. DHHC3 has a higher preference for palmitoyl (C16) over stearoyl (C18) compared to DHHC7. The homologous pair of Tyr181-Ser29 in DHHC20 is Ile182-Phe53 in DHHC3. After Ile 182 was replaced with Ser (a small amino acid), DHHC3 has a higher preference for stearoyl (C18)–CoA (100, 119). Therefore, a large hydrophobic residue in DHHC20 (Tyr181) and DHHC3 (Ile182) was sufficient to select the length of a lipid substrate.

2. Aims of the study

The role of the amphiphilic helix and transmembrane region in the efficient acylation of M2 from Influenza A virus

Both the M2 protein and HA of Influenza A virus are acylated by the DHHC proteins 2, 8, 15 and 20, a large family of acyltransferases which contain 23 members in humans. How these enzymes recognize their substrates is essentially unknown and hence one focus of this study. Previous research has shown that several cellular proteins contain an acylated cysteine within a membrane-near amphiphilic helix. A similar amphiphilic helix (AH) is also present in M2 of the influenza A virus and the structure of the helix including the adjacent membrane-spanning domain has been resolved which is helpful to plan mutagenesis. In this study, I aimed to investigate whether the AH contains the signal for S-acylation by fusing it to the C-terminus of the red fluorescent protein RFP. I then measured its membrane targeting ability and S-acylation level in transfected cells. To further explore whether conserved amino acids, the biophysical properties of the AH and/or its secondary structure are essential for palmitoylation, I introduced different mutations into the complete M2 protein. To explore whether there are other signals in the M2 protein, I proceeded to truncate a large part of the amphiphilic helix and performed mutagenesis of the transmembrane (TM) region of M2. Since these mutations might affect the targeting of the M2 protein from the ER to the intracellular site of palmitoylation, I used confocal microscopy and co-localization of M2 mutants with a cis-Golgi marker, which is the site where its main enzyme DHHC20 is located. Finally, I asked whether M2 can be co-precipitated with DHHC20 and whether the mutations affect this interaction. The data will be supplemented by a molecular dynamics (MD) simulation of a M2 DHHC20 complex, which was performed in the Theoretical & Computational Biophysics group of Professor Cecilia Clementi (Department of Physics, FU Berlin).

Role of palmitoylation of the Hemagglutinin of Influenza B virus and identification of the enzymes involved

It is already known that S-palmitoylation of the hemagglutinin (HA) is crucial for replication of influenza A virus, but similar studies have not been performed with Influenza B virus, which contains only two (instead of three) S-acylated cysteines at the cytoplasmic tail of HA. Using recombinant viruses, I asked whether the removal of one or both acylation sites affects the generation of viable virus particles and viral titers in cell culture.

DHHC 2, 8, 15, and 20 have been identified to be involved in S-acylation of HA from influenza A virus, but the enzymes required for acylation of HA of Influenza B virus have not been identified. To possibly narrow down the number of DHHCs to be investigated, I first aimed to determine the intracellular compartment of the exocytic compartment where HA of Flu B is acylated. Most of the DHHCs are located in the Golgi network, while only a few are present in the ER and at the plasma membrane. I will then use commercial HAP-1 cells where the genes encoding the DHHCs located in the identified compartment have been inactivated to determine which of them causes a reduction in palmitoylation of Flu B HA.

Thus, my study has two aims focused on understanding the acylation processes of the M2 and HA proteins in Influenza A and B viruses, respectively. By investigating the role of the amphiphilic helix in M2, the study aims to shed light on how acyltransferases recognize their substrates, which are also important for cellular proteins that are acylated at a membrane-near helix. Additionally, the study aims to determine the function of acylation of HA of Influenza B virus and identify the specific DHHCs involved in HA palmitoylation. The findings from these experiments will contribute to a better understanding of the acylation mechanisms in both viruses, potentially identifying novel targets for antiviral interventions.

3. Materials and Methods

3.1 Materials

Reagent type	Designation	Source or reference	Identifiers	Additional
Gene (Influenza A virus)	M2	GenBank: ACF54600.1		A/WSN/1933(H1N1)
Gene (Aequorea victoria)	RFP	addgene	Cat# 26001	RFP was cloned from this plasmid
Gene (virus)	Influenza B Lee 40	NCBI		Taxonomy ID: 518987
Gene	HA	GenBank: DQ792897	Robert Koch-Institute	A gift from Thorsten Wolff group
Gene(virus)	A/WSN/1933(H1N1)	NCBI		Taxonomy ID: 382835
Gene (Influenza A virus)	HA	GenBank: LC333185.1		A/WSN/1933(H1N1)
Cell line	HEK293T	ATCC	Cat# CRL-3216 RRID: CVCL_0063	
Cell line	BHK21	ATCC	Cat# CCL-10 RRID: CVCL_AR44	For IF experiments
Cell line	HAP1	Horizon Discovery		Screen DHHC candidates
Cell line	HAP1 knock out cells	Horizon Discovery		Screen DHHC candidates
Cell line	A549	ATCC		For IF experiments
Cell line	MDCKII	ATCC		Virus infection

antibody	anti-M2 antibody 14C2(Mouse Monoclonal)	Santa Cruz Biotechnology	Cat# sc-32238 RRID: AB_627808	WB: 1:1000 to 1:4000 co-ip: 1:200
antibody	Anti-Flotillin-2(Mouse Polyclonal)	BD	Cat# 610383 RRID: AB_397766	WB: 1:1000
antibody	anti-RFP antibody (Rabbit Polyclonal)	abcam	Cat# ab62341 RRID: AB_945213	WB: 1:1000
antibody	anti-myc-tag antibody (Rabbit Polyclonal)	Proteintech	Cat# 10828-1-AP RRID: AB_2148585	WB: 1:2000 IF: 1:1000
antibody	anti-GM130 cis-Golgi Marker antibody (Rabbit Monoclonal)	abcam	Cat# ab52649 RRID: AB_880266	IF: 1:200
antibody	Influenza A virus H1N1 HA polyclonal antibody from rabbit	Genetex	Cat# GTX127357	WB: 1:3000
antibody	Monoclonal antibodies against HA of Influenza B virus	A gift by Dr. Florian Krammer		WB: 1:1000
antibody	Caveolin-1(N-20) polyclonal antibody from rabbit.	Santa	Cat# Cruz-894	WB: 1:1000
antibody	Rabbit polyclonal to HA tag-ChIP Grade	Abcam	Cat# Ab9110	IF: 1:500

antibody	Influenza B (Haemagglutinin HA2) Mouse Monoclonal Antibody	OriGene	Cat# AM00954PU-N	IF: 1:1000
antibody	Anti-Rabbit IgG VHH Single Domain Antibody (Monoclonal secondary)	abcam	Cat# Ab191866 RRID: AB_2650595	WB: 1:3000-1:5000
antibody	Goat anti-mouse IgG (H + L) (Goat, Polyclonal secondary)	Bio-rad	Cat# 1706516 RRID: AB_11125547	WB: 1:1000-1:4000
antibody	Goat anti-mouse Alexa 488 (polyclonal secondary)	Thermo Fisher Scientific	Cat# A28175 RRID: AB_2536161	IF: 1:1000
antibody	Goat anti-Rabbit Alexa 488(polyclonal secondary)	Thermo Fisher Scientific	Cat# A-11008 RRID: AB_143165	IF: 1:1000
antibody	Goat anti-Rabbit Alexa 568(polyclonal secondary)	Thermo Fisher Scientific	Cat# A-11011 RRID: AB_143157	IF: 1:1000
Plasmid	M2-PCAGGS	This Lab M2 project		Insert the M2 sequence in PCAGGS
Plasmid	M2-AH1 M2-AH2 M2-AH3	M2 project		Insert mutations to change the conserved amino acids in AH of M2 based on M2-PCAGGS
Plasmid	M2-AH4 M2-AH5	M2 project		Insert mutations in AH of M2 based on M2-PCAGGS

Plasmid	M2 1-50 M2 1-53	M2 project		Insert M2 1-50 and M2 1-53 in PCAGGS
Plasmid	M2 1P M2 3P	M2 project		Insert Prolines to break helix in M2 based on M2-PCAGGS
Plasmid	M2 G34A	M2 project		Insert mutation in TM of M2
Plasmid	M2 1-50 G34A	M2 project		Insert mutation in TM of M2 1-50
Plasmid	RFP	M2 project		Insert RFP in PCAGGS
Plasmid	RFP-AH	M2 project		Insert RFP-AH in PCAGGS
Plasmid	RFP-AH-C50S	M2 project		Insert RFP-AH-C50S in PCAGGS
Plasmid	DHHC20-myc (Plasmid)	Masaki Fukata lab		Myc-tagged human DHHC20 clones in pcDNA3.1
Plasmid	pHW-Lee-HA	Thorsten Wolff group		Wild type HA of influenza B virus
Plasmid	pHW-Lee-HA-Ac1 pHW-Lee-HA-Ac2	This Lab FluB project		Mutation removing one S-acylation site.
Plasmid	pHW-Lee-HA-Ac1+2	This Lab FluB project		Removing the two acylation sites
Plasmid	HA-DHHC1,2,3,4 and 6	Masaki Fukata lab		Mouse DHHCs

commercial assay or kit	the subcellular protein fractionation kit for cultured cells	ThermoFishr	Cat# 78840	For the membrane separation experiment
commercial assay or kit	Pierce ECLplus reagent	Thermofisher	Cat# 32132	For WB
commercial assay or kit	innuPREP Virus TS RNA Kit	Analytik Jena	Cat# 845-KS-4710250	Extra the virus RNA
commercial assay or kit	High capacity cDNA reverse transcription kit	Thermo Fisher Scientific	Cat# 4368814	
commercial assay or kit	ER staining kit–Red Fluorescence | Cytopainter	Abcam	Cat# ab139482	Dye the ER
chemical compound, drug	Methyl methanethiosulfonate (MMTS)	Sigma	Cat# 208795	
chemical compound, drug	Tris (2-carboxyethyl) phosphine (TCEP)	Carl Roth	Cat# HN95.2	
chemical compound, drug	Endo H	NEB	Cat# P0703L	
chemical compound, drug	TPCK-trypsin	Sigma	Cat# T1426	For virus infection medium and surface trypsinization experiment
chemical compound, drug	Brefeldin A	Sigma	Cat# B7651	Inhibit protein transportation

chemical compound, drug	NP40 lysis buffer	Thermo Scientific	Cat# 85124	
chemical compound, drug	Protein inhibitor	Roche/Merk	Cat# 11873580001	
chemical compound, drug	lipofectamine 3000 transfection reagent	Thermofisher	Cat# L3000015	
software, algorithm	Image J	https://imagej.nih.gov/ij/index.html	RRID:SCR_003070	For WB experiments
software, algorithm	Heliquest	https://heliquest.ipmc.cnrs.fr/		To predict the helix
software, algorithm	PyMOL	https://pymol.org/2/	RRID:SCR_000305	
software, algorithm	Fiji	https://imagej.net/software/fiji/	RRID:SCR_002285	For IF data and the quantification of the colocalization
software, algorithm	AlphaFold2	https://colab.research.google.com/github/sokrypton/ColabFold/blob/main/AlphaFold2.ipynb		To predict the protein structure
software, algorithm	AlphaFold Protein Structure Database	https://alphafold.ebi.ac.uk/		
other	ProLong Glass antifade mounting medium	Thermo Fisher	Cat# P36984	Make the samples for confocal microscope

other	DAPI	ThermoFisher	Cat# 62247	Dye the nucleus
other	Protein-G Sepharose 4 Fast Flow	GE Healthcare	Cat# GE17-0618-01	For IP experiment
other	S7 Fusion Polymerase	Mobidiag	Cat# MD-S7-500	For PCR and Quickchange method
other	NheI, XbaI XhoI, BglII	NEB		

3.2 Methods

3.2.1 Cloning

I. **Construction of Influenza B HA mutants for reverse genetics**

To rescue influenza B mutant viruses, Quick Change Site-directed mutagenesis was used to generate the mutation on pHW-Lee-HA. Briefly, a complementary primer pair with desired point mutations were designed so they anneal to the target sequence on the plasmid DNA. The Cys581 and Cys 583 at the cytoplasmic tail of HA were individually mutated to serine by changing 2 nucleotides in the amino acid codon (Cysteine TGT to Serine AGC). This was carried out using 2 step PCR method as follows:

PCR Mix	Volume
5x Phusion Buffer	10 µl
dNTPs (10mM)	1 µl
Phusion enzyme	0.5 µl
Plasmid DNA (100ng/µl)	1 µl
Nuclease free water (NFW)	35.5 µl
Total volume	48µl

First, prepare the PCR Mix, then separate it into two tubes (24µl each), one tube added F primer and another added R primer. Then the first PCR was performed as follows:

The aim of this step is to allow the annealing of mutation primers and individual amplification of each strand to serve as a template for the next step. After the first PCR, 25 µl products from both tubes were mixed, and transferred into a new PCR tube, 0.5µl of fresh Phusion enzyme was added and a second PCR was performed using the same protocol but for 35 cycles.

PCR step	Temperature (°C)	Time	Cycles
Initial denaturation	98°C	30s	1x
Denaturation	98°C	10s	
Annealing	55°C	30s	**5 x**
Extension	72°C	3min	
Final extension	72°C	10 min	1x

PCR was treated with the restriction endonuclease DpnI (1 µl) at 37°C overnight to digest only methylated DNA leaving the unmethylated PCR products intact. DH5α E.coli cells were transformed with the treated product for amplification, subsequent purification, and sequencing of the mutated plasmids.

Transformation of competent bacterial cells

For amplification of plasmid DNA, E.coli cells were transformed either with plasmid or with ligation products. 100µl E.coli cells were put on ice, mixed with target plasmid DNA or ligation mixture incubated on ice for 30 minutes. After a 45s "heat shock" at 42°C, cells were directly placed on ice for 2 min. 500 µl LB medium was added and shaken (200 rpm) for 45 min at 37°C. 100µl of the transformed cell culture was subsequently plated on LB plate containing 100 µg/ml of ampicillin. Plates were incubated overnight at 37°C and single colonies were picked for plasmid purification.

II. Construction of plasmids for expression

To get high expression of M2, RFP, HA protein in transfected cells, the full sequences of proteins were individually inserted into the vector pCAGGS through introducing the restriction site XhoI and BgIII for M2 and RFP plasmids, and NheI and XbaI for BHA plasmids. The plasmid construction was done through regular molecular cloning with PCR, restriction digest, ligation, transformation and plasmid purification.

PCR Mix	**Volume**
5x Phusion Buffer	10 µl
dNTPs (10mM)	1 µl
Phusion enzyme	0.5 µl
Primer F (25µM)	1 µl
Primer R (25µM)	1 µl
Plasmid DNA (100ng/µl)	1 µl
Nuclease free water (NFW)	35.5 µl
Total volume	50µl

PCR was performed as follows:

PCR step	Temperature (°C)	Time	Cycles
Initial denaturation	98°C	30s	1x
Denaturation	98°C	10s	
Annealing	55-60°C	30s	**35 x**
Extension	72°C	30s/kb	
Final extension	72°C	11 min	1x

Restriction digest

After gel extraction, both the purified DNA fragments and the vector were digested by the restriction enzyme XhoI and BglII (or NheI and XbaI) for 4h at 37°C. The reaction mixture is listed below.

Component	Volume
10X Buffer	5 µl
Enzyme 1	1 µl
Enzyme 2	1 µl
DNA fragment / vector	X (25 µl/1ug)
Nuclease free water	50-X µl
Total volume	50µl

Ligation

After purified using Monarch PCR/DNA Cleanup Kit, DNA segment and vector were used to prepare the reaction mix. incubated at 16°C overnight to allow successful ligation of HA fragment and linearized vector. The reaction mix followed:

Component	Volume
10X Buffer	2µl
T4 ligase	1µl
DNA fragment	50ng
Vector	100ng
Nuclease free water	To 20µl

Transformation as mentioned above and plasmid purification.

3.2.2 Primers

Primers for restriction cloning

Name	Sequence
M2-XhoI-F	CCGCTCGAGATGAGTCTTCTAACCGAGGTCGAAACGCCTATCAGAAAC GAATGGGGGTGC
M2-BglII-R	GAAGATCTTTACTCCAGCTCTATGTTGACAA
M2-1-50-XhoI-F	CCGCTCGAGATGAGTCTTCTAACCGAGGTCGAAAC
M2-1-50-BglII-R	CAAGATCTTTAGCATTTGAAAAAAAGACG
M2-1-53-BglII-R	CAAGATCTTTAACGATAAATGCATTTGAAAAAAAGACG
RFP-AH-XhoI-F	CCGCTCGAGATGGCCTCCTCCGAGGACGTCATC
RFP-BglII-R	GAAGATCTTTAGGCGCCGGTGGAGTGGCG
RFP-AH-BglII-R	GAAGATCTTTATCTTTTCAAACCGTATTTAAAGCGACGATAAATGCATTT GAAAAAGGCGCCGGTGGAGTGGCGGC
RFP-AH-C50S-BglII-R	GAAGATCTTTATCTTTTCAAACCGTATTTAAAGCGACGATAAATAGATTT GAAAAAGGCGCCGGTGGAGTGGCGGC
M2-1-50-G34A-BglII-R	GAAGATCTTTAGCATTTGAAAAAAAGACGATCAAGAATCCACAATATCA AGTGCAAGATGGCAATGATAT
BHA-NheI-F	CTAGCTAGCATGAAGGCAATAATTGT ACTAC
BHA-XbaI-R	GCTCTAGATCACAGACAGATGGAACAAGAAAC
BHA-Ac1,2-XbaI-R	GCTCTAGATCACAGTGAGATGGATGAAGAAACATTG

Primers of mutates using Quickchange:

Name	Sequence
M2-AH1-F	CGTCTTTTTTTCGAGTGCATTTATCGTCGCTTTAAATACGGTTTG
M2-AH1-R	GCGACGATAAATGCACTCGAAAAAAAGACGATCAAGAATCCACAA
M2-AH1-F	CATTTATGAACGCTTTGAGTACGGTTTGAAAAGAGGGCCTTCTACGGAAGGAG
M2-AH1-R	CTTTTCAAACCGTACTCAAAGCGTTCATAAATGCACTCGAAAAAAAGACGCAC
M2-AH4-F55K-F	TTATCGTCGCAAGAAATACGGTTTGAAAAGAGGGCCTTCTACGG
M2-AH4-F55K-R	CAAACCGTATTTCTTGCGACGATAAATGCATTTGAAAAAAAGACG
M2-AH4-F48, I51K-F	CGTCTTTTTAAGAAATGCAAGTATCGTCGCAAGAAATACGGTTTGAAAAG
M2-AH4-F48, I51K-R	GCGACGATACTTGCATTTCTTAAAAAGACGATCAAGAATCCACAATATCA
M2-AH5-K49, R53F-F	CGTCTTTTTTTCTTCTGCATTTATTTCCGCTTTAAATACGGTTTGAAAAGAGGGCCTTCT
M2-AH5-K49, R53F-R	CGTATTTAAAGCGGAAATAAATGCAGAAGAAAAAAAGACGATCAAGAATCCACAATATCA
M2-AH5-K60R6, 1F-F	TAAATACGGTTTGTTCTTCGGGCCTTCTACGGAAGGAGTGCCAGAGTCTGCCAG
M2-AH5-K60, R61F-R	CTTCCGTAGAAGGCCCGAAGAACAAACCGTATTTAAAGCGGAAATAAATGCAGAA
M2-AH2-Y52A-F	CAAATGCATTGCCCGTCGCTTTAAATACGGTTTGAAAAGAG
M2-AH2-Y52A-R	TAAAGCGACGGGCAATGCATTTGAAAAAAAGACGATCAAG
M2-AH2-L59A-F	TAAATACGGTGCGAAAAGAGGGCCTTCTACGGAAGGAGAGGGC
M2-AH2-L59A-R	GAAGGCCCTCTTTTCGCACCGTATTTAAAGCGACGGGCAAT
M2-AH3-F47A-F	GATCGTCTTGCTTTCAAATGCATTTATCGTCGCTTTAAATACGG
M2-AH3-F47A-R	CTTGATATTGTGGATTCTTGATCGTCTTGCTTTCAAATGCATTTA
M2-I51P-F	CGTCTTTTTTTCAAATGCCCCTATCGTCGC
M2-I51P-R	GCGACGATAGGGGCATTTGAAAAAAAGACG
M2-3P-F	CTTTTTTTCAAATGCATTCCTCCTCCCTTTAAATACGGTTTG
M2-3P-R	CAAACCGTATTTAAAGGGAGGAGGAATGCATTTGAAAAAAAG
M2-G34A-F	CAAATATCATTGCCATCTTGCACTTGATATTG
M2-G34A-R	CAATATCAAGTGCAAGATGGCAATGATATTTG

Name	Sequence
FluB-BHA-AC1-F	CTAGCTCCATCT GTCTGTGAGG GAAATTAAGC CCTGTGTTTTCC
FluB-BHA-AC1-R	CCTCACAGACAGATGGAGCTAG AAACATTGTCTCTGGAGACCAT
FluB-BHA-AC2-F	CTTGTTCCATCAGCCTGTGAGG GAAATTAAGC CCTGTGTTTTCC
FluB-BHA-AC2-R	CCTCACAGGCTGATGGAACAAG AAACATTGTCTCTGGAGACCAT
FluB-BHA-AC1,2-F	CTAGCTCCATCAGCCTGTGAGG GAAATTAAGC CCTGTGTTTTCC
FluB-BHA-AC1,2-R	CCTCACAGGCTGATGGAGCTAGAAACATTGTCTCTGGAGACCAT
FluA-AHA-AC1-F	CTGGATGAGCTCTAATGGGTCTTTGC
FluA-AHA-AC1-R	CATTAGAGCTCATCCAGAAACTGATTGC

3.3 Methods for the project: the role of the amphiphilic helix and transmembrane region in the efficient acylation of M2 from Influenza A virus

3.3.1 Membrane separation experiment

3µg plasmids encoding RFP, RFP-AH or RFP-AH-C50S were transfected into 293T cells using lipo3000 transfection reagent. After 24 hours, the subcellular protein fractionation kit for cultured cells was used to separate cells into cytoplasm and membranes. All the buffers were prepared with protein inhibitors from the kit in advance. Cells ($1x10^6$), PBS-washed and pelleted in a microfuge (500xg, 5min), were incubated with 150ul of the cytoplasmic extraction buffer CEB at 4°C for 10 minutes with gentle mixing. This buffer permeabilizes the plasma membrane and releases the cytosol. The opened cells are pelleted (500xg, 5min) and the supernatant (cytosol) is removed. 150ul membrane extraction buffer MEB was added to the pellet, first vortex the tube for 5 seconds and incubate tube at 4°C for 10 minutes with gentle mixing This dissolves all membranes with the exception of the nuclear membrane. Centrifugation (3000 × g for 5 min) pellets the nuclei, the supernatant contains extracts from the plasma membrane, mitochondria, and ER/Golgi membranes. 10% of the cytosol preparation and 20% of the membranes were analysed by western blotting using anti-RFP antibodies (1:1000) and secondary anti-rabbit IgG VHH single domain antibody (1:3000) as described below.

3.3.2 Co-Immunoprecipitation experiments

Plasmids (1.5µg) encoding M2-wt or M2 mutants were co-transfected with the plasmid (1.5µg) encoding human DHHC20 fused at its cytosolic C-terminus to a myc tag into 293T cells grown in 6-well plates. 24h after transfection cells were lysed with 250 µl NP40 lysis buffer (final concentration 0.5%) diluted in IP buffer (500 mM Tris-HCl, 20 mM EDTA, 30 mM sodium pyrophosphate decahydrate, 10 mM sodium fluoride, 1 mM sodium orthovanadate, 2 mM benzamidine, 1 mM PMSF, 1 mM NEM) with protein inhibitor for 1h on ice. Cell debris were removed by centrifugation for 10 min at 10000 rpm in a table top centrifuge. To determine the expression level (input control) 10% of the resulting supernatant was removed and subjected to western-blotting with either anti-M2 monoclonal antibody from mice (1:4000) or anti-myc-tag polyclonal antibody from rabbit (1:2000). 1µl of the M2 antibody (diluted in 200ul 3% BSA buffer) was added to the remaining supernatant and incubated for 1 hour at 4°C with shaking. Later 30 µl of protein-G Sepharose 4 Fast Flow (GE Healthcare, prepared according to manufacturer instructions) were added to the samples and incubated at 4°C with shaking overnight. Samples

were then centrifuged for 5 min at 5000 rpm and the supernatant was removed. After three times washing with IP buffer, the pellet was dissolved in 40 µl of 2X SDS-PAGE loading buffer and subjected to western-blotting, first with anti-myc-tag antibody and secondly with anti-M2 antibody using the appropriate secondary antibodies as described below. The relative amount of DHHC20-myc coprecipitated with the M2 antibodies was calculated using the band density of the DHHC20-myc band divided by the density of the M2 band visualized on the same membrane.

3.3.3 Acyl-Resin assisted capture (Acyl-RAC)

Protein S-acylation was analyzed by the Acyl-RAC assay (47). Transfected 293T cells were washed with PBS twice, and each well of the 6-well plate was lysed in 500µl buffer A (0.5%Triton-X100, 25 mM HEPES (pH 7.4), 25 mM NaCl, 1 mM EDTA, and protease inhibitor cocktail). Aliquots of the sample was used to check for total protein expression by western blotting. Disulfide bonds were reduced by adding Tris (2-carboxyethyl) phosphine (TCEP) to a final concentration of 20mM and incubated at RT for 1h. Free SH-groups were then blocked by adding methyl methanethiosulfonate (MMTS), dissolved in 100 mM HEPES, 1 mM EDTA, 87.5mM SDS to a final concentration of 1.5% (v/v) and incubated for 4 h at 40 °C. 3 volumes of ice-cold 100% acetone were added to the cell lysate and incubated at -20°C overnight. Precipitated proteins were pelleted at 5,000xg for 15 minutes at 4°C. Pelleted proteins were washed five times with 70% (v/v) acetone, air-dried, and then re-suspended in 1ml binding buffer (100 mM HEPES, 1 mM EDTA, 35mM SDS) with protein inhibitor. An aliquot, adjusted according to the expression level was removed and served as input. Another aliquot of the sample, also adjusted according to the expression level, was treated with hydroxylamine (0.5 M final concentration, added from a 2M hydroxylamine stock adjusted to pH 7.4) to cleave thioester bonds. The same volume of the sample was treated with 0.5M Tris-HCl (pH 7.4). 40µl Thiopropyl Agarose, which were washed twice in binding buffer in 1000rpm 10min before use was added at the same time to capture free SH-groups. Samples were incubated with beads overnight at room temperature on a rotating wheel. The beads were then washed 4 times in binding buffer and proteins were eluted from the beads with 2x reducing SDS-PAGE sample buffer for 10 minutes at 95°C. Samples were subjected to western blot as described below.

3.3.4 SDS-PAGE and Western blot

After sodium dodecyl sulphate-polyacrylamide gel electrophoresis (SDS-PAGE) in 12% gels, wet electroblotting (100V for 1h) was used to transfer proteins onto polyvinylidene difluoride (PVDF) membranes. After blocking (blocking solution: 5% skim milk powder in phosphate buffered saline (PBS) containing 0.1% Tween-20 (PBST)) for 1h at room temperature, membranes were incubated with the indicated primary antibody diluted in 3% BSA in PBST overnight at 4°C. The following commercial antibodies were used anti-M2 (1:1000), Purified Mouse Anti-Flotillin-2 (1:1000). Anti-RFP antibody (1:1000), anti myc-tag antibody (1:2000). Monoclonal anti-BHA from mouse (1:1000), Purified Mouse Anti-Flotillin-2(1:1000). Influenza A virus H1N1 HA antibody from rabbit (1:3000), Caveolin-1(N-20) antibody from rabbit (1:1000). After washing 3 times for 10min with PBST, membranes were incubated with horseradish peroxidase-coupled secondary antibody diluted in 3% BSA for 1 hour at room temperature. The following commercial secondary antibodies were used anti-rabbit IgG VHH Single Domain (1:3000 to 1:5000) and goat anti-mouse IgG (H + L), (1:1000 to 1:3000). After washing three times, signals were detected by chemiluminescence using the Pierce ECLplus reagent and SuperSignal West Dura extended Duration substrate with the Fusion SL camera system (Peqlab, Erlangen, Germany). The density of bands was quantified with Image J software as described in the figure legends.

3.3.5 Confocal microscopy

Co-localization of M2 with cis-Golgi marker GM130 in BHK21 cells were seeded at 50% confluency one day before transfection on glass coverslips in 24-well cell culture plates. Cells were transfected with 500ng plasmids encoding M2 (wt or mutants) using lipofectamine 3000 transfection reagent according to manufacturer´s instructions. 24h post transfection, cells were fixed with 4% paraformaldehyde (PFA) for 20min at room temperature, washed two times with PBS, permeabilized with Triton X-100 (0.1% in PBS) for 10 min and again washed twice with PBS. To coat non-specific protein binding sites, cells were incubated with 3% bovine serum albumin (BSA in PBS containing 0.1% Tween-20) for 1h at room temperature. BSA was removed and cells were incubated with the first antibody for 1h at room temperature, the anti-M2 antibodies (1:1000 dilution in 3%BSA) was used. After washing with PBS three times for 5 min, cells were incubated with fluorescent anti-mouse Alexa flour 488 from goat (1:1000). Cells were washed 3 times for 5 min with PBS and then incubated with anti-GM130 antibody (1:200) for one hour. Cells were then washed 3x for 5 min with PBS and then treated for 1hr protected from light at RT, cells were stained simultaneously with anti-rabbit Alexa 568 from goat (1:1000) for 1h at room temperature. Cells were washed 3 times for 5 min with PBS.

Co-localization of M2 with DHHC20

To detect DHHC20-myc and M2, 300 ng of each plasmid were co-transfected in BHK21 cells. M2 was visualized as described above. Then anti myc-tag rabbit antibody (1:1000) followed by anti-rabbit Alexa fluor 568 from goat antibody (1:1000) were used to detect DHHC20-myc location.

Cells were subsequently stained with DAPI (4',6-diamidino-2-phenylindole, 1:1000 dilution in BSA) for 10 min at RT to visualize nuclei. Cells were washed three times with PBS and coverslips were mounted on glass slides with ProLong Glass antifade mounting medium and allowed to cure in a dark place overnight.

Visualization of RFP

500ng plasmids encoding RFP (wt or fused to the amphiphilic helix of M2) were transfected into BHK21 cells. Cells were fixed and mounted on glass slides as described above.Cells were illuminated via laser lines at 405nm (DAPI), 488 nm (Alex Fluor 488) and 568 nm (Alexa Fluor 568 and RFP protein) and visualized with the VisiScope confocal FRAP System (VisiTron Systems GmbH), equipped with iXon Ultra 888 EMCCD camera using the 100X objective. The images were then processed using Fiji software. Co-localization of M2/M2 mutates with the cis-Golgi marker was quantified from at least 40 cells with the Pearson's correlation coefficient method using the JACoP plugin of the Fiji software.

3.3.6 Bioinformatic procedures

The helical wheel plots were made with Heliquest (https://heliquest.ipmc.cnrs.fr/) using the amphiphilic helix (residues 47 to 61) of the M2 sequence (ACF54600.1). Protein structures were analysed with PyMOL (Molecular Graphics System, Version 2.0 Schrödinger, LLC, https://pymol.org/2/).

3.4 Methods for the project: role of palmitoylation of the Hemagglutinin of Influenza B virus and identification of the enzymes involved

3.4.1 Transfection-mediated recovery of recombinant Influenza B virus

To generate recombinant Influenza B virus, the eight plasmids pHW-PB2, pHW-PB1, pHW-PA, pHW- HA, pHW-NP, pHW-Lee-NA, pHW-Lee-M, and pHW-Lee-NS (0.5 µg each) were transfected into a co-culture of 293T and MDCKII cells grown in 6-well plates using Lipofectamine 3000. After 5h, Opti-MEM medium was replaced by DMEM medium with 0.1% FBS and 0.5 µg/ml TPCK-trypsin and cells were incubated at 37°C. 72 h after transfection, the supernatant was collected, cell debris were removed by centrifugation (5000rpm, 10min) and the supernatant was kept frozen at -80°C before further usage. One aliquot (500µl, 25%) of this passage 1 (P1) virus was used to infect MDCKII cells in 6 well plates. After 1h the inoculum was removed, cells were washed twice with PBS before adding 2ml infection medium (DMEM with 0.1%FBS and 2 µg/mL TPCK-trypsin). The supernatant was collected after 48h. Another aliquot (200µl) of the P1 virus was injected into the allantois cavity of 9-day-old embryonated chicken eggs which were incubated at 33 °C for 72 hours before the allantois fluid was collected. The resulting P2 viruses from either eggs or MDCK II cells were further passaged using first T25 flasks (P3 virus) and then T75 flasks (P4 virus). TCID50 and HA-assay was used to quantify virus particles.

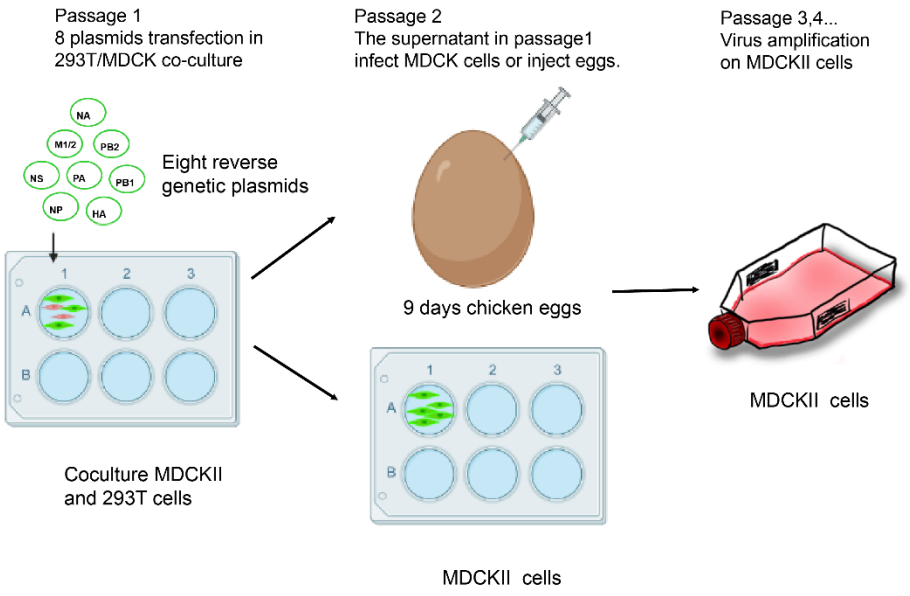

Figure 8. Transfection-mediated recovery of recombinant Influenza B virus

3.4.2 Immunofluorescence of transfected and infected cells to generate recombinant Flu B virus

48h post-transfection or infection, cells were fixed with 4% paraformaldehyde (PFA) for 20min at room temperature, washed two times with PBS, permeabilized with Triton X-100 (0.1% in PBS) for 10 min and again washed twice with PBS. Cells were stained with mouse monoclonal antibody against Influenza B virus HA at a dilution of 1:1000 for 1h. Cells were washed 3 times for 5 min with PBS and later covered with anti-mouse coupled to Alexa 488 fluorescent antibody (1:1000) for 1h. Cells were washed 3 times for 5 min with PBS. Cells were illuminated via laser lines at 488 nm (Alex Fluor 488) and visualized with ZEISS Colibri7, 20X objective was used.

3.4.3 RNA extraction and RNA reverse transcription

200µl cell culture supernatant or allantois fluid was used to extra the RNA using innuPREP Virus TS RNA Kit according to protocol 1 of the manufacturer's instructions. Reverse transcription was done with the high capacity cDNA reverse transcription kit with RNase Inhibitor. The reactions were prepared following the manufacturer's instructions to a total volume of 20µl.The following primers were used to amplify a part of the HA-encoding sequence of Flu B virus. BHA-F: CCAACGAAGGGATAATAAACAGTG, BHA-R: TAACGTTTCTTTGTAATGGTGACAAGC. The S7 Fusion polymerase was used in the PCR reaction and the reaction system was prepared according to the manufacturer's instructions. The PCR starts at 98°C for 10min and the following program was used for 35 cycles: 98°C for 30s, 55°C for 30 s, and 72°C for 30s, followed by one cycle at 72°C for 10 min. Later the amplified segments were sequenced and compared to the sequence of the wild type.

3.4.4 Surface trypsinization of cells TPCK-trypsin experiment

70%-80% confluent 293T cells in a 6 well plate were transfected with 3µg HA wt or HA Ac1+2 cloned into the PCAGGS plasmid using lipo3000 transfection reagent. After 48h, the medium was removed, the cells were gently washed twice by PBS and 1ml DMEM with 15µg/ml TPCK-trypsin (Sigma) was added to cover the cells. 1ml DMEM without trypsin was added to the control cells. Cells were then incubated at 37℃ for 30min, scraped from the plate, pelleted at 5000rpm for 5min, washed twice with lysed in 150µl NP40 lysis buffer (final concentration is 1% dilute with millipore water) with protease inhibitor. The Western blot experiment was used to detect the BHA transportation ability. Flotillin2 is the loading control.

3.4.5 Brefeldin A(BFA) experiment

MDCKII cells grown to 90% confluency in 6-well plates (Endo-H experiment) or in T25 flasks (acyl-RAC experiment) were infected with Influenza A or B virus at a MOI of 1. After 1h, the inoculum was removed and cells were washed twice with PBS and 1 ml DMEM with 2% FBS was added. After 2h, Brefeldin A was added to the medium from the stock solution (5 mg/ml) prepared in methanol to the final concentration of 3 µg/ml. Influenza A virus-infected cells were scraped from the plate after 12h and Influenza B virus-infected cells after 24h. Cells were pelleted at 5000rpm for 5min, washed twice with PBS and lysed with 200ul NP40 lysis buffer (final NP40 concentration is 1%) with protein inhibitor on ice for 1h. Insoluble material was pelleted at 10000rpm for 10min at 4°C. Aliquots of the samples were not digested or digested for 3h at 37°C with Endo H according to the manufacturer's instructions. For the acyl-RAC experiment, the sample from each T25 was lysed on ice for 2h with 1mL buffer A. 10µl 4XSDS-PAGE reducing loading buffer was added and samples heated at 95℃ for 10min prior to western blotting.

3.4.6 Screen the DHHCs candidate by infection of HAP-1 knockout cells

HAP-1 cells and HAP-1 knock-out cells were seeded in T75 flash to a confluency of 80%. Influenza B virus MOI=0.5 was used to infect the cells, after 1h, the viruses were removed and washed twice by PBS. And change to 10ml 2%FBS DMDM medium. After 24h, the cells were collected and centrifugated for 10 min at 5000 rpm to remove the supernatant. The sample from each T75 flash was lysed on ice for 2h with 2ml buffer A. The S-acylation level was measured using Acyl-RAC method.

3.4.7 SDS-PAGE and western blot

After sodium dodecyl sulfate-polyacrylamide gel electrophoresis (SDS-PAGE) using 12% polyacrylamide, wet electroblotting (100V for 1h) was used to transfer proteins onto polyvinylidene difluoride (PVDF) membranes (GE Healthcare). After blocking (blocking solution: 5% skim milk powder in PBS with 0.1% Tween-20 (PBST)) for 1h at room temperature, membranes were incubated with the primary antibody overnight at 4°C. After washing 3 times for 10min with PBST, membranes were incubated with horseradish peroxidase-coupled secondary antibody for one hour. After again washing three times, signals were detected by chemiluminescence using either the Pierce ECLplus reagent or for weak signals SuperSignal West Dura extended Duration substrate with the Fusion SL camera system (Peqlab, Erlangen, Germany). The density of bands

was analyzed with Image J software. Quantification and statistics are fully described in the figure legends.

The first antibodies were used at the following dilutions: monoclonal anti-HA of Flu B from mice: 1:1000, polyclonal antiserum against HA from Influenza A virus H1N1 from rabbit: 1:3000, Purified Anti-Flotillin-2 from mice: 1:1000. The horseradish peroxidase-conjugated secondary antibodies were used at the following dilutions: recombinant anti-rabbit IgG VHH Single Domain: 1:3000 -1:5000, anti-mouse IgG (H + L) from goat: 1:2000 -1:3000. The primary and secondary antibodies were diluted in PBS containing 3% BSA and 0.1% tween.

3.4.8 Confocal microscopy to co-localize DHHCs with the ER or with HA of Flu B

Colocalization with the ER

BHK 21 and A549 cells were seeded at 50% confluency one day before transfection on glass coverslips in 24-well cell culture plates. Cells were transfected with 500ng plasmids encoding mouse DHHC 1, 2, 3, 4 or 6 fused at the C-terminus to a HA-tag with using lipofectamine 3000 transfection reagent according to manufacturer instructions. 24h post-transfection, cells were fixed with 4% paraformaldehyde (PFA) for 20min at room temperature, washed twice with PBS, permeabilized with Triton X-100 (0.1% in PBS) for 10 min and again washed twice with PBS. To coat non-specific protein binding sites, cells were incubated with bovine serum albumin (BSA, 3% in PBST) for 1h at room temperature. BSA was removed and cells were incubated with the primary rabbit polyclonal antibody to HA tag (1:500 dilution in 3%BSA) for 1h at room temperature. After washing three times with PBS for 5 min, cells were incubated with anti-rabbit coupled to Alexa 488 fluorescent secondary antibody (1:1000) in the dark. Cells were washed 3 times for 5 min with PBS. The ER was stained with staining kit–Red Fluorescence Cytopainter at 1:1000 dilution (with 1X assay buffer from the kit) for 15 min at 37°C. Cells were washed 3 times for 5 min with PBS.

Colocalization with HA

BHK 21 cells were seeded at 50% confluency one day before transfection on glass coverslips in 24-well cell culture plates. Cells were co-transfected with 250ng the HA gene in pCAGGS and 250ng plasmids encoding mouse DHHC 1, 2, 4, and 6 fused with HA tag using lipofectamine 3000 transfection reagent according to manufacturer instructions. After 24 h cells were washed and fixed and then incubated with the rabbit polyclonal antibody to the HA-tag (1:500 dilution in 3%BSA) for 1h at room temperature and later with anti-rabbit coupled to Alexa 561 fluorescent secondary antibody (1:1000). HA was detected by the monoclonal antibody against Influenza B

virus HA (1:1000) and anti-mouse coupled to alexa 488 fluorescent secondary antibody (1:1000).

Cells were subsequently stained with Hoechst 33342 from the kit (1:2000 dilution in 1X assay buffer) for 10 min at room temperature to visualize nuclei. Cells were washed 3 times with PBS and coverslips were mounted on glass slides with ProLong Glass antifade mounting medium and allowed to cure in a dark place overnight.

Cells were illuminated via laser lines at 405nm (Hoechst 33342), 488 nm (Alex Fluor 488) and 561 nm (ER-staining and Alex Fluor 568) and visualized with the Leica Stellaris 8 FALCON Confocal Microscope (Leica) using the objective: HC PL APO 63x/1.40 OIL SC2. WD 0.14 mm. The images were then processed using Fiji software.

3.4.9 Predicted structures of DHHCs and of the C-terminus of HA using Alphafold2

The predicted structures of human DHHCs were downloaded from the alphafold protein structure database: https://alphafold.ebi.ac.uk/. The accession numbers are: DHHC 2: AF-Q9UIJ5-F1, DHHC 4: AF-Q9NPG8-F1, DHHC 6: AF-Q9H6R6-F1. Since no predicted structures of viral proteins are in this database, we used CoLabFold V1.5.2. to make our own prediction of the C-terminus of HA of Flu A and B:
(https://colab.research.google.com/github/sokrypton/ColabFold/blob/main/AlphaFold2.ipynb
The amino acid sequence used for the predictions are shown in the legend of S1 Fig.
Alphafold2 generates a PDB file and a confidence score, called the predicted local distance difference test (pLDDT), which indicates the confidence in the local structure prediction. The scale ranges from 0 to 100 and an IDDT value above 90 indicates very high accuracy, equivalent to structures determined by experiments, which allows for the investigation of details of individual side chains. A value from 70 to 90 indicates high accuracy, where the predictions of the protein's backbone are reliable. A value of 50 to 70 indicates lower accuracy, but the predictions of the individual secondary structural elements, α-helices and β-strands are probably correct, but how they are aligned in space is uncertain. Values below 50 might be an indication of an intrinsically unstructured region. The PDB files with the predicted structure contain this information in the B-factors, which can be highlighted in the 3D protein structure. Areas with high B-factors, which indicates high confidence, are colored red, while low B-factors are colored blue.
The figures were generated with PyMol (Molecular Graphics System, Version 2.0 Schrödinger, LLC, https://pymol.org/2/).

4. Results

4.1 The role of an amphiphilic helix and transmembrane region in the efficient acylation of M2 from Influenza A virus

4.1.1 The amphiphilic helix of M2 contains intrinsic signals for S-palmitoylation

A M2 monomer, which contains 97 amino acids is composed of a short, unglycosylated ectodomain, a single transmembrane domain (TM, aa 26-43) and a cytoplasmic tail that contains an amphiphilic helix (AH, aa47-61) and an intrinsically disordered region (62-80). M2 is a homo-tetramer, which is stabilized by formation of disulphide bonds between Cys17 and Cys19 in the ectodomain (Figure 9A).

Figure 10 B shows the NMR structure of the TM and AH domain integrated into a virtual lipid bilayer(62). The four helical TM run through the membrane at an angle and are slightly bent in the middle due to the presence of Gly34, and connected by a short 90° turn to the amphiphilic helix. The helix runs almost parallel to the membrane and contains the acylated Cys50 at the beginning of the hydrophobic face, so the fatty acid can insert into the lipid bilayer. The C-terminal parts of two TMs are connected by an ionic bond between Asp44 and Arg45 and two AHs by a hydrogen bond between Lys49 and Gly62 (Figure 9C). The AH contains many amino acids with distinctive side chains, such as Phe, Tyr, His, Arg, Lys, which are localized on its surface and could bind to a DHHC enzyme (Figure 9C, D). Note, however that the sequence of the AH is not conserved through all Influenza strains. The M2 protein we used contains two non-conservative (Phe54Arg, Glu56Arg) and one conservative amino acid exchange (His57Tyr, stained in cyan Figure 9B) relative to the M2 for which the NMR structure was determined (Figure 9E). It thus corresponds better to the consensus sequence calculated for all M2 proteins (Figure 9F).

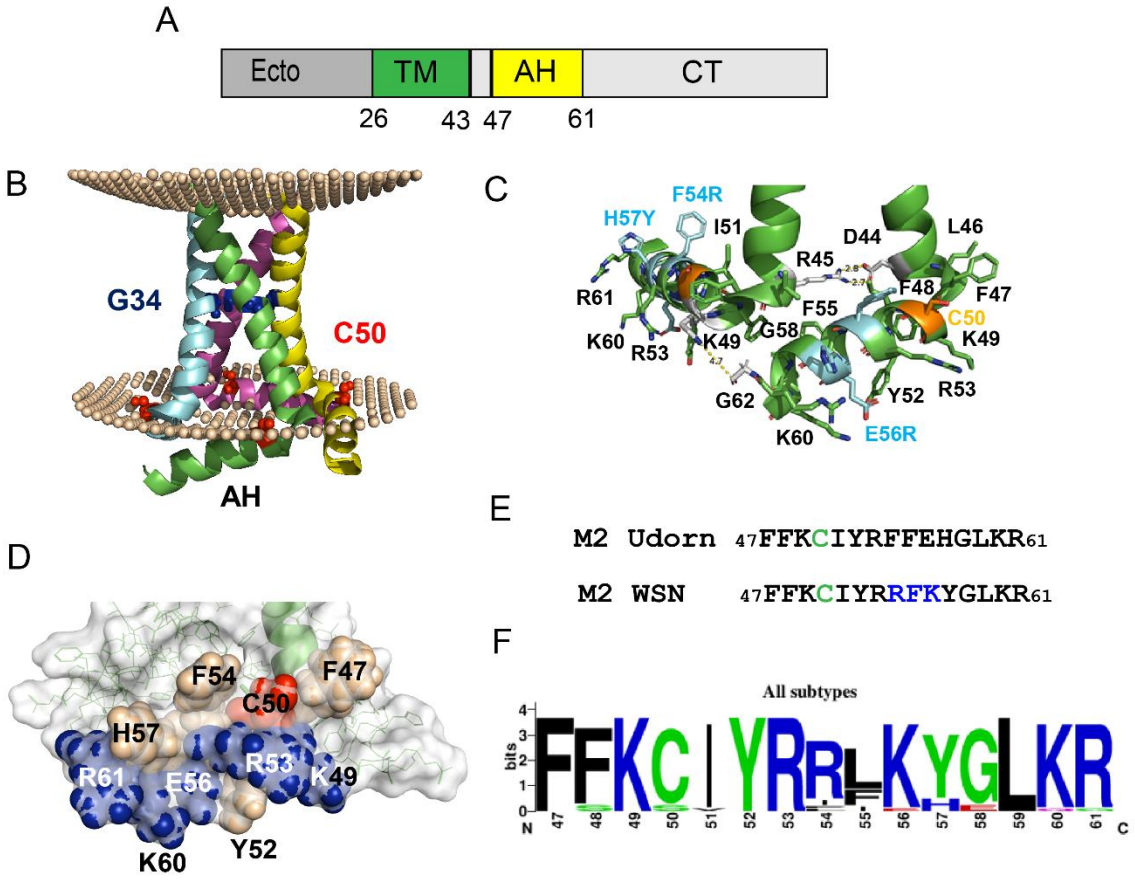

Figure 9. Primary and 3D structure of M2 of Influenza A virus

(A) Scheme of M2 of influenza A virus: Ectodomain (Ecto), transmembrane region (TM, aa 26-43), and cytoplasmic tai l(CT) an amphiphilic helix (AH, aa 47-61) exist at the beginning of the CT.

(B) NMR structure shows TM and AH of M2 embedded in a virtual lipid bilayer. G34(glycine) locates in the middle of the TM, forming a kink. C50 is the acylation site at the beginning of the AH.

(C) The side chains of the amino acids in AH. The three residues differ between the M2(NMR, the Udorn strain) and for M2(from the WSN strain) highlighted in cyan. Two monomers have hydrophilic interactions through D44 and R45, and K49 and G62.

(D) Surface representation in the tetramer of the AH domain. Aromatic amino acids in wheat, charged amino acids in blue, and acylated Cysteine 50 in red.

(E) Amino acid sequence of the AH in M2 used for structural analysis (upper row) and in this study (lower row).

(F) The Web-Logo shows the conserved and variable residues in the AH from M2 sequence of all the influenza A subtypes.

To investigate whether the helix of M2 becomes acylated in the absence of the TM, we fused its sequence, either corresponding to the wt helix or a Cys50Ser mutant, to the C-terminus of the red fluorescent protein (RFP). Confocal microscopy of transfected BHK21 cells revealed, that RFP, which has no intrinsic membrane targeting features, localizes to the cytosol and to the

nucleus. In contrast, RFP-AH and RFP-AH-C50S are excluded from the nucleus and redistributed to intracellular compartments, especially to a perinuclear region, which is partially stained by antibodies against GM130, a component of the cis-Golgi, an intracellular site where DHHC20 (in addition to the ER) is located(75) (Figure 10A). We then performed a membrane fractionation assay to analyze the distribution of the proteins between cytosol and membranes. As expected, RFP is present only in the cytosolic fraction, whereas RFP-AH and also RFP-AH-C50S are also membrane bound, ~30% of total RFP-AH is in the membrane fraction (Figure 10 B). Thus, the amphiphilic helix of M2 has the capacity to interact with cellular membranes, even in the absence of the acylation site. However, quantification of three independent experiments revealed that membrane binding of RFP-AH-C50S is 35% reduced relative to RFP-AH (Figure 10 C).

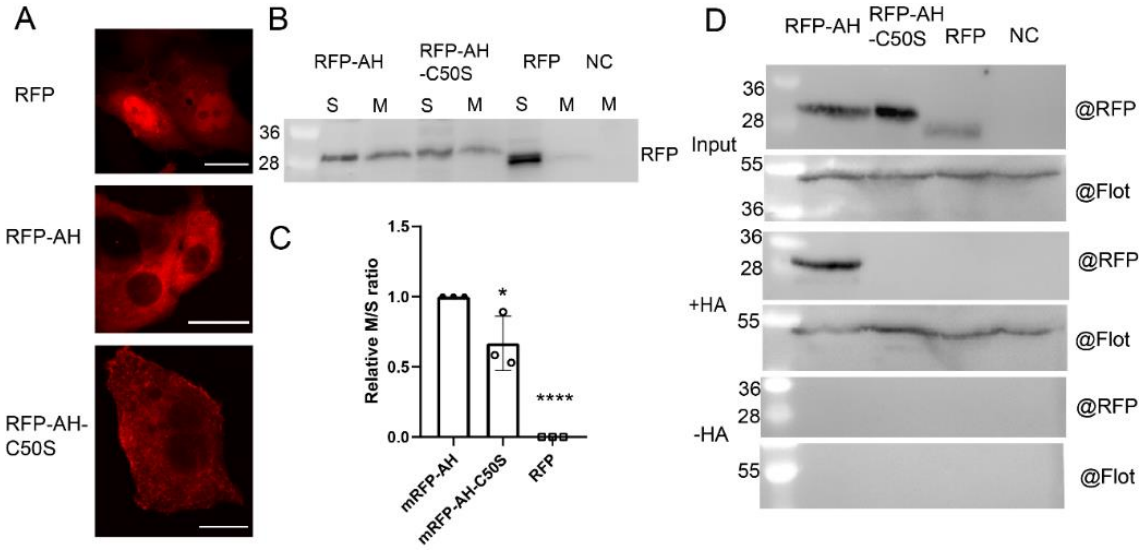

Figure 10. Membrane localization and acylation of the amphiphilic helix of M2 fused to RFP

(A) Immunofluorescence shows the location in BHK21 cells of RFP, RFH-AH, and RFP-AH-C50S. The scale bar is 20 µm.

(B) Membrane separation experiment results show the membrane ability of RFP, RFH-AH, and RFP-AH-C50S in 293T cells. The proteins were detected using anti-RFP antibodies. Soluble proteins (S), and membranous proteins(M).

(C) Quantification of this and two other independent experiments. The ratio of the density of the M and S bands was calculated, normalized to RFP-AH (=1). The mean ± SD are shown. One-way ANOVA followed by multiple comparison Dunnett test was applied for statistical analysis. *: $P < 0.05$, ****:$P < 0.0001$ versus RFP-AH.

(D) S-acylation of RFP, RFH-AH, RFP-AH-C50S. The S-acylation level was measure using Acyl-RAC method. RFP was detected using antibody against RFP and flotillin-2 as the loading control.

To test whether RFP-AH becomes acylated, we used the Acyl-RAC (resin-assisted capture) assay, which exploits thiol-reactive resins to capture SH-groups in proteins. 24 hours after transfection, cells were lysed and 10% of the total extract (TE) was removed from the lysate to determine the expression levels. Disulphide bonds in proteins present in the remaining part were reduced and newly exposed -SH groups were blocked. The sample was then equally split: one aliquot was treated with hydroxylamine (+HA) to cleave thioester bonds, and the other aliquot was treated as control with Tris-HCl buffer (-HA). After pull-down of proteins with the thiol-reactive resin, samples were subjected to western blotting using antibodies against the RFP. To exclude that proteins were lost during sample preparation, we used antibodies against the cellular palmitoylated protein flotillin 2 as an internal control. The results clearly show that RFP-AH is acylated, since it is precipitated by the thiol-reactive beads, which is not the case for RFP and RFP-AH-C50S (Figure 10D).

4.1.2 Mutations in the helix reduce but do not abolish palmitoylation of M2

To investigated which features of the helix are essential for acylation of M2, we used the authentic M2 protein, which is targeted to the ER by its TM region and then transported through the exocytic pathway to the plasma membrane such that all molecules have access to DHHC enzymes(117) (118). We exchanged amino acids exposed at the molecule´s surface, that alter the charge of the helix and/or its biophysical properties, such as hydrophobicity and hydrophobic moment. In M2 AH-1 the positively charged Lys49, Arg53 and Arg56 exposed at the frontside of the AH were exchanged by negatively charged Glu (Figure 11A). The localization of mutated amino acids in a surface representation of M2 shown in Figure 12.

These substitutions do not greatly alter the hydrophobicity and the hydrophobic moment of the helix as calculated by the tool heliquest, but they eliminate its positive net charge (Figure 11B). In M2-AH-2, two long hydrophobic residues (Tyr52, Leu59) located at the back bottom of the AH were replaced by less hydrophobic Alanine residues. In M2-AH-3, Phe47, which forms a distinct protrusion at the beginning of the helix near the acylated cysteine, has been replaced by Alanine. The helices of M2-AH-2 and M2-AH-3 are less hydrophobic, but still exhibit an amphiphilic character. M2-AH-4 contains three positively charged lysine instead of three hydrophobic residues (Phe48, Ile51, Phe55), located at the back bottom of the helix. In AH-5, four positively charged residues (Lys49, Arg53, Lys60, Arg61), which are exposed at the frontside of the AH, were replaced by Phe. The mutations in M2-AH-4 and M2-AH-5 essentially destroyed the amphiphilic character of the helix. AH-4 is hydrophilic and AH-5 is more hydrophobic compared to the wt-helix.

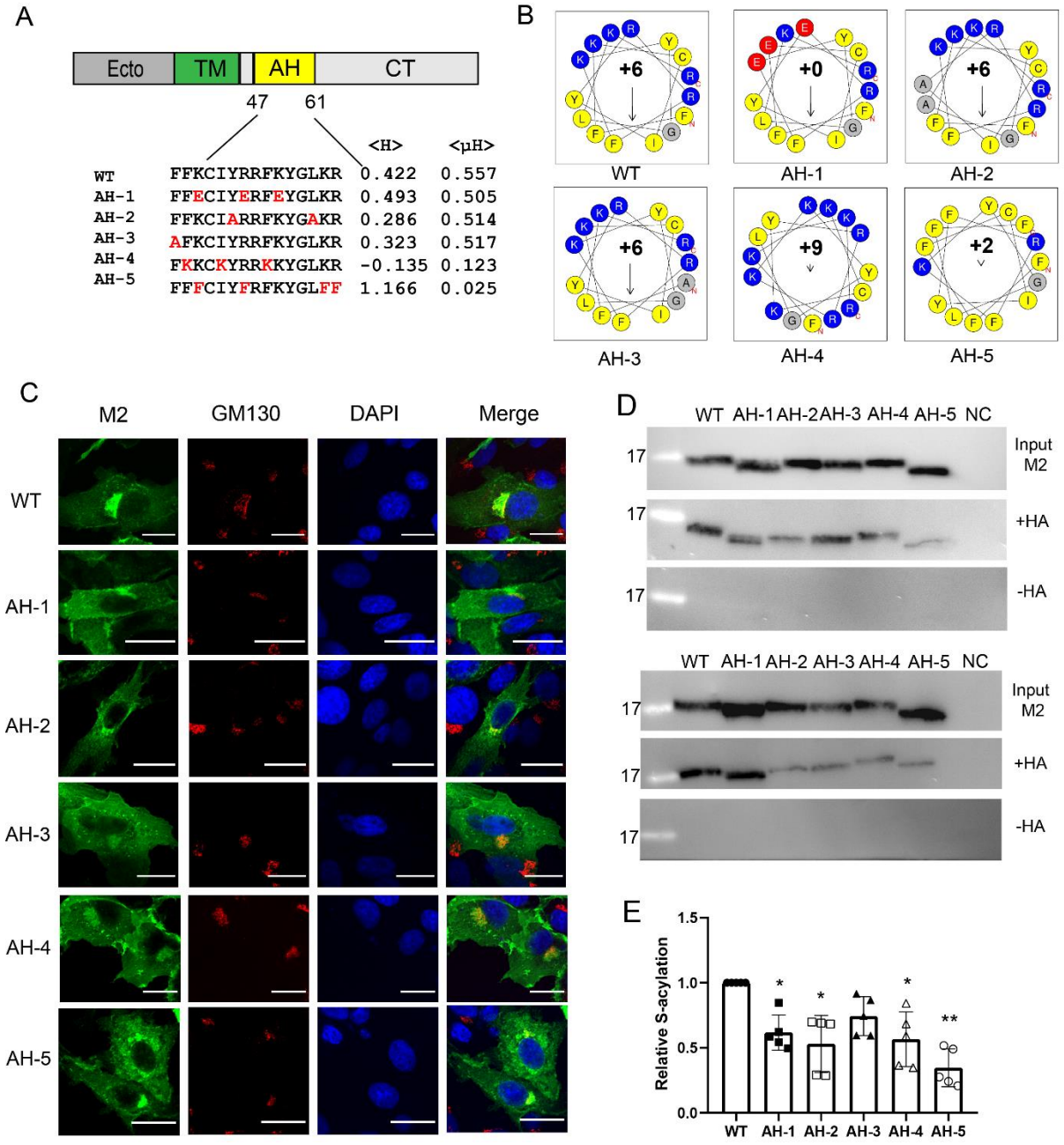

Figure 11. Palmitoylation and intracellular localization of M2 with mutations in the amphiphilic helix that affect its biophysical properties

(A) Scheme of M2 and the mutations inserted in AH of M2 (mutated amino acids are in red). The hydrophobic moment <μH> and hydrophobicity <H> of the AH were calculated using Heliquest (https://heliquest.ipmc.cnrs.fr/).

(B) Helical wheel plots of the AH of M2 and the M2-AH mutants. Positive amino acids(blue), negative amino acids (red), and hydrophobic amino acids (yellow) are shown. The arrow points to the hydrophobic face of AH. The length of the arrow corresponds to the < μH>. The numbers indicate the net charge of the helix.

(C) Immunofluorescence shows M2/M2 mutates the location and colocalization with Golgi. M2 and M2 mutates were transfected in BHK21 cells. Cells were permeabilized and stained with antibodies against M2(green), the cis-Golgi marker GM130 (red) and with DAPI (blue) to highlight the nucleus. The scale bar is 20 µm.

(D) S-acylation level of M2 wt and the mutants. M2 and M2 mutants were expressed in 293T cells. For the input samples different volume of the lysate was removed to adjust to a similar level. The remainder was divided into two aliquots that were adjusted to the same extent. One aliquot was not treated (−HA) and one treated with hydroxylamine (+HA) to cleave cysteine-bound fatty acids before pulling down proteins with a free SH group. Samples were subjected to Western blotting with antibodies against M2. The results of two independent experiments are shown.

(E) Quantification of these two and two other Acyl-RAC assays. The density of the bands with hydroxylamine (+HA) bands was divided by the density of the input bands and normalized to M2 wild type (=1)). The mean ± SD are shown. One-way ANOVA followed by multiple comparison Dunnett test was applied for statistical analysis. *, $P < 0.05$, **, $P < 0.01$ versus wild type.

The resulting mutants were expressed in 293T cells, which were analysed by western blotting with M2 antibodies. The signals of M2-AH-1, M2-AH-3 and M2-AH-5 are substantially reduced compared to those of M2 wt and the other mutants. We were concerned that the mutations would lead to misfolding and subsequent degradation of M2 by the cell's quality control system, which would manifest as blockage of transport out of the ER. Confocal microscopy revealed for M2 wt and all mutants reticular staining in the cytosol, likely representing the ER, transport to the plasma membrane and especially bright perinuclear staining, which overlaps with the cis-Golgi marker GM 130 (Figure 11C). Thus, the M2 mutant proteins expressed are localized to the same compartments as M2 wt. Calculation of the Pearson’s correlation coefficient revealed that four M2 mutants co-localize to the same extent as M2 wt with the marker GM130. Only transport of M2-AH-4 to the cis-Golgi was slightly reduced (Figure 16A). Therefore, the mutations are unlikely to cause misfolding of M2 and a defect in its transport to the intracellular acylation site.

However, to compare the acylation of the M2-AH mutants, we had to adjust the amount of cell lysate used as input and accordingly the amount incubated with the thiol-reactive beads to account for the different expression levels. This prevented us from using flotillin as internal acylation control. Instead, we performed each Acyl-RAC assay four times to compensate for random loss of protein during sample preparation. Two of the results are shown in Figure 11D to demonstrate the variability between experiments. The quantification of the five experiments (ratio of hydroxylamine-treated to input M2 normalized to M2 wt) is shown in Figure 11E. Each mutation reduced acylation of M2 in each experiment. The reduction was greatest in M2-AH5 (reduced to 30% relative to M2 wt), followed by M2-AH-2 (50%), M2-AH-4 (54%) M2-AH-1 (62%) and least in AH-3 (75%). Although the differences between the experiments are relatively large,

the mean values for most mutants (with the exception of M2 AH-3) were statistically significantly different from those for M2 wt.

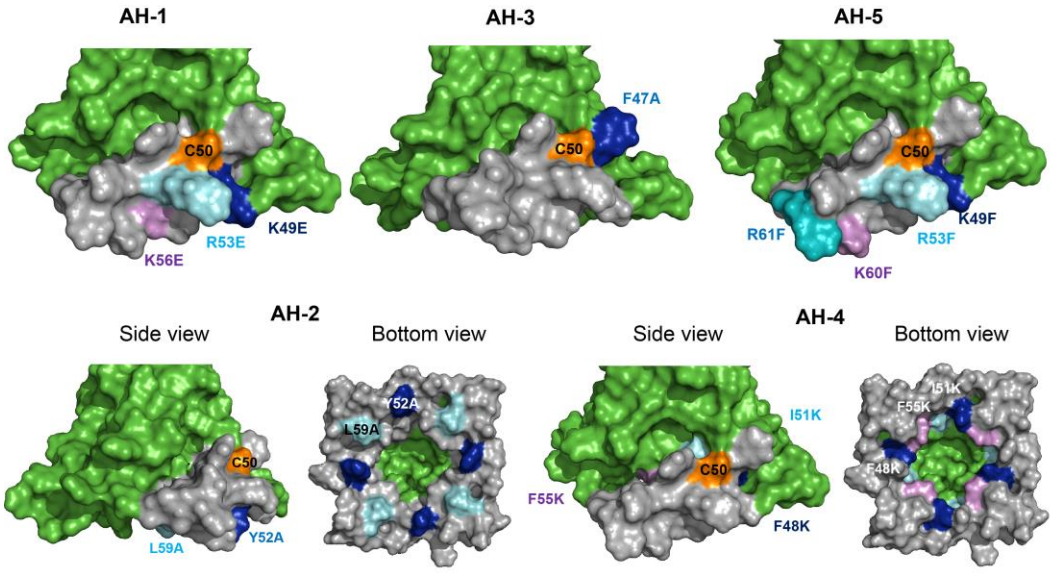

Figure 12. Location of the amino acids exchanged in the amphiphilic helix of M2

Surface representation of the NMR structure of the M2 tetramer. Amino acids of one amphiphilic helix are in grey, the acylation site in orange and the amino acids exchanged in AH-1, AH-2, AH-3, AH-4 and AH-5 are in dark or light blue or in magenta.

4.1.3 Truncation and destruction of the helix reduces, but does not abolish palmitoylation of M2

We investigated next whether a helical structure downstream of Cys50 is required for the basal acylation of M2. We created two mutants where the cytoplasmic tail of M2 including most parts of the helix were deleted. Mutant M2 1-50 retains the first four helical residues including Cys50, M2 1-53 contains three additional residues downstream of the acylation site (Figure 13A). M2 1-53 and especially of M2 1-50 are expressed at lower levels than M2 wt. However, confocal microscopy revealed for both mutants the staining pattern typical for M2, including strong perinuclear staining. M2 1-50 even showed slightly enhanced co-localization with the cis-Golgi marker compared to M2 wt and M2 1-53 (Figure 13B, 16C). The Acyl-RAC assay showed that the acylation of the mutants is greatly reduced but still clearly detectable (Figure 13C). Quantification of four experiments showed a statistically significant reduction of about 45% for M2 1-50 and 40% for M2 1-53, but with relatively large variation between experiments (Figure 13D).

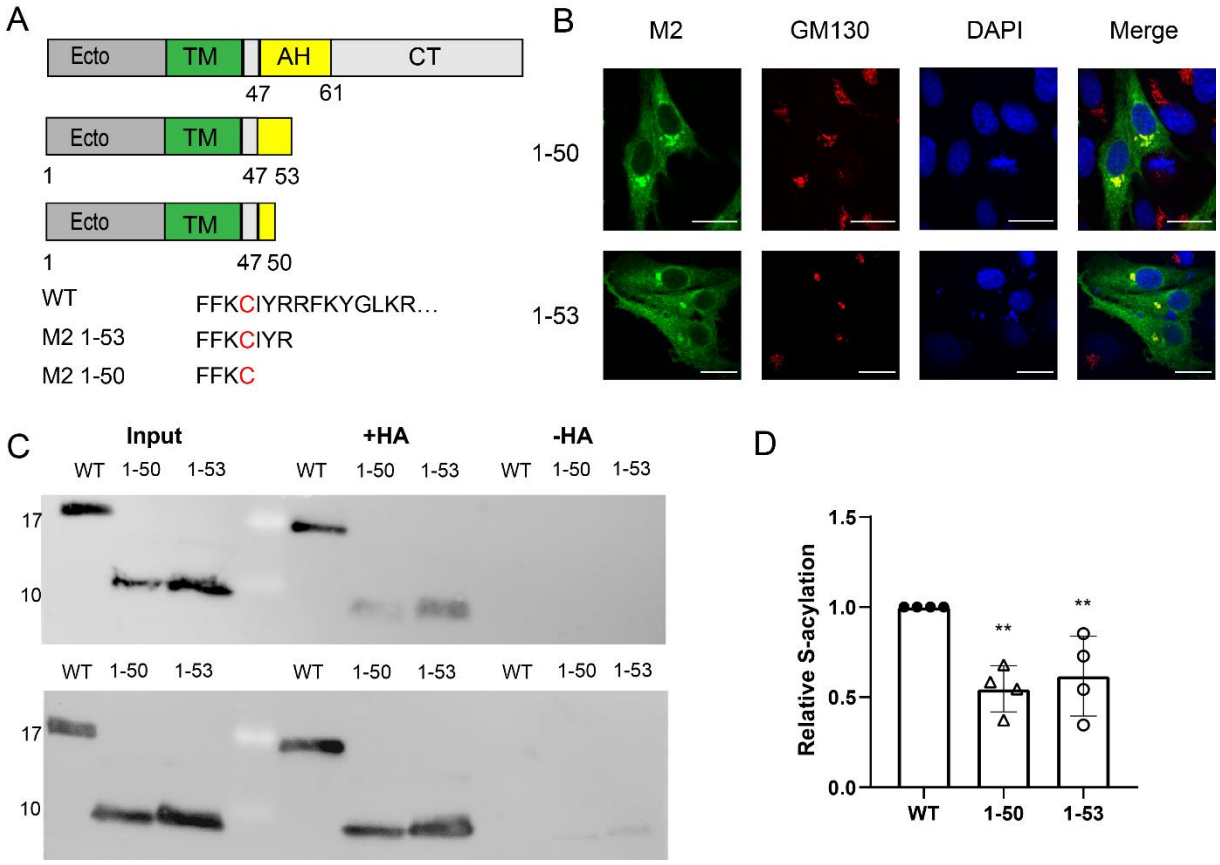

Figure 13. Palmitoylation and intracellular localization of M2 truncated mutants

(A) Scheme and sequence of M2 and truncated mutants.

(B) Confocal microscopy of mutants in transfected BHK21 cells. Cells were permeabilized and stained with antibodies against M2(green), the cis-Golgi marker GM130 (red) and with DAPI (blue) to highlight the nucleus. The scale bar is 20 µm.

(C) S-acylation: M2 wt and the mutants were expressed in 293T cells. For the input samples, different volume of the lysate was removed to adjust for the reduced expression level of some mutants. The remainder was used to measure the S-acylation level. Samples were subjected to Western blotting with antibodies against M2. The results of two independent experiments are shown.

(D) Quantification of these two and two other independent experiments. The mean ± SD and the results from four independent experiments are shown. One-way ANOVA followed by multiple comparison Dunnett test was applied for statistical analysis. **, $P < 0.01$ versus wild type.

Two further mutants were made inserting helix-destroying proline residues. In the M2-1P mutant, Ile 51 next to the acylated cysteine was replaced by a proline. The M2-3P mutant contains three prolines to replace Tyr52, Arg53 and Arg54 (Figure 14A). M2-1P expressed at a lower level, but it co-localizes with the cis-Golgi marker to the same extent as M2-3P and M2-wt (Figure 14B, 16B). The acylation level of the mutant M2-1P is greatly reduced to 30% compared to M2 wt.

The effect of the insertion of three Prolines is less obvious. The mean value of acylation from four individual experiments is 82%, but the results are not statistically significantly different from M2 wt (Figure 14C and D). These results confirm that an amphiphilic helix is essential for efficient acylation of M2, but that a basal level of acylation is maintained even in the absence of a helical structure downstream of the acylation site. This suggests that amino acids in the transmembrane region of M2 might also affect the acylation.

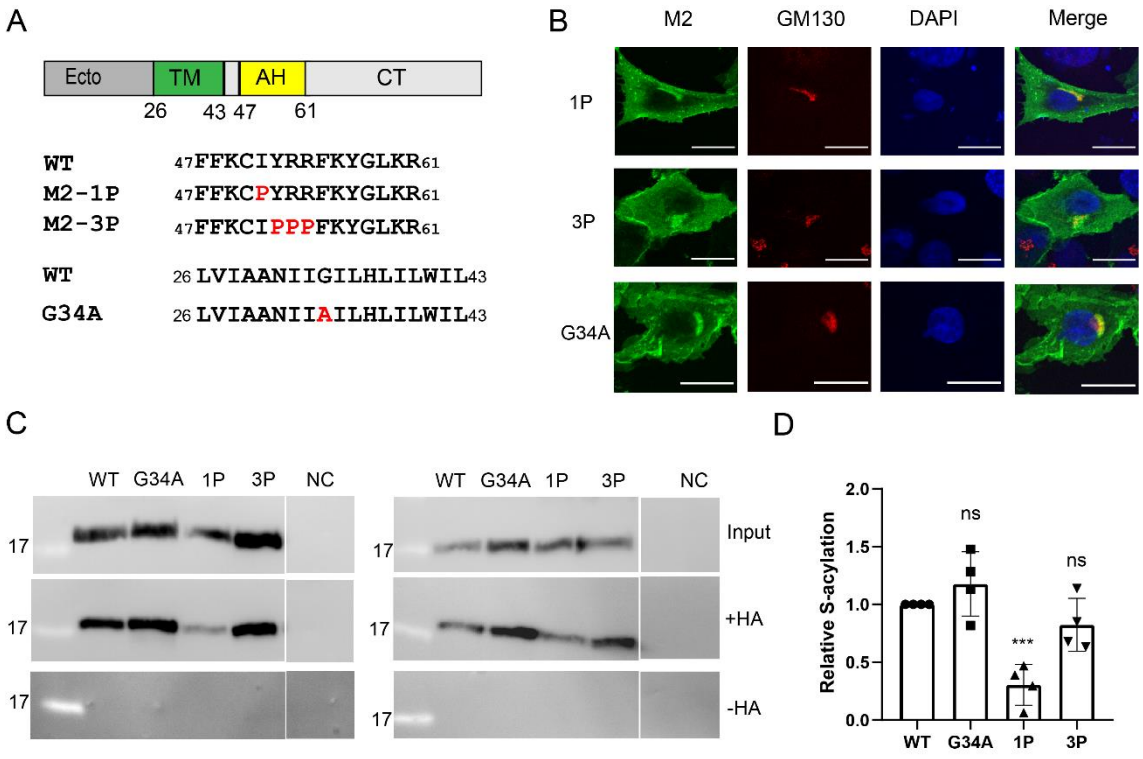

Figure 14. Palmitoylation and intracellular localization of M2 mutants with disrupted amphiphilic helix and replacement of a glycine in the transmembrane region

(A) Scheme and sequence of M2, wild type and mutants with one or three Prolines inserted into the helix and with the Gly34Ala exchange in the TM.

(B) Confocal microscopy of mutants in transfected BHK 21 cells. Cells were permeabilized and stained with antibodies against the cis-Golgi marker GM130 (red) and with DAPI (blue) to highlight the nucleus. The scale bar is 20 µm.

(C) S-acylation: M2 wt and the mutants were expressed in 293T cells. For the input samples, different volume of the lysate was removed to adjust for the reduced expression level of some mutants. The remainder was used to measure the S-acylation level. Samples were subjected to Western blotting with antibodies against M2. The results of two independent experiments are shown.

(D) Quantification of 5C and two other independent experiments. The mean ± SD and the results from four independent experiments are shown. One-way ANOVA followed by multiple comparison Dunnett test was applied for statistical analysis. ns, not significant, ***, $P < 0.001$ versus wild type.

4.1.4 Replacement of kink-inducing glycine in the transmembrane helix increases palmitoylation of M2

The transmembrane region of M2 (sequence LVIAANIIGILHLILWIL) contains many of the hydrophobic amino acids commonly found in such a region, which are unlikely to be a specific recognition feature for a DHHC enzyme. Two particular and conserved residues are His37 and Trp41 but their side chains are pointing into the pore formed by tetrameric transmembrane region, and they are known to be essential for proton transport. One peculiar feature of the transmembrane region is a highly conserved Glycine in its middle that causes a slight kink in the helix.

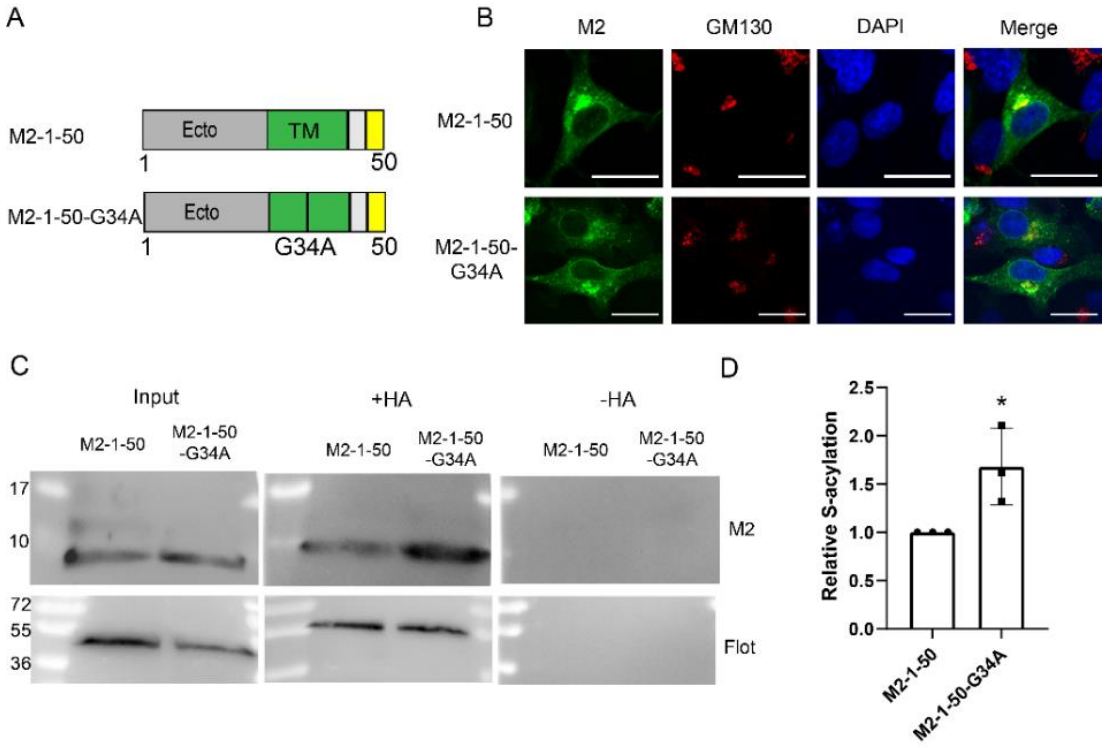

Figure 15. Palmitoylation and intracellular localization of M2 mutants with truncated amphiphilic helix and replacement of a glycine in the transmembrane region

(A) Scheme and sequence of M2 1-50, wild type and mutants with the Gly34Ala exchange in the TM.

(B) Confocal microscopy of mutants in transfected BHK21 cells. Cells were permeabilized and stained with antibodies against the cis-Golgi marker GM130 (red) and with DAPI (blue) to highlight the nucleus. The scale bar is 20 µm.

(C) S-acylation: M2 1-50 and M2 1-50-G34A were expressed in 293T cells. For the input samples, same volume of the lysate was removed to detect expression level. The remainder was used to measure the S-acylation level. Samples were subjected to Western blotting with antibodies against M2 and, subsequently against flotillin-2, an endogenous acylated protein.

(D) Quantification of 6C and two other independent experiments. The mean ± SD and the results from three independent experiments are shown. Unpaired t-test was applied for statistical analysis. *, $P < 0.05$, versus M2-1-50.

We changed the helix-disfavouring Glycine to an Alanine, a common amino acid in helical transmembrane regions. The resulting mutant M2-G34A is expressed at a higher level as M2 wt and shows the same intracellular staining pattern in confocal microscopy (Figure 14B, 16D). Quantification of four Acyl-RAC assays indicates that the acylation level of M2-G34A might be slightly higher than that of M2-wt (118%), but the difference was not statistically significant (Figure 14C, D). We suspected that the relevance of the transmembrane region on acylation would become more pronounced if we minimize the influence of the helix. Thus, we introduced the G34A mutation into the truncated mutant M2 1-50 (Figure 15A). Both proteins are expressed at the same level and show a similar intracellular staining pattern in confocal micrographs (Figure 16D) but the Acyl-RAC assay revealed a 50% increase in acylation (Figure 15C and D).

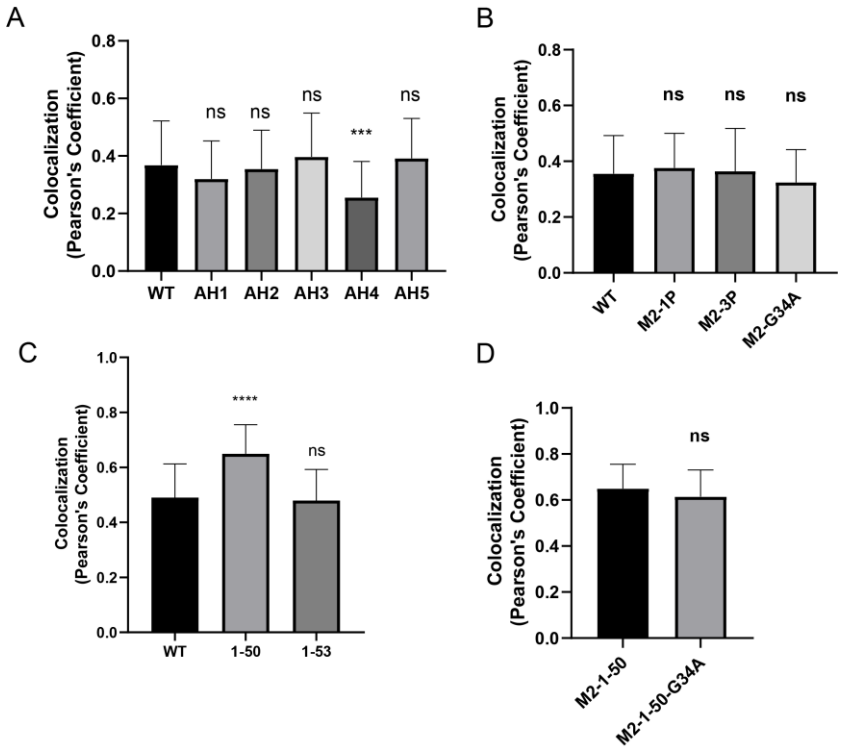

Figure 16. The quantification of the IF experiments

(A). The quantification of the colocalization of Figure 11C

(B). The quantification of the colocalization of Figure 13B

(C). The quantification of the colocalization of Figure 13B

(D). The quantification of the colocalization of Figure 14B

4.1.5 Mutations in the helix of M2 do not prevent binding to DHHC20

M2 wt substantially overlaps with DHHC20 in co-transfected BHK21 cells revealing mainly a reticular ER-like and perinuclear staining pattern (Figure 17). Some substrates can be co-immunoprecipitated with their cognate DHHC indicating a long-term, stable interaction during the enzymatic reaction(119, 120).

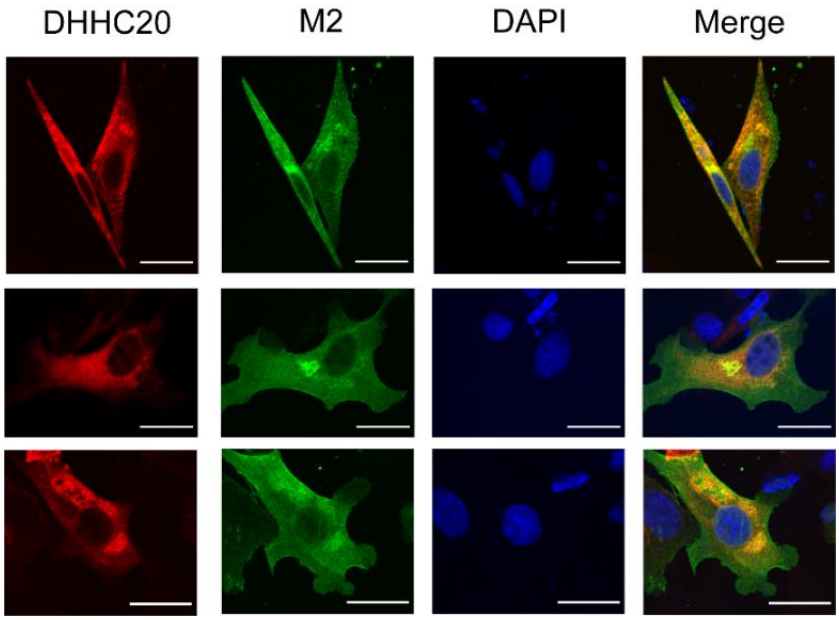

Figure 17. Colocalization of DHHC20 with M2

M2 wt and DHHC20-myc were co-expressed in BHK21 cells, which were fixed, permeabilized and stained with anti-myc and anti-M2 antibodies. The scale bar is 20 µm.

We asked whether this also applies for the M2-DHHC20 complex and how the most severe helix mutations, M2-1P, M2-3P, M2-AH4 and M2-AH5 affect this interaction. Since the specificity of most commercially available antibodies against DHHCs have not been validated, we used a plasmid encoding human DHHC20 fused at its C-terminus to a myc-tag. DHHC20-myc and M2 were co-expressed in 293T cells, and co-ip was used to detect the interaction. Roughly 1% of total DHHC20-myc was co-precipitated with M2-wt and the M2 mutants also interact with DHHC20-myc (Figure 18A). The experiments were performed three times and the ratio of co-precipitated DHHC20-myc and M2 were calculated and normalized to the values of M2-wt (Figure 18B). The results show that the introduction of helix-breaking proline residues does not

affect the interaction with DHHC20-myc, but AH-4 and AH-5 have a clear but opposite effect on DHHC20 binding. It is reduced to ~20% for M2-AH-5, but increased around 2fold for M2-AH-4.

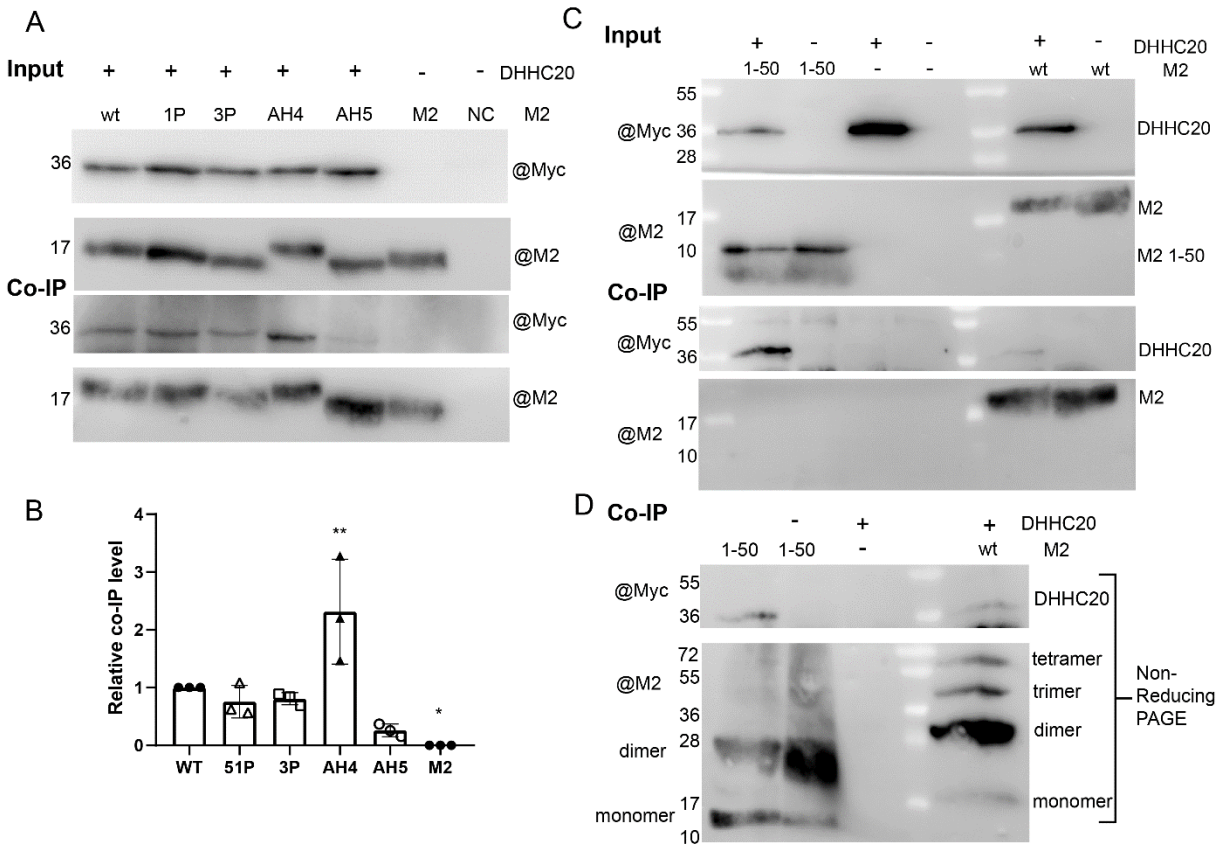

Figure 18. Co-precipitation of DHHC20 with M2 wt and M2 mutants with reduced acylation

(A) Input: DHHC20-myc and M2, either wild type and the indicated mutants were expressed in 293T cells. Cells were lysed with non-denaturating detergent, different volumes of the lysate were removed to adjust for the reduced expression level and samples were subjected to reducing SDS-PAGE and blotting with anti-myc and anti M2 antibodies. Co-IP: The remainder of the lysate was divided into two aliquots that were adjusted to the same extent. Samples were then subjected to immunoprecipitation with M2 antibodies and to reducing SDS-PAGE and blotting with anti-myc and anti-M2 antibodies.

(B) Quantification of this and two other independent experiments. One-way ANOVA was applied for statistical analysis. ns, not significant, *P < 0.05, **P < 0.01 versus wild type.

(C) DHHC20-myc and M2 wild type and M2 1-50 were expressed in 293T cells. Cells were lysed with non-denaturating detergent, different volumes of the lysate were removed to adjust for the reduced expression level of M2 1-50 and samples were subjected to reducing SDS-PAGE and blotting with anti-myc and anti M2 antibodies. Co-IP: The remainder of the lysate was divided into two aliquots that were adjusted to the same extent. Samples were then subjected to immunoprecipitation with M2 antibodies and to reducing SDS-PAGE and blotting with anti-myc and anti-M2 antibodies.

(D) Co-IP from C subjected to non-reducing SDS-PAGE.

Finally, we analyzed the truncated M2 mutant 1-50 for binding to DHHC20-myc. Blotting the M2 antibody precipitate with myc antibodies shows the DHHC20-myc band, even stronger than the DHHC20-myc band obtained after co-expression with M2 wt. Surprisingly, no M2 1-50 was detected, (after longer exposure very little was found), when probing the same membrane with M2 antibodies, although both M2 wt and M2 1-50 are detected at similar levels in the input (Figure 18C). However, when the M2 antibody precipitate was subjected to non-reducing SDS-PAGE, M2 1-50 can be clearly detected, mainly as a disulphide-linked dimer. M2 wt also appears mainly as a dimer, but also forms some disulphide-linked trimers and tetramers, as already described (37). The DHHC20-myc band is also present in samples separated by non-reducing SDS-PAGE, and to a slightly higher extent if co-expressed with M2 1-50 (Figure 18D). It thus appears that M2 1-50 forms unusual large aggregates during immunoprecipitation that fail to penetrate the gel under reducing conditions. Nevertheless, M2 1-50, which basically consists of one transmembrane region binds to DHHC20 inside cells. The experimental results are summarized in table 1. We conclude that the reduced acylation of most M2 mutants is not due to reduced binding to the enzyme. Rather, it is more likely that the subsequent step, the transfer of the fatty acid to M2, is impaired.

4.1.6 Molecular modelling of the M2 DHHC 20 interaction

To identify the contact surface between M2 and DHHC20 we cooperated with the group of Cecilia Clementi (Theoretical and Computational Biophysics, Department of Physics, Free University Berlin). Clark Templeton performed a molecular dynamics simulations of a complex between M2 and the enzyme DHHC20. A snapshot of the simulation of the complex is shown as a surface representation in Figure 19A. The figure shows that the amphiphilic helix of M2 docks to a 25Å wide cavity in the cytoplasmic domain of DHHC20 close to its transmembrane region. Contact analysis shows that the proteins form 18 interactions involving 13 residues in DHHC20 and 12 residues in M2. These interactions can be broken into interactions residing in the transmembrane and amphiphilic sections of M2. In the transmembrane helix four residues of M2 interact with four residues located on the outside of TM1 of DHHC20. Ile39 of M2 also interacts with Trp158, which is located near the hydrophobic tunnel and is supposed to act as a gate (Figure 19B) (121).

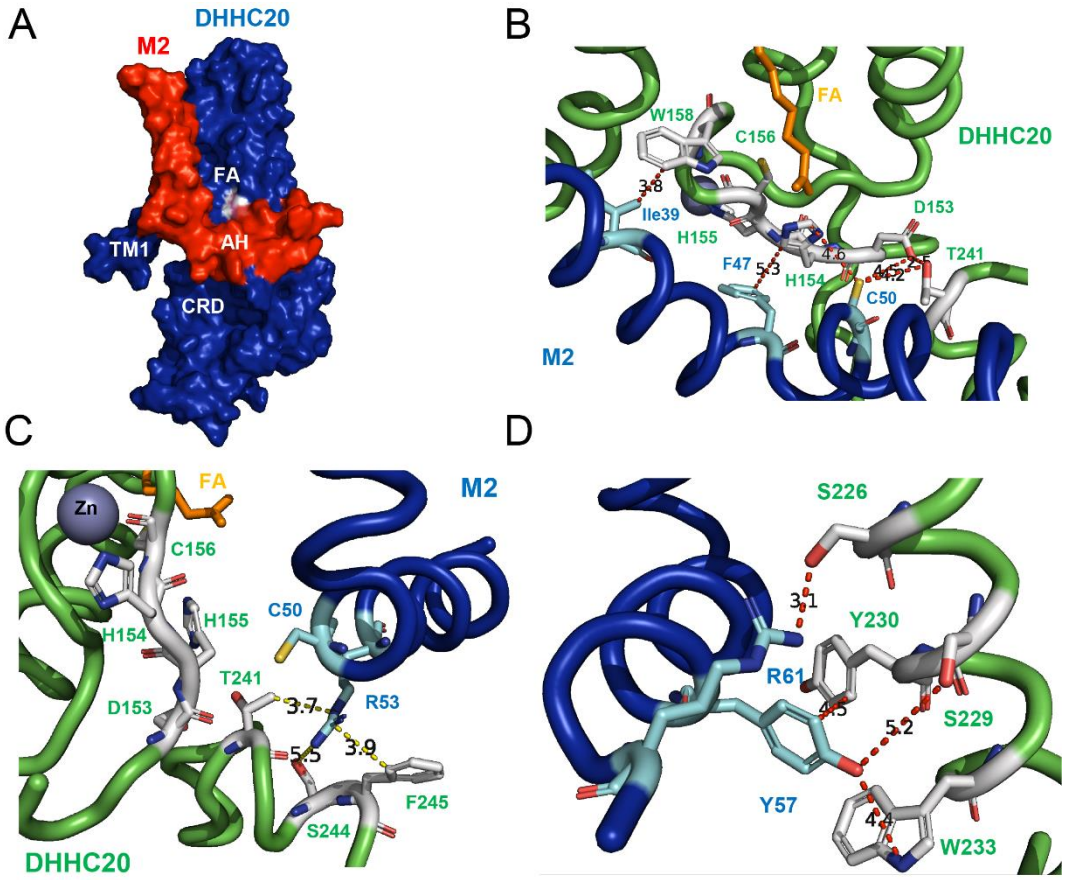

Figure 19. Molecular dynamics simulation of the M2 DHHC20 complex

(A) Surface representation: M2 in red, AH: amphiphilic helix. DHHC20 in blue. CRD: cysteine-rich domain in the cytoplasmic domain. TM1, TM4: transmembrane region 1 and 4.

(B, C, D) Residues in the amphiphilic helix of M2 (blue) that contact residue in DHHC20 (green) important for catalysis. Residues in M2 are highlighted as cyan sticks and in DHHC as white sticks. The distance is indicated in angstroms. Orange stick: Fatty acid. Zn: Zinc ion. One snapshot of the MD simulation is shown. The MD simulation experiments was done by Clark Templeton in the group of Cecilia Clementi (Theoretical and Computational Biophysics, Free University Berlin). My supervisor Michael Veit made this figure. Permission got from both of them to better explain this project.

The other residues in M2 contacting DHHC20 are located in its amphiphilic helix. Interestingly, the 153DHHC156 motif of DHHC20 has contact to several M2 residues: Cys50 of M2 contacts DHHC residue Asp 153 & His154 and M2 Phe47 with DHHC His 154 & His155 (Figure 19B). Likewise, Thr241 in the conserved 240TTXE243 motif is in contact with both Cys50 and Arg53 (Figure 19C). The C-terminal part of the helix wraps around TM4 of DHHC20 where Tyr57 is contacts Ser229, Tyr 230 and Trp 233 (Figure 19D).

4.2 Role of palmitoylation of the Hemagglutinin of Influenza B virus and identification of the enzymes involved

4.2.1 Palmitoylation of HA is essential for replication of Influenza B virus

Two acylated Cysteines were replaced in the cytoplasmic tail of HA of the Influenza B virus (Lee40 strain) by Serine, either separately (Ac1 and Ac2) or together (Ac1+2, Figure 20A). The mutant HA plasmid, together with seven additional plasmids encoding the other viral proteins, was transfected into a co-culture of 293T and MDCKII cells after the two nucleotide alterations TGT to AGC were confirmed by sequencing (Figure 21A). 72 hours later the supernatant was collected and the remaining cells were subjected to immunofluorescence with antibodies against HA to show that transfection was successful (Figure 20B, upper row). An aliquot of the supernatant (P1 virus) was amplified in fertilized eggs (P2 virus) and subsequently in MDCKII cells (P3). The cellular supernatant was used to infect MDCKII cells. Immunofluorescence revealed that most of the cells were infected with wild type, fewer cells were infected with Ac1 and no cells were infected with Ac2 and Ac1+2 (Figure 20B, lower row). The second aliquot from the transfection was passaged three times in MDCKII cells and the resulting supernatants were subjected to HA assay. The wild-type virus from passage 3 (P3 virus) and 4 (P4 virus) produced HA titres of 2E7, while no agglutination was measurable with P4 virus from Ac1, Ac2 and Ac1+2 (Figure 20C). We performed two more transfections with a subsequent amplification in eggs or in MDCK cells, but were never able to detect infectious virus particles for Ac2 and Ac1+2. Note also that Ac1 could only be successfully rescued if the supernatant of the transfection was subsequently amplified in embryonated eggs.

A

Virus	Cyt.tail (Amino acids)	Cytoplasmic tail (Nucleotide)	Virus rescue
Wild	RDNVS**C**SI**C**L*	…**TGT**TCCATC**TGT**CTGTGA	+
Ac1	RDNVS**S**SI**C**L*	…**AGC**TCCATCTGTCTGTGA	+
Ac2	RDNVS**C**SI**S**L*	…TGTTCCATC**AGC**CTGTGA	-
Ac1+2	RDNVS**S**SI**S**L*	…**AGC**TCCATC**AGC**CTGTGA	-

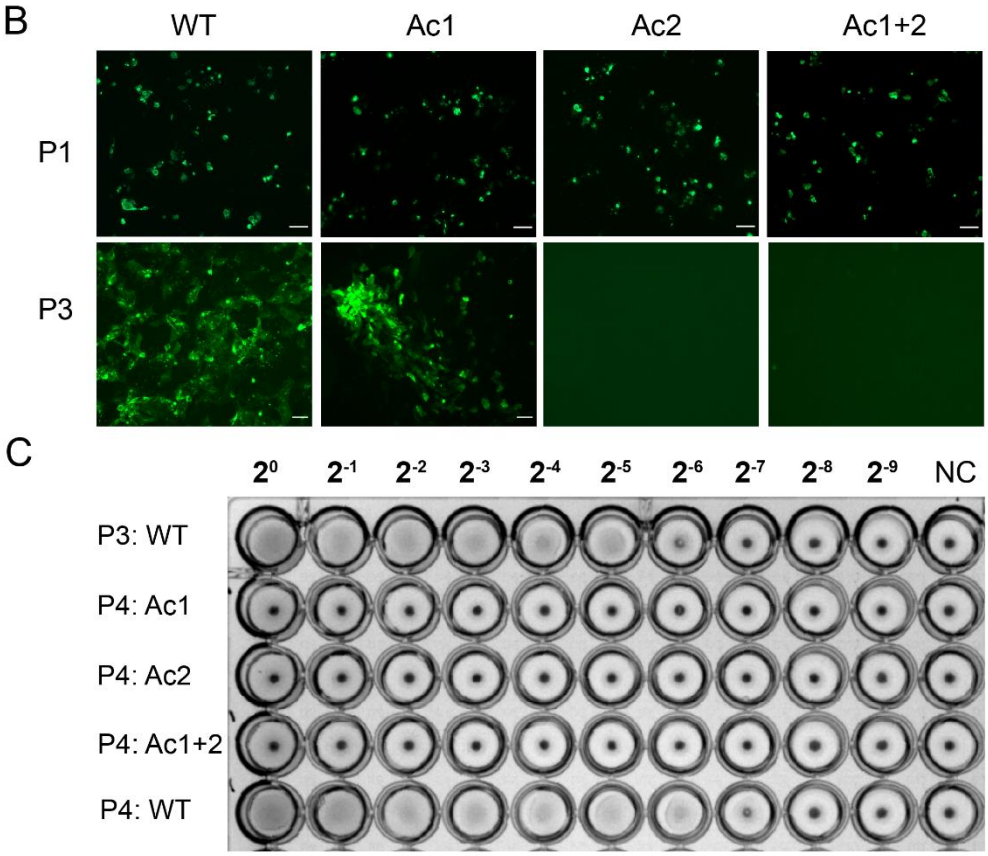

Figure 20. Palmitoylation of HA is essential for Influenza B virus replication

(A) Amino acid and nucleotide sequence of HA from the Influenza B virus strain B/Lee/40. Acylated cysteines and the encoding nucleotide triplets are in bold. The mutations are highlighted in red. An asterisk indicates the stop codon. + and - indicates whether or not virus could be rescued.

(B) Upper row: Immunofluorescence of a co-culture of 293T and MDCKII cells transfected with seven Flu B plasmids and the indicated HA plasmid. Lower row: Immunofluorescence of MDCKII cells infected with P3 virus, which was generated by amplification of the transfection supernatants in eggs and subsequently in MDCKII cells. Undiluted for Ac1, Ac2 and Ac1+2, 1:10 diluted for wt-infected cells. The scale bar is 100 µm.

(C) HA-assay with P3 and P4 virus, which was generated by two and three amplification steps of the transfection supernatants only in MDCKII cells. Note, that we could rescue the Flu B Ac1 only, if the supernatant of the transfection was first amplified in embryonated eggs.

To test for the genetic stability of the inserted mutation, Flu B Ac1 from embryonated eggs (P2 virus) was amplified two more times in MDCK II cells and after each amplification step, cDNA was prepared and ~300 nucleotides at the 5' end of the HA gene were sequenced to analyse whether the mutation is still present (Figure 21A). Whereas the P2 virus still contains the codon AGC introduced into the plasmid, the sequencing chromatogram of the P3 virus reveals two peaks at position one (A or T) and two at position three (T or C) of this codon. It thus contains a mixture of viruses having either a Ser (AGC, AGT) or a Cys (TGC, TGT) in HA. After a further amplification in MDCK II cells the resulting P4 virus contains exclusively TGT which is identical to the codon present in HA wt (Figure 21A). We conclude that a fatty acid attached to the membrane-near Cys is beneficial for virus growth, since viruses having this amino acid rapidly outgrow viruses with a Ser. Since a simultaneous exchange of two nucleotides in one amplification step is unlikely, the sequence of reversions from AGC (Ser) to AG**T** (Ser) and to **T**GC (Cys) in passage 3 and to TGT (Cys) in passage 4 seems most probable. The original codon TGT is apparently also preferred over the codon TGC, which also codes for cysteine.

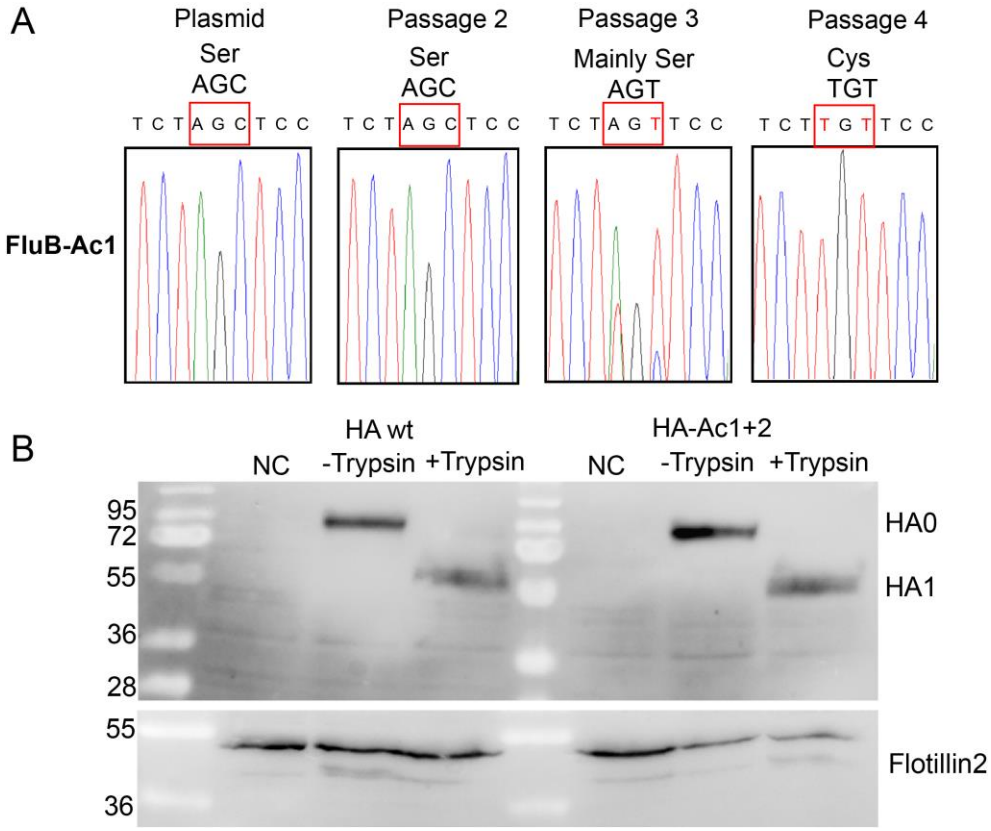

Figure 21. Flu B Ac1 rapidly reverted back to the wild-type sequence

(A) Sequence chromatograms of the plasmid used to rescue Ac1 and of the recombinant virus after one passage in embryonated eggs (P2 virus) and one (P3) or two (P4) passages in MDCKII cells.

(B) Expression of HA wt and HA Ac1+2 and cell surface trypsinisation. HA wt and HA Ac1+2 were expressed in 293T cells, which were treated after 48h with trypsin for 30 minutes. Cells were lysed and subjected to western blot with anti-HA antibody. Flotillin2 is the loading control.

Palmitoylation may be crucial for the stability and intracellular trafficking of viral glycoproteins(103). In order to determine if the inability to rescue the Ac1+2 recombinant is due to impaired transport of HA to the budding site, we expressed HA Ac1+2 and HA wt in 293T cells, which were subsequently subjected to trypsin treatment. Only when HA is exposed at the cell surface does the enzyme cleave it into its subunits HA1 and HA2. In the absence of trypsin, a HA band of similar intensity is detected for HA wt and HA Ac1+2. In the presence of trypsin HA0 wt as well as HA0 Ac1+2, is completely cleaved into HA1 and HA2, the latter band is not visible since the monoclonal antibody binds to the HA1 subunit (Figure 21B). Thus, palmitoylation does not affect the stability of HA or its intracellular transport, as previously reported for HA of Flu A and HEF of Flu C (92) (122).

4.2.2 Palmitoylation of HA of Influenza B virus occurs in the ER

In an effort to reduce the number of DHHCs potentially implicated in palmitoylation of HA of Flu B, we investigated in which compartment along the exocytic the modification happens and whether it varies from the compartment where HA of Flu A is acylated. Brefeldin A (BFA), a drug that prevents proteins from leaving the ER, was used to study this(123) (124). Although no tool exists to test directly for protein exit from the ER, transport of HA to the medial Golgi can be monitored using endoglycosidase-H (Endo-H), which removes carbohydrates of the high mannose type. Posttranslational proteolytic cleavage of HA into HA1 and HA2 subunits is another criterion for vesicular transport. Despite having a monobasic cleavage site, HA of Flu B is partially proteolytically activated in MDCK II cells by a transmembrane serine protease(125) (126, 127). Similarly, HA of the Influenza A strain WSN is also partially cleaved in these cells, either by endogenous proteases or facilitated by recruitment of serum plasminogen and its conversion to the protease plasmin(128–130).

First, we explored various experimental setups and discovered that a modest dose of BFA, given three hours after infection and present the entire time, prevented HA transport while also allowing enough HA to be synthesized to test it for acylation. In untreated cells Endo-H removes carbohydrates from approximately half of the uncleaved HA molecules but not from HA1 because cleavage of HA occurs after the acquisition of Endo-H resistant carbohydrates. Because the antibody only binds to the HA1 subunit, HA2 is not visible in the blot. Only a small part of HA molecules is cleaved in the presence of BFA, and both uncleaved HA and HA1 are entirely sensitive to Endo-H digestion, showing that cleavage occurs under BFA treatment before HA develops Endo-H resistant carbohydrates (Figure 22A).

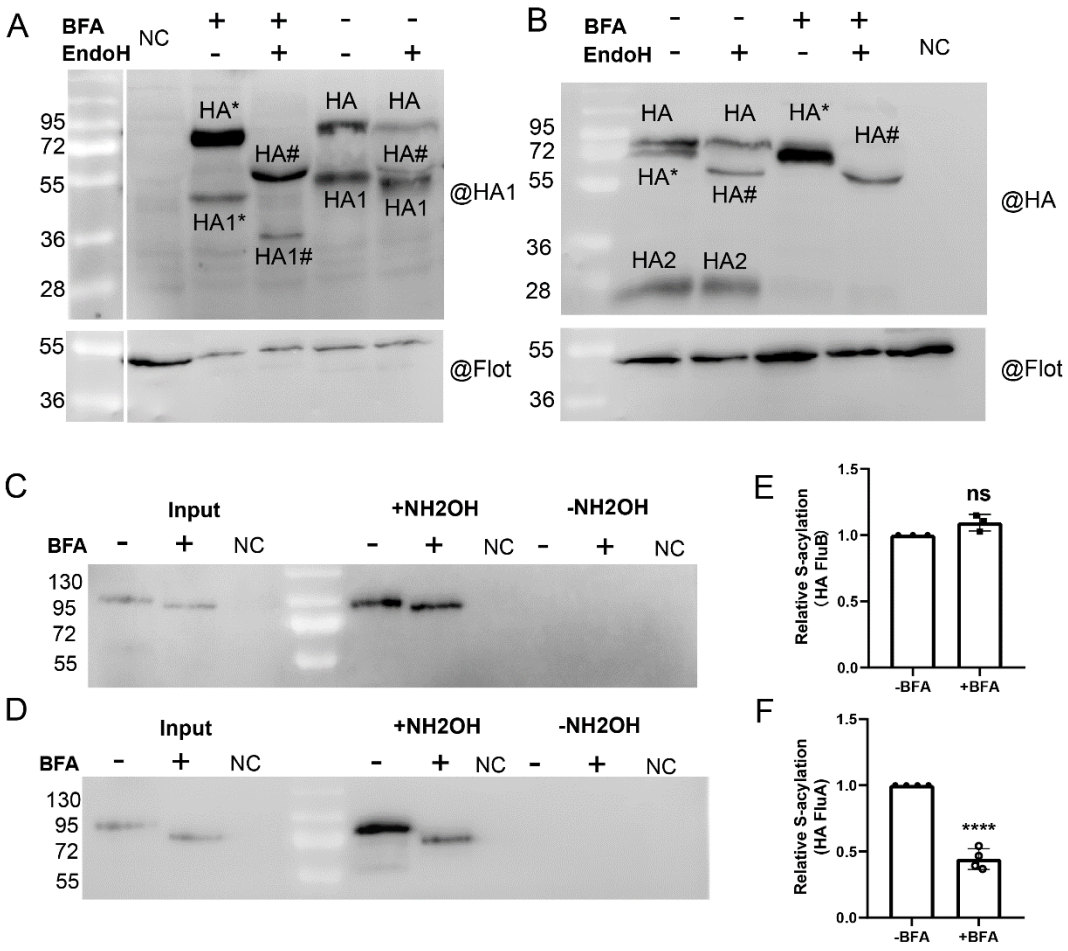

Figure 22. Palmitoylation of HA of Flu B occurs in the ER

(A, B) Validating the effect of brefeldin A. MDCKII cells were infected with Influenza B virus (A) or Influenza A virus (B) at an MOI of 1. 3hours later BFA (3µg/ml) was added and cells were incubated for 24 (A) or 12 (B) hours. Cells were lysed using NP40 lysis buffer and treated or not treated with Endo H glycosidase. Lysates were then subjected to western blot with antibodies against Influenza B Virus HA (A) or Influenza A virus HA (B). Labelling of bands: HA: uncleaved HA, HA1, HA2: cleaved subunits, #: HA with carbohydrates removed by Endo-H digestion. *: Glycosylated HA with lower molecular weight due to the BFA-induced transport block. Note that HA bands in untreated cells are weaker since the protein was lost due to virus budding, which does not occur if HA transport is blocked.

(C, D) S-acylation level of HA of Flu B (C) or Flu A (D) in the presence of BFA. MDCKII cells were infected with Influenza B virus (C) or Influenza A virus (D) and treated with BFA as described. Cell lysates were then subjected to Acyl-RAC assay, which is based on pull-down of proteins with thiol-active resins. Input: aliquot of the cell lysate to compare expression levels. NH2OH: samples treated (+) or not treated (-) with hydroxylamine to cleave thioester-bound fatty acids. Note that a larger amount of the cell lysate was used from all samples from non-treated cells to account for protein loss caused by virus budding. No HA1 of Flu B and very little HA2 of Flu A were detected in these blots.

(E, F) Quantification of three independent experiments with Influenza B (E) and four with Influenza A (F) virus. Densities of the +NH2OH bands were divided by the densities of the input bands and normalized to experiments without BFA. Unpaired t-test was applied for statistical analysis, ns, not significant, ****, $P < 0.0001$ versus wild type without BFA

The same experiment performed with Influenza A virus strain WSN provides almost identical results: BFA prevents cleavage of HA and also the conversion of uncleaved HA to an Endo-H resistant form (Figure 22B). Also take note of the fact that uncleaved HA0 in BFA-treated cells of both Influenza A and B virus has a slightly lower molecular weight than uncleaved HA0 in untreated cells. This is because ER-located glycoproteins have shorter, trimmed carbohydrate chains, while in the Golgi the side chains are extended.

Once the experimental parameters for blocking HA transport had been established, we compared the acylation of HA in BFA-treated and untreated cells. We employed the Acyl-RAC (resin-assisted capture) assay, which makes use of thiol-reactive resins to capture SH-groups that had just been released as a result of hydroxylamine cleavage of thioester linkages. MDCKII cells were infected with the Influenza B virus in the presence or absence of BFA, lysed, and a 10% aliquot was used to compare the levels of HA expression (input). The remaining protein sample was equally split, one aliquot was treated with hydroxylamine (+NH2OH), the other aliquot was treated with Tris–HCl (-NH2OH) to assess the binding specificity of the resin. All samples were then subjected to western blotting with antibodies against HA (Figure 22C, D). Quantification of the results from three independent experiments revealed that acylation of HA of Flu B was undiminished, whereas acylation of HA of Flu B was reduced to ~45% with very little variation between experiments (Figure 22E, F).

In these experiments, only a very small fraction of HA of Flu A was cleaved in untreated cells and HA of Flu B revealed no cleavage (not shown). We have no conclusive explanation for the inter-experimental variability other than the MDCK-II cell line being a mixture of three different cell types that differ in the expression of proteolytic enzymes. We conclude that acylation of HA of Flu A Influenza HA begins in the ER but continues in the Golgi, which is consistent with previous findings(131). In contrast, acylation of Flu B HA occurs exclusively in the ER.

4.2.3 HA of Influenza B virus is acylated by DHHC enzymes 1, 2, 4 and 6

To identify the DHHCs involved in acylation of HA of Influenza B virus we used commercial HAP1 cells, where various DHHCs were knocked-out using the CRISPR/Cas9 technology. Wild-type HAP1 cells express all human DHHCs, except DHHC 19 (84). They can be infected with Influenza B virus and synthesize HA, which is transported to the plasma membrane as demonstrated by the binding of erythrocytes to infected cells. However, HAP1 cells do not release virus particles into the medium as analyzed by hemagglutination and plaque assays, as

already observed for Influenza A virus (not shown). Note also that cleavage of HA was not observed in any experiment with HAP1 cells.

In the first screening experiments we used cell lines where the ER-located DHHCs 1, 2, 4 and 6, the Golgi-located DHHCs 5, 7, 8, 15, 16 have been inactivated [5, 6]. The HAP1 cells were infected with virus, lysed 24 hours later and subjected to Acyl-RAC to determine whether acylation of HA is reduced in any of the infected cells. The results of two independent experiments are shown in Figure 23 A and B and their quantification (densities of the +NH2OH bands relative to densities of the input bands) in Figure 23C. In both experiments acylation of HA was quite markedly reduced only in ΔDHHC 2 and ΔDHHC 4 cells and slightly in ΔDHHC 1 cells. Most other knock-out cell lines revealed a large variation between both experiments, except for ΔDHHC 8 cells, which exhibit a small increase.

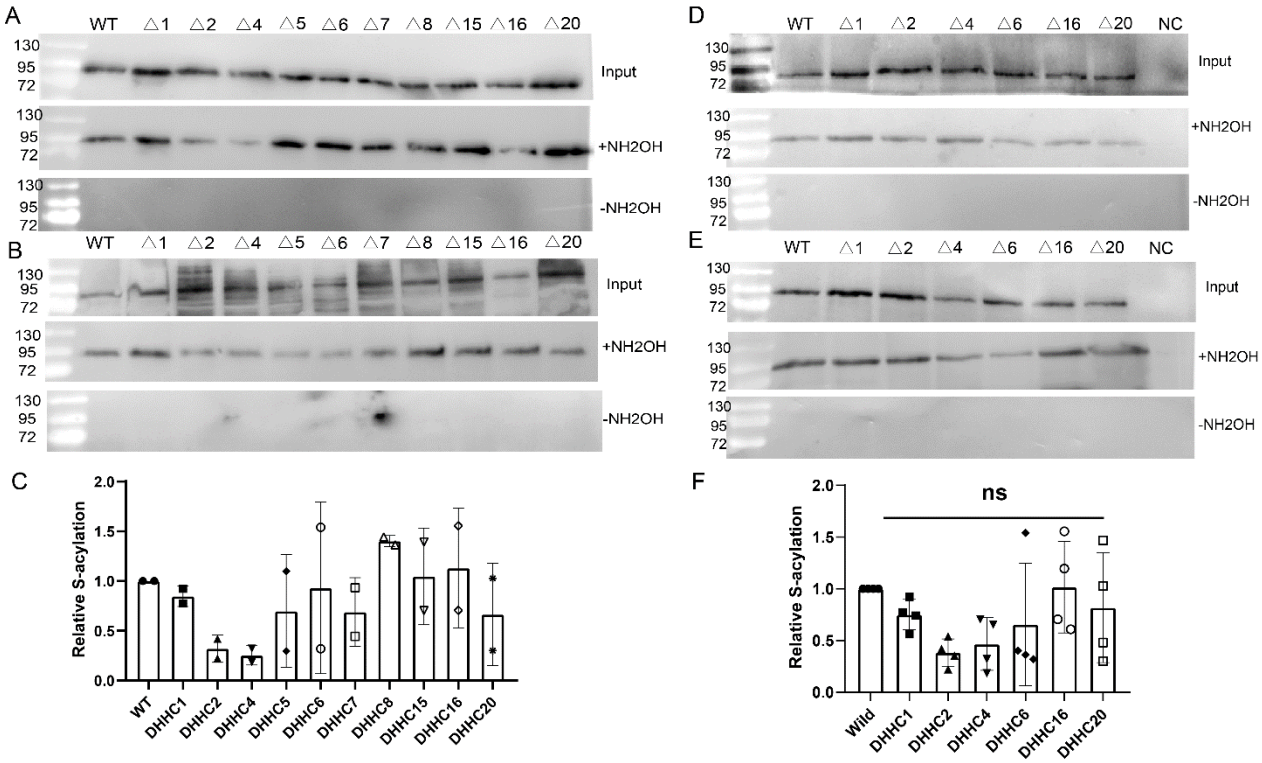

Figure 23. Testing HA acylation in cells deficient in ER- and Golgi-located DHHCs

(A, B, D, E) HAP1 cells where the indicated DHHC genes were knocked-out using the CRISPR/Cas9 technology were infected with Influenza B virus at an MOI of 1. 24 hours later, acylation of HA was analysed using Acyl-RAC.

(C) Quantification of data from A and B.

(D) Quantification of data from A, B, D and E. The mean ± SD is shown. One-way ANOVA followed by multiple comparison Dunnett test was applied for statistical analysis. ns, not significant compared to WT.

In the next screening round, we used the ΔDHHC 2 and ΔDHHC 4 cell lines, the ΔDHHC 1 and ΔDHHC 6 cells, where the other ER-located DHHCs have been inactivated and ΔDHHC 16 and ΔDHHC 20 cells. The results of two independent experiments show again a marked reduction in acylation of HA in ΔDHHC 2 and ΔDHHC 4 cells and a small reduction in ΔDHHC 1 cells. HA acylation was also markedly reduced in both experiments with ΔDHHC 6 cells, but no consistent effect was seen in ΔDHHC 16 and ΔDHHC 20 cells (Figure 23 D-F). However, quantification of the four experiments performed so far showed no statistically significant differences compared to wild-type cells for any of the knockout cells.

To further statistically validate the results, we performed the same experiment two more times with ΔDHHC 1, ΔDHHC 2, ΔDHHC 4 and ΔDHHC 6 cells. To exclude that proteins were lost during sample preparation, we used antibodies against the cellular palmitoylated protein flotillin 2 as an internal control (Figure 24 A and B). Acylation of HA is reduced in all four knockout cells, most obviously in ΔDHHC 2 and ΔDHHC 4 cells and quantification of all six experiments showed a statistically significant difference for these cells (Figure 24 C). In five of the six experiments, infection of ΔDHHC 6 cells showed a substantial decrease in acylation of HA. However, since the first experiment showed an increase in acylation, the evaluation of all experiments revealed no statistically significant difference to wt cells. When the first experiment is removed from the analysis, the average reduction in acylation is now significant and at the same level as in the ΔDHHC 2 and ΔDHHC 4 cells, namely a reduction to about 40 %. Similarly, the small reduction (10 %) in acylation of HA in ΔDHHC 1 cells is now also statistically significant (Figure 24D). We conclude that DHHC 1, 2, 4 and 6 are involved in acylation of HA of Flu B.

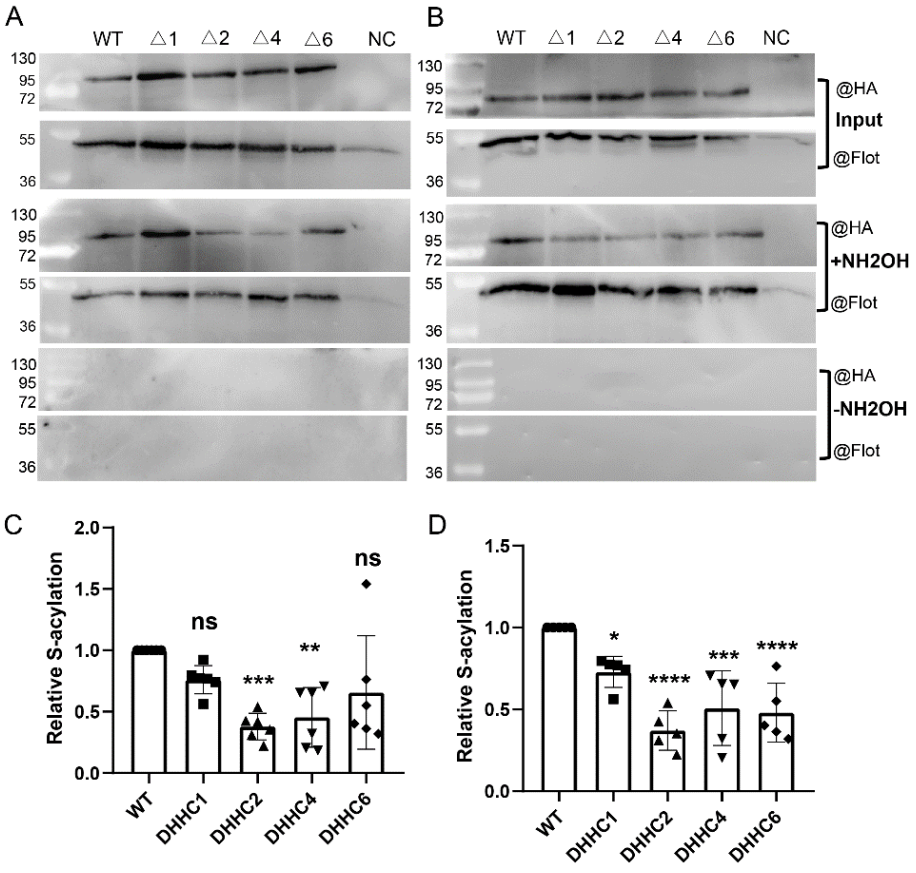

Figure 24. HA of Influenza B virus is acylated by DHHC 1, 2, 4 and 6

(A, B) HAP1 cells where the indicated DHHC genes were knocked-out using the CRISPR/Cas9 technology were infected with Influenza B virus at an MOI of 1. 24 hours later, acylation of HA was analyzed using Acyl-RAC. Input: aliquot of the cell lysate to compare expression levels. NH2OH: samples treated (+) or not treated (-) with hydroxylamine to cleave thioester-bound fatty acids.

(C) Quantification of data from all six experiments in Figure 23 and 26. The mean ± SD is shown. One-way ANOVA followed by multiple comparison Dunnett test was applied for statistical analysis. ns, not significant, **, P <0.01, ***, P <0.001 versus WT.

(D) Quantification of data from five experiments, excluding data from Figure 23A. The mean ± SD is shown. One-way ANOVA followed by multiple comparison Dunnett test was applied for statistical analysis. *, P <0.05, ***, P <0.001, ****, P <0.0001 versus WT.

4.2.4 DHHC 1, 2, 4 and 6 are located in the ER in cultured cells and expressed in epithelia cells of the human respiratory tract

DHHC 4 and 6 are ER-localized transmembrane proteins with a C-terminal lysine-based retention signal and DHHC1 remains in the ER by an unknown mechanism [43, 44]. DHHC 2 associates with the plasma membrane, recycling endosomes, and vesicular structures in neurons(132) and in T-cells it localizes primarily to the endoplasmic reticulum and Golgi

apparatus(133). We investigated the intracellular localization of DHHC 1, 2, 4 and 6 by confocal microscopy in transfected BHK cells, which were subsequently stained with an ER-marker (Figure 25A). Quantification revealed the highest Pearson´s correlation coefficient~0.75 for DHHC 1, 4 and 6, but the value for DHHC 2 is only slightly lower~0.7. In contrast, DHHC 3, which resides mainly in the cis-Golgi(75) revealed a different, perinuclear staining pattern and a lower Pearson´s correlation coefficient (~0.48). In addition, HA of Flu B shows substantial overlap with DHHC 1, 2, 4 and 6 in double transfected BHK cells (Figure 25C).

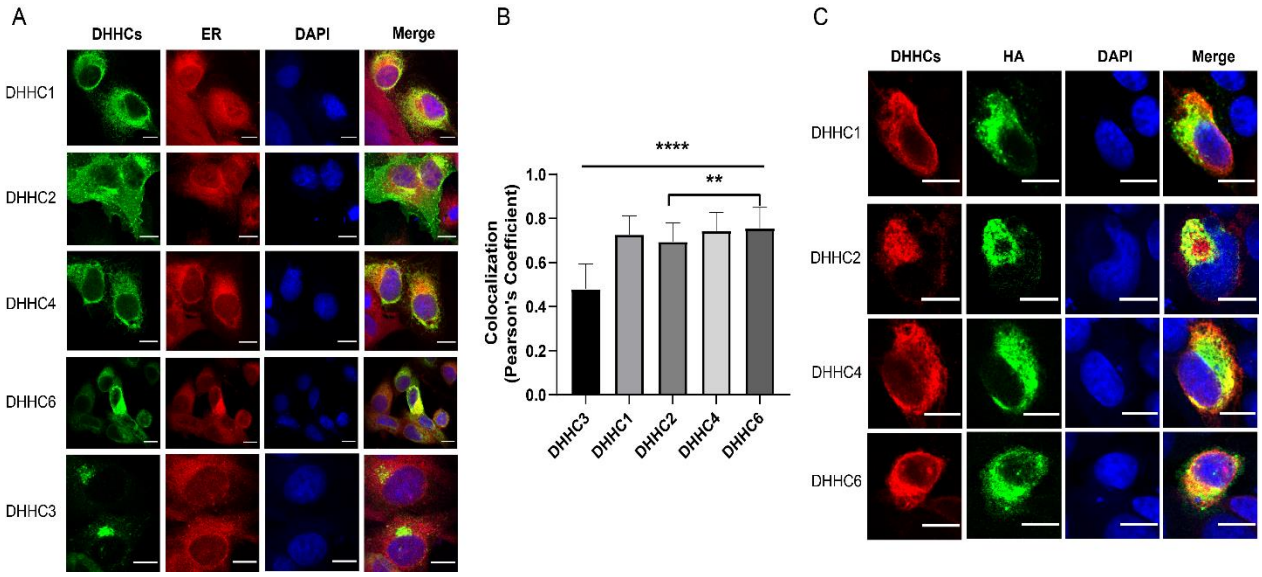

Figure 25. Co-localization of DHHCs responsible for acylation of HA with ER marker/HA

(A) Confocal microscopy of BHK21 cells transfected with the indicated mouse DHHCs fused to a HA tag. Cells were permeabilized and stained with antibodies against HA tag (green), with ER staining kit (red), and with DAPI (blue) to highlight the nucleus. The scale bar is 10 µm.

(B) Co-localization of DHHCs and ER from at least 50 cells was quantified with Pearson's correlation coefficient method using the JACoP plugin of the Fiji software. One-way ANOVA followed by multiple comparison Tukey test was applied for statistical analysis. ****, P <0.0001 DHHC 3 versus DHHC 1,2,4 and 6; **, P <0.01 DHHC 2 versus DHHC 6. DHHC 1,4,6 has no significant differences from each other. There is no significant difference between DHHC 1, DHHC 4, and DHHC 6.

(C) Confocal microscopy of BHK21 cells co-transfected with the indicated mouse DHHCs fused to a HA tag and Influenza B virus HA. Cells were permeabilized and stained with antibodies against HA- tag (red) and against Flu B HA (green), and with DAPI (blue) to highlight the nucleus. The scale bar is 10 µm.

We also investigated localization of DHHC 2, 4 and 6 in A549 cells, a model for alveolar Type II pulmonary epithelium, where Influenza viruses replicate (Figure 26). We calculated the same

Pearson correlation coefficient as in BHK cells, ~0.75 for DHHC 4 and 6 and only slightly lower (~0.7) for DHHC 2. We conclude that the DHHCs responsible for the acylation of HA of Influenza B virus are located in the ER, which is consistent with the intracellular site of its acylation.

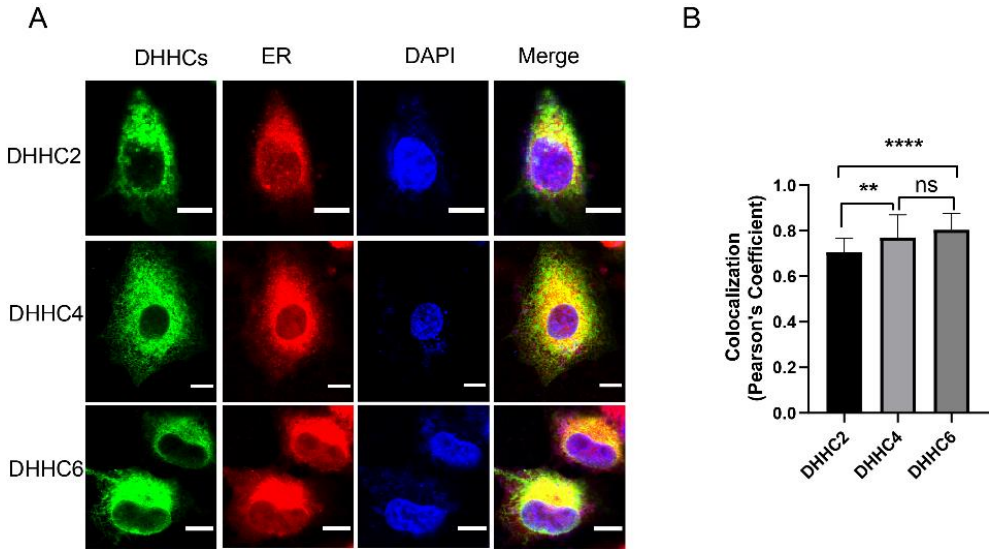

Figure 26. Co-localization of DHHC 2, 4 and 6 with an ER-marker in human lung A549 cells

(A) Confocal microscopy of A549 cells transfected with the indicated mouse DHHCs fused to a HA tag. Cells were permeabilized and stained with antibodies against the HA-tag (green), with the ER staining kit (red), and with DAPI (blue) to highlight the nucleus. The scale bar is 10 µm.

(B) Quantification of co-localization from at least 40 cells with Pearson's correlation coefficient method using the JACoP plugin of the Fiji software. One-way ANOVA followed by multiple comparison Tukey test was applied for statistical analysis. ****, P <0.0001 DHHC 2 versus DHHC 6; **, P <0.01 2 versus DHHC 4. DHHC 4 and 6 has no significant differences from each other.

Influenza viruses replicate in epithelia cells of the upper and lower respiratory tract, as well as in alveolar cells of the lung in more severe cases. It is therefore interesting to determine whether these cells express the DHHCs involved in HA acylation. We used "CellPalmSeq," a curated RNAseq database of palmitoylating enzyme expression in human tissues and cells, for this purpose(134). The expression of DHHC 4 and 6 in the whole lung tissue is much higher than that of DHHC 1 and 2. The enzyme with the highest expression in single cells of the lung is DHHC 4, followed by DHHC 6. Except for alveolar type 1 and 2 cells, where DHHC 2 is most abundant, DHHC 2 is the third most expressed DHHC of the four. DHHC 1 is expressed at the lowest level and not at all in alveolar cells (Table 1). We hypothesis that DHHC 4 and 6 are responsible for the majority of acylation reactions of Flu B HA in human lung cells. It should be

highlighted, nevertheless, that the stability and activity of the enzyme are just as important as the degree of RNA expression.

	DHHC1	DHHC2	DHHC4	DHHC6
Whole Lung tissue	12.4	14.3	21.9	20
Basal respiratory cells	1.3	4.1	63.4	23.2
Respiratory ciliated cells	5.5	7.7	32.5	13.4
Club cells	1.4	10.5	42.4	27.4
Lonocytes	2	6.1	42.7	10.2
Alveolar type 1	0	44.8	38.5	22.4
Alveolar type 2	0	25.4	20.1	20.1
Calu-3 cell (mean)	11.4	27.6	71.4	28.2

Table 1. Expression of DHHC 1, 2, 4 and 6 in human lung tissue and various cell types

Expression levels of the indicated DHHCs in whole lung tissue and specialized lung cell types. The results are based on RNA-Seq experiments and the units are transcripts per million (nTPM). Data were taken from the "CellPalmSeq" database (https://cellpalmseq.med.ubc.ca/), which is based on the human protein atlas (https://www.proteinatlas.org/)

4.2.5 The shape of HA´s transmembrane region might explain the acylation by different DHHCs

The HAs of Influenza A and B viruses are acylated by different DHHCs, only DHHC 2 has an effect on both proteins. We were therefore interested in whether the transmembrane regions or the cytoplasmic domains of the two HA proteins have peculiar structural features that could act as recognition motifs for their respective DHHC enzymes. Apart from the cryo-EM structure of a group 1 HA, in which, however, only the outer part of the transmembrane region was resolved, no other experimentally determined structures are available for full-length HA proteins(135). Similarly, the alphafold2 database does not contain predicted HA structures(136). We therefore used a colab version of alphafold2 multimer to predict the structures of the transmembrane region and cytoplasmic tail of HA of Flu B and of one group 1 and one group 2 HA of Flu A(137). To estimate the accuracy of the prediction, alphafold2 supplies a per residue confidence metric called the predicted local distance difference test (pLDDT), which indicates the confidence in the local structure prediction. The pLDDT scores are displayed on the predicted structure in rainbow colours, ranging from red (high confidence) to blue (low confidence). The cytoplasmic tails have a very low pLDDT score below 50, which might suggest that they are intrinsically disordered.

The transmembrane region, especially the inner part is predicted with a higher confidence score of 60 to 70 suggesting that at least the structural elements are predicted correctly (Figure 27, left part). This is consistent with CD spectroscopy of purified peptides, that also revealed a trimeric helix for the transmembrane region of HA(138). A surface representation of the transmembrane region allows to locate the amino acids exposed at the molecule´s surface which might function as binding site of DHHC enzymes (Figure 27, right part). However, the TMRs of HA of Flu B and Flu A revealed a similar pattern: large hydrophobic amino acid (Leu, Ile) are followed by two or three amino acids with -OH groups (Ser, Thr), which are followed by five or six hydrophobic amino acids, one or two of which are aromatic residues (Phe, Tyr, Trp). Looking only at the protein backbone, we see that the three helices in the HA of Flu B are straight and parallel to each other, whereas the helices of the HA s of Flu A are slightly bent. The kink in the helix is caused by a Gly localised in the lower part of the TMR. In the Cryo-EM structure of HA the region following the Gly splays out from the upper part of the transmembrane region(83). Since a glycine is not present in the TMR of HAs from Flu B, its kink-inducing capacity is a feature that distinguishes HA from Flu A and Flu B.

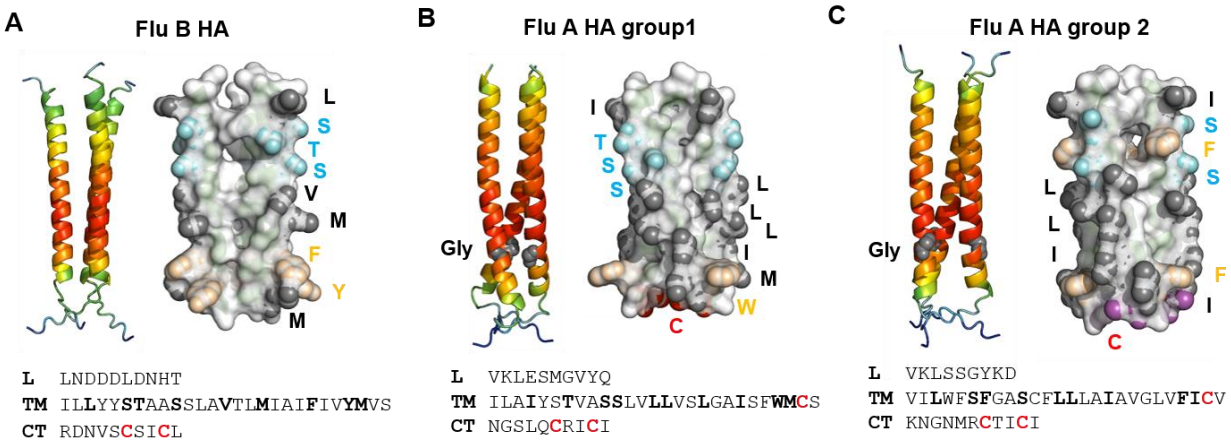

Figure 27. Predicted structure of the transmembrane region of HA of Flu A and B

(A) Flu B HA **(B)** Flu A HA group 1 **(C)** Flu A HA group 2. Left part: Cartoon of the structure predicted by alphafold2. The confidence score is colour coded from red (high confidence) to blue (low confidence). Right part: Surface representation of the transmembrane region. Amino acid side chains located at the surface are highlighted as spheres. Cyan spheres: Hydroxy amino acids, black spheres: long and hydrophobic amino acids, wheat spheres: aromatic amino acids. Lower part: amino acid sequence used for the prediction divided into L: linker region, TM: transmembrane, CT: cytoplasmic tail. Amino acids highlighted in the surface representation are bold, the acylated cysteines in red. Sequences are from Flu B Lee strain, Flu A/WSN/1933(H1N1) group 1 HA, Flu A/FPV/Rostock/34, H7N1 group 2 HA.

4.2.6 Exclusive attachment of palmitate to the HA of Flu B virus is not encoded in the responsible DHHCs

The crystal structure of the autoacylated form of DHHC 20 provided a model for the fatty acid specificity of the acylating enzymes. The hydrogen bond established between Ser29 in TM1 and Tyr181 in TM3 in DHHC 20 closes the narrow end of the cavity in which the fatty acid is inserted. It was proposed that the specificity of a DHHC enzyme's fatty acid binding depends on whether large or small amino acids are present at this position, which we investigated for DHHC 2, 4 and 6. Crystal structures are not available for any of these DHHCs, but the alphafold2 database contains predicted models with a per-residue confidence score (pLDDT) of >90 for the transmembrane regions, which are thus equivalent to experimentally determined structures. Other parts of the enzymes, especially domains down- or upstream of the four transmembrane regions, have a pLDDT score below 50 and hence are likely to be intrinsically disordered (Figure 28, left part). The predicted models were superimposed with the structure of DHHC 20 to identify the crucial amino acids (Figure 28, middle part). All three DHHCs, especially DHHC2 align very well with DHHC 20, especially over the entire transmembrane domain, including the cysteine-rich domain. DHHC 2 also possess a Ser in TM1 and a Tyr in TM3, which can be perfectly superimposed on their DHHC 20 counterparts (Figure 28, right part). In addition, DHHC 2 contains a Tyr (instead of a Phe) in TM3, which forms an additional hydrophilic interaction with Ser in TM1 sealing the cavity further. DHHC 4 also contains a Ser/Tyr pair at the end of the hydrophobic cavity, but the order is reversed compared to DHHC 20. Tyr 80 is in TM1 and Ser204 in TM3 and both residues form a hydrophilic interaction. DHHC 6 contains Cys34 instead of Ser29 in TM1 and Gly154 instead of the bulky Tyr in TM3 and this pair of small amino acids is highly unlikely to prevent access of stearate into the hydrophobic cavity. The helix is only tightly sealed further up by a layer of hydrophobic amino acids. We conclude that the specific attachment of palmitate to HA of Flu B is not encoded in the DHHCs required for its acylation. Longer fatty acids, such as stearate, can likely be accommodated by DHHC 2, 4 and 6, which can transfer them to the HA of Influenza B virus.

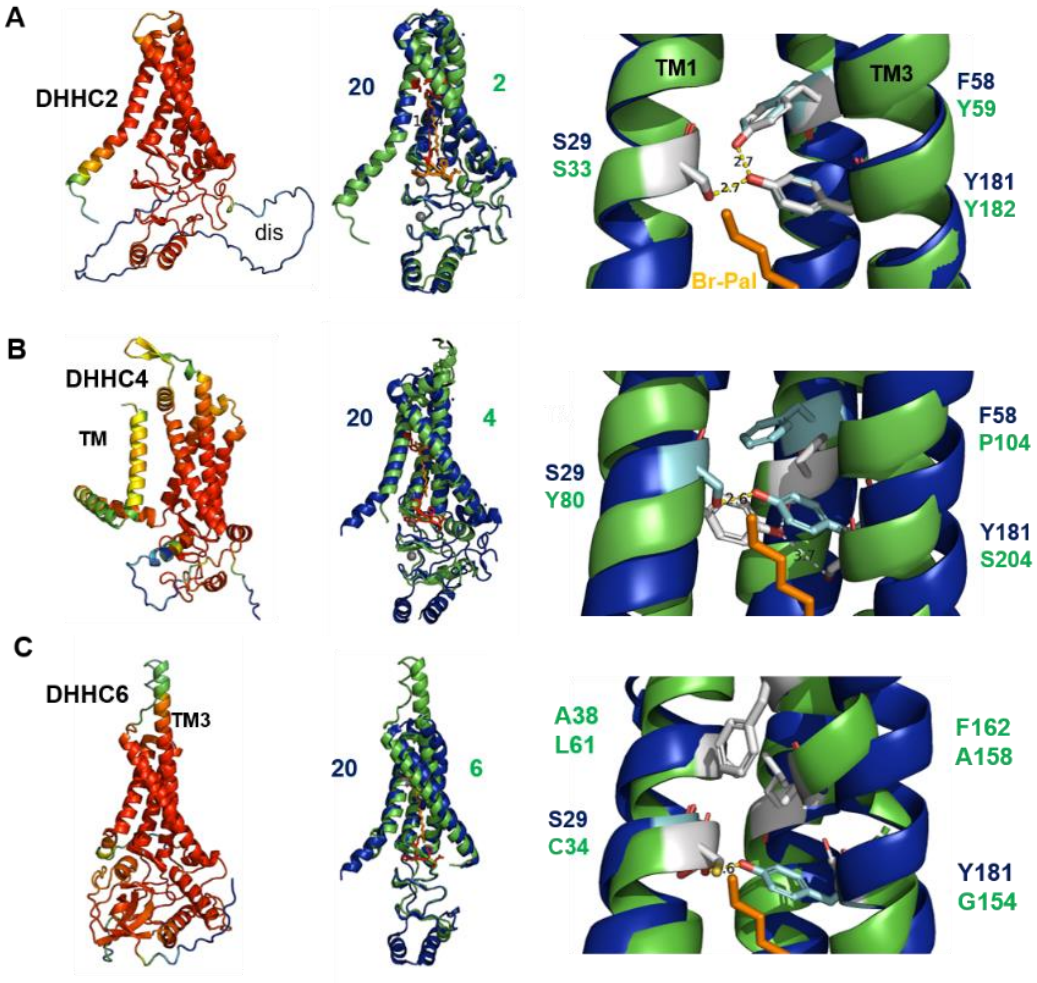

Figure 28. Amino acids at the ceiling of the hydrophobic cavity in DHHC 2, 4 and 6

(A) DHHC 2 structure, **(B)** DHHC 4 structure, **(C)** DHHC 6 structure. Left part: Alphafold 2 model of the respective human DHHC showing the confidence level of prediction colour-coded from red (high confidence) to blue (low confidence). Dis: disordered region, TM: additional transmembrane region in DHHC 4. TM3: longer transmembrane region in DHHC 6. Accession numbers for the alphafold database: DHHC 2: AF-Q9UIJ5-F1, DHHC 4: AF-Q9NPG8-F1, DHHC 6: AF-Q9H6R6-F1. Middle part: Alignment of DHHC 20 with the respective DHHCs. Root-mean-square deviation of atomic positions (RMSD): DHHC 2 = 0.459Å. DHHC 4: 4.326Å, DHHC 6: 2.387Å. The N-terminal extensions in DHHC 2 and DHHC 4 were deleted prior to the alignment. Right part: Detail of the alignment showing the amino acids sealing the celling of the cavity as cyan sticks (DHHC 20) or white sticks (DHHC 2, 4 or 6). TM4 was removed from the structure for clarity.

5. Discussion

5.1 The role of an amphiphilic helix and transmembrane region in the efficient acylation of M2 from Influenza A virus

5.1.1 The amphiphilic helix of M2 contains the required information for palmitoylation

The AH of M2 becomes palmitoylated when fused to the C-terminus of the RFP indicating that the information for fatty acid attachment is encoded in the helix. The helix also redistributes RFP from its usual cytosolic location to cellular membranes. This also occurs, although is reduced by about 30%, when the acylation site is replaced by a Serine. Thus, the AH of M2 has intrinsic propensity to target to cellular membranes, which is then stabilized by palmitoylation(139). A substantial proportion of RFP-AH (~70%) is located in the cytosol, making it unlikely that acylation is stochiometric, since palmitoylated molecules are (almost) always membrane-bound. There are several mutually exclusive explanations for this observation: some of the fatty acids are cleaved by thioesterases, the initial palmitoylation is substoichiometric because the AH does not contain all the information for complete acylation, and/or due to incomplete targeting to membranes not every molecule has access to the membrane-bound DHHC.

5.1.2 Mutations in the amphiphilic helix reduce, but do not eliminate palmitoylation of M2

To further investigate the signals in the amphiphilic helix, we used the full-length M2 protein, as it is a transmembrane protein and transported to the plasma membrane via the exocytic pathway, and thus has complete access to DHHC enzymes(118). As described previously(140) some of the mutations reduced the expression level of M2 but this is unlikely to be due to misfolding, since all mutants were transported along the exocytic pathway and co-localized with a cis-Golgi marker to the same extent as M2 wt. Each mutation we introduced into the amphiphilic helix reduced the acylation of M2, but to varying degrees, from 30% to 82% compared to M2 wt (results are summarized in table 2). The strongest reduction to 30% was achieved by eliminating the hydrophobic moment of the AH, increasing its hydrophobicity (M2 AH-5), and by inserting a proline adjacent to the acylated cysteine (M2-1P). The latter mutant still contains all amino acids identified by molecular dynamics to interact with DHHC20.

In M2 AH-4, none of the interacting amino acids were exchanged either, although acylation was determined to be reduced by about 50%. This indicates that the conformation of the helix and its biophysical properties, such as hydrophobicity and hydrophobic moment play a role for efficient acylation. Note, that the inherent variability of the Acyl-RAC assay makes it difficult to assess

whether certain mutations have stronger effects than others. The acylation level of two mutants, M2 AH-3 (to 74%) and M2-3P (to 82%), was not statistically significantly different from M2 wt, although the reduction was seen in almost every experiment. It is therefore safe to conclude, that any of the mutations we introduced to change the conserved amino acids and change the biophysical properties into the AH, reduces but does not eliminate fatty acid transfer to M2. Even after removal of all residues beyond Cys50, M2 is still about 50 % acylated compared to M2 wt. This suggests that the amino acids preceding the acylation site also affect acylation.

Name	**Sequence**	**Acylation**	**Binding**	**Features AH**
wt	FFKCIYRRFKYGLKR	100%	+	
AH-1	FF**E**CIY**E**RF**E**YGLKR	62%	n.a.	No net charge
AH-2	FFKCI**A**RRFKYG**A**KR	49%	n.a.	<H> ↓
AH-3	**A**FKCIYRRFKYGLKR	74%(ns)	n.a.	<H> ↓
AH-4	F**K**KC**K**YRRKKYGLKR	54%	++	<μH>↓ <H> ↓↓
AH-5	FF**F**CIY**F**RFKYGL**FF**	30%	+/-	<μH>↓<H>↑
1P	FFKC**P**YRRFKYGLKR	30%	+	H destroyed
3P	FFKCI**PPP**FKYGLKR	82%(ns)	+	H destroyed
1-50	FFKC	54%	++	truncated
1-53	FFKCIYR	62%	n.a.	truncated

Table 2. Summary of the effects of the amino acid mutations in the amphiphilic helix of M2

"Acylation" is the normalized acylation level relative to M2 wt, "Binding" summarizes the results of the Co-IP experiments with DHHC20 and "features AH" the effect of the mutations on the biophysical property of the amphiphilic helix AH. <H>: overall hydrophobicity and <μH> hydrophobic moment of the helix. ↑ and ↓ indicate an increase and decrease, respectively of these features. Mutated amino acids are in red. N.a.: not analysed, Ns: not significant.

5.1.3 The transmembrane region effects acylation of M2

Replacing a kink-inducing Glycine in the middle of the transmembrane helix with an Alanine increased palmitoylation of M2, which was statistically significant in the context of the M2 1-50 mutant. Glycine is not one of the residues identified by MD simulations to contact DHHC20, but it does cause a small kink in the middle of the helix. We therefore suggest that the altered conformation of the transmembrane region presents the cysteine in a more favourable way to the active site of the acyltransferase. Note also that the acylated cysteine is always at position 50 in each variant of M2, suggesting that its position plays an important role. This is in contrast to the acylated cysteines in the cytoplasmic domain of the spike proteins of corona and influenza viruses, whose positions have shifted during viral evolution(77).

5.1.4 Mutations in the helix of M2 do not prevent binding to DHHC20

Using co-immunoprecipitation assays we investigated whether M2 stably interacts with DHHC20 and whether this interaction is affected by the mutations induced. If we assume that the binding of M2 to DHHC20 represents the formation of an enzyme-substrate complex, then this is reduced only for M2 AH-5 which at least partly explains its reduced acylation level. The interaction of two other mutants M2-1P and M2-3P with DHHC20 is basically undiminished and two mutants, M2-AH-4 and M2 1-50 bind even stronger to DHHC20, although acylation was significantly reduced. We conclude that the fatty acid transfer is affected in these mutants, perhaps because binding happens in an unfavourable manner.

This assumption is supported by molecular dynamics simulations of M2 mutants with DHHC20. The acylation site of truncated M2 1-50 moves away from the catalytic center of the enzyme but the protein remains associated with TM1 and helps to explain why DHHC20 can be co-precipitated with M2 1-50 but acylation is reduced. Likewise, MD of the mutant M2-1P showed that the insertion of the Pro does not only destroy the part of the helix upstream of Cys50, but also decreases the angle between the helix and the transmembrane region. This does not change the distance between Cys156 in DHHC20 and Cys50 in M2 but causes “misalignment” of the helix with the catalytic center of DHHC20.

In summary, we have shown that M2 requires an amphiphilic helix for efficient acylation. Based on MD simulations we speculate that specific interactions of amino acids in the helix of M2 with the DHHC and TTXE motif of DHHC20 initiate the fatty acid transfer. However, since several of the mutants contain exchanges in residues that do not contact DHHC20, general biophysical features of the helix, such as charge, hydrophobicity and hydrophobic moment play a crucial role

for efficient acylation. Evidence of this is seen as M2 with mutations in the amphiphilic helix can still bind to DHHC20 but the subsequent step, the transfer of the fatty acid to M2, is impaired.

5.2 Role of palmitoylation of the Hemagglutinin of Influenza B virus and identification of the enzymes involved

5.2.1 The function of acylation of Influenza B virus HA

We demonstrate that palmitate modification in the cytoplasmic tail of HA is essential for Influenza B virus replication. The failure to rescue virus particles is not due to instability or reduced transport of HA to the budding site, since removal of both acylation sites does not diminish the amount of HA expressed on the cell surface. HA from Flu A and B, and HEF from Flu C behave identically in this respect, as removal of acylation sites does not affect their plasma membrane transport(122). In contrast, acylation of the functionally similar spike protein of SARS-CoV-2 at ten cytoplasmic cysteines is important for the protein´s stability.

We have not looked into the particular role of acylation of HA during the viral replication cycle, but in expression experiments deleting one acylation site had an effect on the opening of a fusion pore, which corresponds to a late phase in virus entry. This finding is similar to what has been reported for various subtypes of HA of Flu A and HEF of Flu C virus, although the effect was minor for the latter(83, 141, 142).

The effect of acylation site removal on viral replication distinguishes Influenza A and B viruses from Influenza C viruses. S-acylation of HA of Influenza A and B virus is essential for virus replication since Influenza virus mutants could not be generated if two or three palmitoylation sites were removed. Similarly, rapid reversion of single mutations to cysteines were observed for both viruses. Mutants with one deleted acylation site in the cytoplasmic tail revealed greatly reduced growth rates in cell culture. In contrast, removing the stearoylated cysteine at the end of the TM of influenza A HA and also of HEF had only a minor effect. Hence, cytoplasmic cysteines connected to palmitate are more critical for virus propagation than transmembrane cysteines bound to stearate. Whether this is due to the specific fatty acid or to the localization of the acylated cysteine is unclear, and also difficult to test experimentally, as shifting a transmembrane cysteine into the cytoplasm also leads to more palmitate being attached(143).

We also found a difference at the intracellular site along the exocytic pathway where HA of Flu A and B are acylated. Blocking ER exit had no impact on acylation of Flu B HA but lowered Flu A HA acylation to 40%. Thus, acylation of HA of Flu A begins in the ER and proceeds to completion in the Golgi, as has been reported for acylation of the SARS-CoV-2 spike. Both viral glycoproteins

are palmitoylated by the enzyme DHHC 20, which is found in both the ER and the Golgi. In contrast, acylation of Flu B HA occurs in the ER and thus corresponds to acylation of the Gp5/M membrane protein of an Arterivirus(144). The previous findings on the acylation of the hemagglutinating glycoproteins of Influenza viruses A, B and C are summarized in the Figure 29.

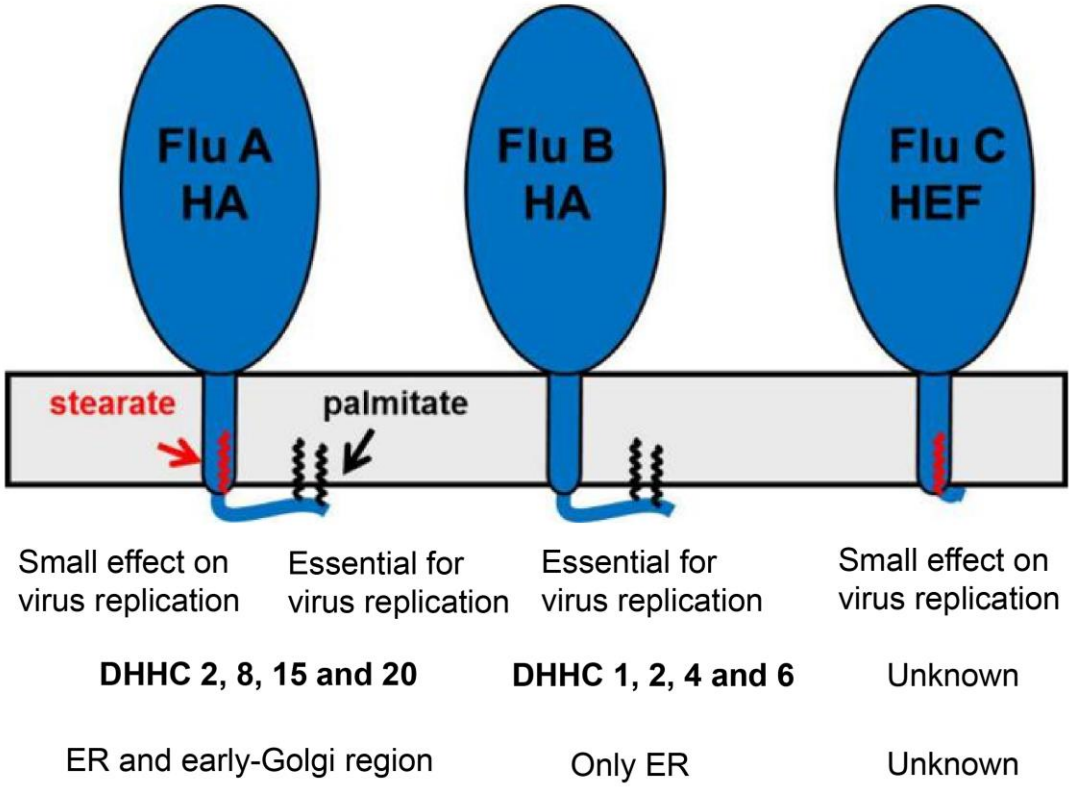

Figure 29. Summary of results on acylation of hemagglutinating glycoproteins of Influenza A, B and C virus

Schematic of HA and HEF protein embedded within a membrane. Fatty acids linked to cysteine residues are shown as blue (palmitate) or red (stearate) zigzag line. The impact of removing individual acylation sites, the DHHCs involved in acylation and the intracellular site are listed. In addition, whereas HA of Influenza A and B virus are associated with membrane rafts, cholesterol- and sphingolipid-enriched nanodomains of the plasma membrane, HEF is thought to localize to the bulk phase of the plasma membrane

5.2.2 Identification of DHHC enzymes involved in palmitoylation of Influenza B virus HA

The localization of the intracellular acylation site of HA allowed us to narrow down the number of DHHCs possibly involved in palmitoylation. In order to find the enzymes, we have chosen HAP1

cells with individual DHHCs knock-out as the experimental system. We started with a screen using cells knock out ER- and Golgi-localized DHHCs. Since the acyl-RAC assay can produce somewhat variable results, we repeated the experiments until the ΔDHHC cells that caused a significant reduction in HA acylation were confidently identified. Only cells lacking DHHC 1, 2, or 4 showed a decrease in acylation of HA in all six experiments. However, the effect in ΔDHHC 1 cells was small, a reduction of only 10%. In five of six experiments, we observed a substantial decrease in acylation of HA in ΔDHHC 6 cells. When the first experiment was removed from the analysis, there was a statistically significant difference, and the average reduction in acylation was at the same level as for ΔDHHC 2 and ΔDHHC 4 cells, around 40%. Interestingly, DHHC 6 requires palmitoylation at three cytoplasmic cysteines by DHHC 16 and selenoprotein K as a cofactor to be active(108, 109), although the latter claim is controversial(145) and these dependencies might have caused atypical results.

DHHC 4 and 6 are typical ER-localized proteins with a C-terminal lysine-based retrieval signal and DHHC 1 also resides in the ER by an unknown mechanism(146). DHHC 2 has been identified in various compartments in different cell types. We show here that all four DHHCs co-localize with HA of Flu B virus and also with an ER-marker in transfected BHK cells. More importantly, DHHC 2, 4 and 6 also resides in the ER in human respiratory A549 cells, which is consistent with the intracellular organelle where palmitoylation occurs. Since DHHC 4 and 6 are more highly expressed than DHHC 1 and 2 in most human lung cells (table 1), we assume that they are responsible for the majority of Flu B HA acylation reactions during an Influenza B virus infection. Each of these DHHC enzymes acylates a variety of proteins with different functions and membrane topologies. However, the exact molecular mechanisms by which the DHHCs recognize their substrate proteins are still largely unknown.

5.2.3 Possible molecular determinants for acylation of Flu A and B HA by different DHHCs enzymes

Although the HA proteins of influenza A and B viruses have similar structure and function, their TMR and short cytoplasmic tail may have minor structural differences that explain acylation by different DHHC enzymes. We predicted the structure of the TMR and cytoplasmic tail of HAs of Flu A and B using alphafold2. Overall, the accuracy of the prediction was quite low, especially for the cytoplasmic tails, which hence might be intrinsically disordered regions. In addition, mutations in the cytoplasmic tail of HA of Flu A and B had no impact on acylation(147, 148). The middle of the trimeric TMR was predicted with higher confidence, and both the TMRs of Flu A and B contain a region with Ser and Thr residues, flanked by hydrophobic and aromatic residues. However, the

backbone of the helices looks different, kinked by the presence of a Gly in the case of the HA of Flu A and straight in the case of the HA of Flu B. Cryo-EM revealed that the transmembrane region of group 1 HA of Flu A splayed out following the Gly. Therefore, the conformation of the TMR, straight or kinked, might allow specific interactions with different DHHCs and present the acylation sites differently to the catalytic domain of DHHCs. The exact mechanism of how DHHC enzymes recognize their substrates is still unknown, but studying the differences between the HAs of Flu A and B may provide insight into this process.

5.2.4 The specific acylation of HA of Flu B with palmitate is not encoded in the responsible DHHCs

Unlike HA from Influenza A virus which is acylated with both palmitic and stearic acid, HA of the Influenza B virus is known to be modified with only palmitic acid(78). We explored the possible molecular determinants for this fatty acid specificity of HA acylation. One possibility is that DHHC enzymes responsible for attaching the fatty acid to HA may not be able to take up longer-chain fatty acids due to a narrow hydrophobic cavity. However, we found that DHHC 2, 4, and 6 have identical or similar amino acids in the critical position at the end of the transmembrane region as DHHC 20, which can accept both palmitic and stearic acid (Figure 29). There is also experimental evidence that DHHC 2 and DHHC 4 exhibit no marked fatty acid preference and DHHC 6 can attach stearic acid to one of its substrates(149, 150). Therefore, it is unlikely that DHHC enzymes determine the specificity of HA acylation.

Another possible mechanism is the regulation of the availability of acyl-CoAs for DHHCs. Acyl-CoAs are provided by long-chain acyl-CoA synthetases (ACSLs), transmembrane proteins, of which there are five isoforms in humans. The distinct subcellular localization of different ACSL isoforms could cause the compartmentalization of acyl-CoA. A similar role could be played by acyl-CoA binding domain containing proteins (ACBDs), a large multigene family of diverse proteins. Experimental evidence for the regulation of fatty acid specificity has been provided for ACBD6, which binds to the enzyme N-myristoyltransferase (NMT). The interaction stimulates the transfer of the rare fatty acid myristate, since it locally sequesters Pal-CoA. This explains how the NMT reaction can proceed in the presence of the very abundant substrate Pal-CoA(151, 152). Therefore, the connection between protein acylation and lipid metabolism may be stronger than previously thought and requires further investigation(153).

Our study demonstrates the essential role of palmitoylation in the replication of Influenza B virus, which has not been previously studied. Additionally, we identified the responsible DHHC enzymes,

which differ from the ones identified previously for acylation of HA of Influenza A virus. Future research can build on these observations by elucidating the specific interactions between viral glycoproteins and DHHC acyltransferases to develop inhibitors that block viral replication.

6. Summary

Influenza viruses are major respiratory viruses, that cause annual epidemics and occasional pandemics. S-palmitoylation, the covalent attachment of long chain fatty acids to membrane proteins, is catalyzed by members of the DHHC family of protein acyl transferases. Protein palmitoylation regulates cellular processes and pathogens like Influenza viruses use the S-palmitoylation machinery of host cells to promote infection, but how substrates are recognized by DHHCs is unknown. In the first part of my work, I used the M2 protein of influenza A virus, which has one acylated cysteine at a membrane-near amphiphilic helix (AH), to study molecular determinants for palmitoylation and binding to its cognate enzyme DHHC20.

After fusion of the amphiphilic helix of M2 with the fluorescent protein RFP, the reporter protein was membrane bound and palmitoylated. Changing the biophysical properties of the amphiphilic helix, its truncation, or destroying its secondary structure greatly reduced but does not eliminate the S-palmitoylation of full-length M2. Furthermore, the exchange of a kink-inducing glycine in the transmembrane (TM) region increased acylation. DHHC20, one of the enzymes involved in palmitoylation of M2, can be co-precipitated with M2 mutants and two of them bind even more strongly than M2 wildtype. Molecular dynamic simulations, performed by Clark Templeton in the group of Cecilia Clementi (Theoretical and Computational Biophysics, Free University Berlin) revealed that M2 associates via both its TM and AH with DHHC20. Amino acids of the helix interact with the catalytically important DHHC and TTXE motifs of the enzyme and some contacts are lost in M2 mutants.

In the second part of my thesis, I studied the role of palmitoylation of the main glycoprotein hemagglutinin of Influenza B virus for virus replication and identified the DHHC enzymes required for the acylation. I found that palmitoylation is essential for influenza B virus replication since removing the two sites where the palmitate is attached to the HA protein or the cysteine located at the end of the cytoplasmic tail prevented generating viable viruses. Viruses with an exchange of the membrane-distal cysteine rapidly reverted back to wild-type viruses.

Using Brefeldin A to block the exit of proteins from the endoplasmic reticulum (ER), I show that palmitoylation of HA of Influenza B virus occurs in the ER, whereas acylation of HA of Influenza A virus happens also in the Golgi. Infecting HAP-1 cells where genes for individual DHHCs have been inactivated revealed that HA of the Influenza B virus is acylated by the ER-localized DHHCs 1, 2, 4, and 6, which are mostly different from those previously identified to be involved in palmitoylation of HA of Influenza A virus. Overall, these results prove that palmitoylation of HA

plays an essential role in the replication of Influenza B virus, as has previously been demonstrated for Influenza A virus. However, the responsible enzymes and their intracellular localization are different for Influenza A and B viruses.

Overall, my research enhances our understanding of the molecular mechanisms underlying influenza virus replication and the role of S-palmitoylation in viral infection. The findings provide valuable insights into the interplay between viral proteins and host cellular processes, offering potential targets for antiviral interventions. Additionally, the identification of virus-specific differences in palmitoylation pathways emphasizes the importance of studying individual influenza strains to develop tailored therapeutic strategies.

7. Zusammenfassung

Strukturelle, enzymologische und funktionelle Untersuchungen zur Bindung von Fettsäuren an das Hämagglutinin und das M2-Membranprotein von Influenzaviren

Influenzaviren sind wichtige respiratorische Viren, die jährlich Epidemien und gelegentlich Pandemien verursachen. S-Palmitoylierung, die kovalente Bindung langkettiger Fettsäuren an Membranproteine, wird durch Mitglieder der DHHC-Familie der Proteinacyltransferasen katalysiert. Die Palmitoylierung reguliert zelluläre Prozesse und Krankheitserreger wie Influenzaviren nutzen die S-Palmitoylierungsmaschinerie von Wirtszellen, um Infektionen zu fördern, aber wie Proteinsubstrate von DHHC Enyzmen erkannt werden, ist unbekannt. Im ersten Teil meiner Arbeit habe ich das M2-Protein des Influenza-A-Virus, das an einem Cystein in einer membrannahen amphiphilen Helix (AH) acyliert ist, verwendet, um molekulare Determinanten für die Palmitoylierung und die Bindung an das Enzym DHHC20 zu untersuchen.

Nach der Fusion der amphiphilen Helix von M2 an das fluoreszierenden Protein RFP war das Reporterprotein membrangebunden und palmitoyliert. Eine Änderung der biophysikalischen Eigenschaften der amphiphilen Helix, ihre Verkürzung oder die Zerstörung ihrer Sekundärstruktur verringert die S-Palmitoylierung von M2 erheblich, beseitigt sie jedoch nicht. Darüber hinaus erhöhte der Austausch eines Glycins in der Transmembranregion (TM) die Acylierung. DHHC20, eines der Enzyme, die an der Palmitoylierung von M2 beteiligt sind, kann mit M2-Mutanten co-präzipitiert werden und zwei von ihnen binden sogar stärker als der M2-Wildtyp. Molekulardynamische Simulationen, durchgeführt von Clark Templeton in der Gruppe von Cecilia Clementi (Theoretische und computergestützte Biophysik, Freie Universität Berlin), zeigten, dass M2 sowohl über seine TM als auch über seine AH mit DHHC20 assoziiert ist. Aminosäuren der Helix interagieren mit den katalytisch wichtigen DHHC- und TTXE-Motiven des Enzyms und einige dieser Kontakte gehen in M2-Mutanten verloren.

Im zweiten Teil meiner Dissertation untersuchte ich die Funktion der Palmitoylierung des Hauptglykoproteins Hämagglutinin des Influenza B Virus für die Virusreplikation und identifizierte die für die Acylierung erforderlichen DHHC-Enzyme. Ich fand heraus, dass die Palmitoylierung für die Replikation des Influenza-B-Virus essentiell ist, da die Entfernung der beiden acylierten Cysteine, oder von einem Cystein am Ende des zytoplasmatischen Schwanzes die Entstehung lebensfähiger Viren verhinderte. Viren mit einem Austausch des membrannahen Cysteins verwandelten sich schnell wieder in Wildtypviren.

Indem ich Brefeldin A verwende, um den Transport von Proteinen aus dem endoplasmatischen Retikulum (ER) zu blockieren, zeige ich, dass die Palmitoylierung des HAs des Influenza B Virus im ER stattfindet, wohingegen die Acylierung von HA des Influenza A Virus auch im Golgi passiert. Die Infektion von HAP-1-Zellen, bei denen Gene für einzelne DHHCs inaktiviert wurden, ergab, dass das HA des Influenza B Virus durch die ER-lokalisierten DHHCs Enzyme 1, 2, 4 und 6 acyliert wird. Insgesamt belegen diese Ergebnisse, dass die Palmitoylierung des HAs eine wesentliche Rolle bei der Replikation des Influenza B Virus spielt, wie bereits zuvor für das Influenza A Virus nachgewiesen wurde. Allerdings sind die verantwortlichen Enzyme und ihre intrazelluläre Lokalisierung bei InfluenzaA- und B Viren unterschiedlich.

Insgesamt hat meine Forschung unser Verständnis der molekularen Mechanismen, die der Replikation des Influenzavirus zugrunde liegen, insbesondere der Rolle der S-Palmitoylierung bei der Virusinfektion verbessert. Die Ergebnisse liefern wertvolle Einblicke in das Zusammenspiel zwischen viralen Proteinen und zellulären Prozessen des Wirtes und bieten potenzielle Angriffspunkte für antivirale Maßnahmen. Darüber hinaus unterstreicht die Identifizierung virusspezifischer Unterschiede in den Palmitoylierungswegen, wie wichtig die Untersuchung einzelner Influenzastämme für die Entwicklung maßgeschneiderter therapeutischer Strategien ist.

8. References

1. M. Koutsakos, T. H. Nguyen, W. S. Barclay, K. Kedzierska, Knowns and unknowns of influenza B viruses. *Future Microbiol* 11, 119–135 (2016).

2. K. Asha, B. Kumar, Emerging Influenza D Virus Threat: What We Know so Far! *J Clin Medicine* 8, 192 (2019).

3. K. Ciminski, T. Thamamongood, G. Zimmer, M. Schwemmle, Novel insights into bat influenza A viruses. *J Gen Virol* 98, 2393–2400 (2017).

4. S. Tong, *et al.*, A distinct lineage of influenza A virus from bats. *Proc National Acad Sci* 109, 4269–4274 (2012).

5. A. C. A. Campos, *et al.*, Ahead of Print - Bat Influenza A(HL18NL11) Virus in Fruit Bats, Brazil - Volume 25, Number 2—February 2019 - Emerging Infectious Diseases journal - CDC. *Emerg Infect Dis* 25, 333–337 (2019).

6. L. Jennings, *et al.*, Literature review of the epidemiology of influenza B disease in 15 countries in the Asia-Pacific region. *Influenza Other Resp* 12, 383–411 (2018).

7. S. Su, X. Fu, G. Li, F. Kerlin, M. Veit, Novel Influenza D virus: Epidemiology, pathology, evolution and biological characteristics. *Virulence* 8, 1580–1591 (2017).

8. J. Treanor, Influenza Vaccine — Outmaneuvering Antigenic Shift and Drift. *New Engl J Medicine* 350, 218–220 (2004).

9. S. E. Hensley, *et al.*, Hemagglutinin Receptor Binding Avidity Drives Influenza A Virus Antigenic Drift. *Science* 326, 734–736 (2009).

10. R. W. H. Ruigrok, L. J. Calder, S. A. Wharton, Electron microscopy of the influenza virus submembranal structure. *Virology* 173, 311–316 (1989).

11. T. Samji, Influenza A: understanding the viral life cycle. *Yale J Biology Medicine* 82, 153–9 (2009).

12. T. K. W. CHEUNG, L. L. M. POON, Biology of Influenza A Virus. *Ann Ny Acad Sci* 1102, 1–25 (2007).

13. D. P. Nayak, R. A. Balogun, H. Yamada, Z. H. Zhou, S. Barman, Influenza virus morphogenesis and budding. *Virus Res* 143, 147–161 (2009).

14. D. Dou, R. Revol, H. Östbye, H. Wang, R. Daniels, Influenza A Virus Cell Entry, Replication, Virion Assembly and Movement. *Front Immunol* 9, 1581 (2018).

15. T. Betakova, M. V. Nermut, A. J. Hay, The NB protein is an integral component of the membrane of influenza B virus. *J Gen Virol* 77, 2689–2694 (1996).

16. M. Hatta, Y. Kawaoka, The NB Protein of Influenza B Virus Is Not Necessary for Virus Replication In Vitro. *J Virol* 77, 6050–6054 (2003).

17. M. W. Shaw, P. W. Choppin, R. A. Lamb, A previously unrecognized influenza B virus glycoprotein from a bicistronic mRNA that also encodes the viral neuraminidase. *Proc National Acad Sci* 80, 4879–4883 (1983).

18. J. A. Mould, *et al.*, Influenza B Virus BM2 Protein Has Ion Channel Activity that Conducts Protons across Membranes. *Dev. Cell* 5, 175–184 (2003).

19. C. Ma, J. Wang, Functional studies reveal the similarities and differences between AM2 and BM2 proton channels from influenza viruses. *Biochimica et Biophys. Acta BBA - Biomembr.* 1860, 272–280 (2018).

20. J. J. Skehel, D. C. Wiley, RECEPTOR BINDING AND MEMBRANE FUSION IN VIRUS ENTRY: The Influenza Hemagglutinin. *Annu Rev Biochem* 69, 531–569 (2000).

21. K. Shimizu, A. Iguchi, R. Gomyou, Y. Ono, Influenza Virus Inhibits Cleavage of the HSP70 Pre-mRNAs at the Polyadenylation Site. *Virology* 254, 213–219 (1999).

22. J. F. Cros, A. García-Sastre, P. Palese, An Unconventional NLS is Critical for the Nuclear Import of the Influenza A Virus Nucleoprotein and Ribonucleoprotein. *Traffic* 6, 205–213 (2005).

23. S. Reich, *et al.*, Structural insight into cap-snatching and RNA synthesis by influenza polymerase. *Nature* 516, 361–366 (2014).

24. T. Shimizu, N. Takizawa, K. Watanabe, K. Nagata, N. Kobayashi, Crucial role of the influenza virus NS2 (NEP) C-terminal domain in M1 binding and nuclear export of vRNP. *Febs Lett* 585, 41–6 (2010).

25. K. Martin, A. Heleniust, Nuclear transport of influenza virus ribonucleoproteins: The viral matrix protein (M1) promotes export and inhibits import. *Cell* 67, 117–130 (1991).

26. G. Neumann, M. T. Hughes, Y. Kawaoka, Influenza A virus NS2 protein mediates vRNP nuclear export through NES-independent interaction with hCRM1. *Embo J* 19, 6751–6758 (2000).

27. S. Huang, *et al.*, A Second CRM1-Dependent Nuclear Export Signal in the Influenza A Virus NS2 Protein Contributes to the Nuclear Export of Viral Ribonucleoproteins. *J Virol* 87, 767–778 (2013).

28. G. Neumann, T. Noda, Y. Kawaoka, Emergence and pandemic potential of swine-origin H1N1 influenza virus. *Nature* 459, 931–939 (2009).

29. K. Das, J. M. Aramini, L.-C. Ma, R. M. Krug, E. Arnold, Structures of influenza A proteins and insights into antiviral drug targets. *Nat Struct Mol Biol* 17, 530–538 (2010).

30. R. T. Armstrong, A. S. Kushnir, J. M. White, The Transmembrane Domain of Influenza Hemagglutinin Exhibits a Stringent Length Requirement to Support the Hemifusion to Fusion Transition. *J Cell Biology* 151, 425–438 (2000).

31. E. Böttcher-Friebertshäuser, W. Garten, M. Matrosovich, H. D. Klenk, The hemagglutinin: a determinant of pathogenicity. *Curr Top Microbiol* 385, 3–34 (2014).

32. R. Webby, *et al.*, Responsiveness to a pandemic alert: use of reverse genetics for rapid development of influenza vaccines. *Lancet Lond Engl* 363, 1099–1103 (2004).

33. A. Stieneke-Gröber, *et al.*, Influenza virus hemagglutinin with multibasic cleavage site is activated by furin, a subtilisin-like endoprotease. *Embo J* 11, 2407–2414 (1992).

34. Y. Ha, D. J. Stevens, J. J. Skehel, D. C. Wiley, H5 avian and H9 swine influenza virus haemagglutinin structures: possible origin of influenza subtypes. *Embo J* 21, 865–875 (2002).

35. R. J. Russell, *et al.*, H1 and H7 influenza haemagglutinin structures extend a structural classification of haemagglutinin subtypes. *Virology* 325, 287–296 (2004).

36. S. J. Gamblin, *et al.*, The Structure and Receptor Binding Properties of the 1918 Influenza Hemagglutinin. *Science* 303, 1838–1842 (2004).

37. F. Ni, E. Kondrashkina, Q. Wang, Structural basis for the divergent evolution of influenza B virus hemagglutinin. *Virology* 446, 112–122 (2013).

38. Q. Wang, F. Cheng, M. Lu, X. Tian, J. Ma, Crystal Structure of Unliganded Influenza B Virus Hemagglutinin. *J Virol* 82, 3011–3020 (2008).

39. C. M. Mair, K. Ludwig, A. Herrmann, C. Sieben, Receptor binding and pH stability — How influenza A virus hemagglutinin affects host-specific virus infection. *Biochimica Et Biophysica Acta Bba - Biomembr* 1838, 1153–1168 (2014).

40. R. A. Medina, A. García-Sastre, Influenza A viruses: new research developments. *Nat Rev Microbiol* 9, 590–603 (2011).

41. T. Ito, *et al.*, Molecular Basis for the Generation in Pigs of Influenza A Viruses with Pandemic Potential. *J Virol* 72, 7367–7373 (1998).

42. G. J. D. Smith, *et al.*, Dating the emergence of pandemic influenza viruses. *Proc National Acad Sci* 106, 11709–11712 (2009).

43. T. Velkov, The specificity of the influenza B virus hemagglutinin receptor binding pocket: what does it bind to? *J. Mol. Recognit.* 26, 439–449 (2013).

44. Q. Wang, X. Tian, X. Chen, J. Ma, Structural basis for receptor specificity of influenza B virus hemagglutinin. *Proc. Natl. Acad. Sci.* 104, 16874–16879 (2007).

45. A. S. Gambaryan, J. S. Robertson, M. N. Matrosovich, Effects of Egg-Adaptation on the Receptor-Binding Properties of Human Influenza A and B Viruses. *Virology* 258, 232–239 (1999).

46. V. Carbone, *et al.*, Molecular characterization of the receptor binding structure-activity relationships of influenza B virus hemagglutinin. *Acta Virol.* 57, 313–32 (2013).

47. R. Kornfeld, S. Kornfeld, Assembly of Asparagine-Linked Oligosaccharides. *Annu Rev Biochem* 54, 631–664 (1985).

48. T. A. Blake, T. L. Williams, J. L. Pirkle, J. R. Barr, Targeted N-Linked Glycosylation Analysis of H5N1 Influenza Hemagglutinin by Selective Sample Preparation and Liquid Chromatography/Tandem Mass Spectrometry. *Anal Chem* 81, 3109–3118 (2009).

49. I. T. Schulze, Effects of Glycosylation on the Properties and Functions of Influenza Virus Hemagglutinin. *J Infect Dis* 176, S24–S28 (1997).

50. S. Sun, Q. Wang, F. Zhao, W. Chen, Z. Li, Glycosylation Site Alteration in the Evolution of Influenza A (H1N1) Viruses. *Plos One* 6, e22844 (2011).

51. M. Ohuchi, R. Ohuchi, A. Feldmann, H. D. Klenk, Regulation of receptor binding affinity of influenza virus hemagglutinin by its carbohydrate moiety. *J Virol* 71, 8377–8384 (1997).

52. K. L. Deshpande, V. A. Fried, M. Ando, R. G. Webster, Glycosylation affects cleavage of an H5N2 influenza virus hemagglutinin and regulates virulence. *Proc National Acad Sci* 84, 36–40 (1987).

53. K. T. Schjoldager, Y. Narimatsu, H. J. Joshi, H. Clausen, Global view of human protein glycosylation pathways and functions. *Nat Rev Mol Cell Bio* 21, 729–749 (2020).

54. D. J. Vigerust, V. L. Shepherd, Virus glycosylation: role in virulence and immune interactions. *Trends Microbiol* 15, 211–218 (2007).

55. M. Aebi, N-linked protein glycosylation in the ER. *Biochimica Et Biophysica Acta Bba - Mol Cell Res* 1833, 2430–2437 (2013).

56. W. G. Dunphy, J. E. Rothman, Compartmental organization of the golgi stack. *Cell* 42, 13–21 (1985).

57. T. Fujiwara, K. Oda, S. Yokota, A. Takatsuki, Y. Ikehara, Brefeldin A causes disassembly of the Golgi complex and accumulation of secretory proteins in the endoplasmic reticulum. *J Biol Chem* 263, 18545–18552 (1988).

58. L. Orcl, *et al.*, Brefeldin A, a drug that blocks secretion, prevents the assembly of non-clathrin-coated buds on Golgi cisternae. *Cell* 64, 1183–1195 (1991).

59. R. Manzoor, M. Igarashi, A. Takada, Influenza A Virus M2 Protein: Roles from Ingress to Egress. *Int J Mol Sci* 18, 2649 (2017).

60. L. J. Holsinger, M. A. Shaughnessy, A. Micko, L. H. Pinto, R. A. Lamb, Analysis of the posttranslational modifications of the influenza virus M2 protein. *J. Virol.* 69, 1219–1225 (1995).

61. B. J. Chen, G. P. Leser, D. Jackson, R. A. Lamb, The Influenza Virus M2 Protein Cytoplasmic Tail Interacts with the M1 Protein and Influences Virus Assembly at the Site of Virus Budding. *J Virol* 82, 10059–10070 (2008).

62. M. Sharma, *et al.*, Insight into the Mechanism of the Influenza A Proton Channel from a Structure in a Lipid Bilayer. *Science* 330, 509–512 (2010).

63. T. Ito, O. T. Gorman, Y. Kawaoka, W. J. Bean, R. G. Webster, Evolutionary analysis of the influenza A virus M gene with comparison of the M1 and M2 proteins. *J Virol* 65, 5491–8 (1991).

64. Y. Tang, F. Zaitseva, R. A. Lamb, L. H. Pinto, The Gate of the Influenza Virus M2 Proton Channel Is Formed by a Single Tryptophan Residue*. *J Biol Chem* 277, 39880–39886 (2002).

65. S. D. Cady, W. Luo, F. Hu, M. Hong, Structure and Function of the Influenza A M2 Proton Channel. *Biochemistry-us* 48, 7356–7364 (2009).

66. E. Alvarado-Facundo, *et al.*, Influenza Virus M2 Protein Ion Channel Activity Helps To Maintain Pandemic 2009 H1N1 Virus Hemagglutinin Fusion Competence during Transport to the Cell Surface. *J Virol* 89, 1975–1985 (2014).

67. M. F. McCown, A. Pekosz, Distinct Domains of the Influenza A Virus M2 Protein Cytoplasmic Tail Mediate Binding to the M1 Protein and Facilitate Infectious Virus Production. *J Virol* 80, 8178–8189 (2006).

68. K. Iwatsuki-Horimoto, *et al.*, The cytoplasmic tail of the influenza A virus M2 protein plays a role in viral assembly. *J Virol* 80, 5233–40 (2006).

69. J. S. Rossman, X. Jing, G. P. Leser, R. A. Lamb, Influenza Virus M2 Protein Mediates ESCRT-Independent Membrane Scission. *Cell* 142, 902–913 (2010).

70. S. S. Sanders, *et al.*, Curation of the Mammalian Palmitoylome Indicates a Pivotal Role for Palmitoylation in Diseases and Disorders of the Nervous System and Cancers. *Plos Comput Biol* 11, e1004405 (2015).

71. H. Jiang, *et al.*, Protein Lipidation: Occurrence, Mechanisms, Biological Functions, and Enabling Technologies. *Chem Rev* 118, 919–988 (2018).

72. E. Kong, *et al.*, Dynamic Palmitoylation Links Cytosol-Membrane Shuttling of Acyl-protein Thioesterase-1 and Acyl-protein Thioesterase-2 with That of Proto-oncogene H-Ras Product and Growth-associated Protein-43*. *J. Biol. Chem.* 288, 9112–9125 (2013).

73. J. Greaves, C. Salaun, Y. Fukata, M. Fukata, L. H. Chamberlain, Palmitoylation and Membrane Interactions of the Neuroprotective Chaperone Cysteine-string Protein*. *J Biol Chem* 283, 25014–25026 (2008).

74. J. Greaves, L. H. Chamberlain, Palmitoylation-dependent protein sorting. *J Cell Biology* 176, 249–254 (2007).

75. A. M. Ernst, *et al.*, S-Palmitoylation Sorts Membrane Cargo for Anterograde Transport in the Golgi. *Dev. Cell* 47, 479-493.e7 (2018).

76. M. Blanc, *et al.*, SwissPalm: Protein Palmitoylation database. *F1000research* 4, 261 (2015).

77. D. A. Abdulrahman, X. Meng, M. Veit, S-Acylation of Proteins of Coronavirus and Influenza Virus: Conservation of Acylation Sites in Animal Viruses and DHHC Acyltransferases in Their Animal Reservoirs. *Pathogens* 10, 669 (2021).

78. L. V. Kordyukova, M. V. Serebryakova, M. Veit, L. A. Baratova, S Acylation of the Hemagglutinin of Influenza Viruses: Mass Spectrometry Reveals Site-Specific Attachment of Stearic Acid to a Transmembrane Cysteine. *Journal of Virology* 82, 9288–9292 (2008).

79. M. Veit, S. Siche, S-acylation of influenza virus proteins: Are enzymes for fatty acid attachment promising drug targets? *Vaccine* 33, 7002–7007 (2015).

80. M. Veit, M. V. Serebryakova, L. V. Kordyukova, Palmitoylation of influenza virus proteins. *Biochem Soc T* 41, 50–5 (2013).

81. L. V. Kordyukova, *et al.*, Two Cytoplasmic Acylation Sites and an Adjacent Hydrophobic Residue, but No Other Conserved Amino Acids in the Cytoplasmic Tail of HA from Influenza A Virus Are Crucial for Virus Replication. *Viruses* 7, 6458–6475.

82. B. J. Chen, M. Takeda, R. A. Lamb, Influenza Virus Hemagglutinin (H3 Subtype) Requires Palmitoylation of Its Cytoplasmic Tail for Assembly: M1 Proteins of Two Subtypes Differ in Their Ability To Support Assembly. *J Virol* 79, 13673–13684 (2005).

83. R. Wagner, A. Herwig, N. Azzouz, H. D. Klenk, Acylation-Mediated Membrane Anchoring of Avian Influenza Virus Hemagglutinin Is Essential for Fusion Pore Formation and Virus Infectivity. *J Virol* 79, 6449–6458 (2005).

84. M. R. Gadalla, L. Abrami, F. G. van der Goot, M. Veit, Hemagglutinin of Influenza A, but not of Influenza B and C viruses is acylated by ZDHHC2, 8, 15 and 20. *bioRxiv*, 2019.12.15.877001 (2019).

85. M. L. Grantham, *et al.*, Palmitoylation of the Influenza A Virus M2 Protein Is Not Required for Virus Replication In Vitro but Contributes to Virus Virulence. *J. Virol.* 83, 8655–8661 (2009).

86. M. Veit, H.-D. Klenk, A. Kendal, R. Rott, The M2 protein of influenza A virus is acylated. *J. Gen. Virol.* 72, 1461–1465 (1991).

87. B. Thaa, *et al.*, Growth of influenza A virus is not impeded by simultaneous removal of the cholesterol-binding and acylation sites in the M2 protein. *J Gen Virol* 93, 282–292 (2012).

88. B. Thaa, S. Siche, A. Herrmann, M. Veit, Acylation and cholesterol binding are not required for targeting of influenza A virus M2 protein to the hemagglutinin-defined budozone. *Febs Lett* 588, 1031–1036 (2014).

89. M. J. Shipston, Ion Channel Regulation by Protein Palmitoylation*. *J Biol Chem* 286, 8709–8716 (2011).

90. M. Ujike, K. Nakajima, E. Nobusawa, Influence of Acylation Sites of Influenza B Virus Hemagglutinin on Fusion Pore Formation and Dilation. *J Virol* 78, 11536–11543 (2004).

91. A. Demers, *et al.*, Palmitoylation is required for intracellular trafficking of influenza B virus NB protein and efficient influenza B virus growth in vitro. *J. Gen. Virol.* 95, 1211–1220 (2014).

92. M. Wang, K. Ludwig, C. Böttcher, M. Veit, The role of stearate attachment to the hemagglutinin-esterase-fusion glycoprotein HEF of influenza C virus. *Cell Microbiol* 18, 692–704 (2016).

93. Y. Muraki, *et al.*, Palmitoylation of CM2 is dispensable to influenza C virus replication. *Virus Res* 157, 99–105 (2011).

94. I. De, S. Sadhukhan, Emerging Roles of DHHC-mediated Protein S-palmitoylation in Physiological and Pathophysiological Context. *Eur J Cell Biol* 97, 319–338 (2018).

95. Y. Ohno, A. Kihara, T. Sano, Y. Igarashi, Intracellular localization and tissue-specific distribution of human and yeast DHHC cysteine-rich domain-containing proteins. *Biochim. Biophys. Acta (BBA) - Mol. Cell Biol. Lipids* 1761, 474–483 (2006).

96. Y. Ohno, A. Kihara, T. Sano, Y. Igarashi, Intracellular localization and tissue-specific distribution of human and yeast DHHC cysteine-rich domain-containing proteins. *Biochimica Et Biophysica Acta Bba - Mol Cell Biology Lipids* 1761, 474–483 (2006).

97. M. E. Linder, B. C. Jennings, DHHC Protein S-Acyltransferases Use Similar Ping-Pong Kinetic Mechanisms but Display Different Acyl-CoA Specificities *. *Journal of Biological Chemistry* 287, 7236–7245 (2012).

98. M. I. P. Malgapo, M. E. Linder, Substrate recruitment by zDHHC protein acyltransferases. *Open Biol.* 11, 210026 (2021).

99. M. S. Rana, *et al.*, Fatty acyl recognition and transfer by an integral membrane S-acyltransferase. *Science* 359 (2018).

100. J. Jumper, *et al.*, Highly accurate protein structure prediction with AlphaFold. *Nature* 596, 583–589 (2021).

101. M. Varadi, *et al.*, AlphaFold Protein Structure Database: massively expanding the structural coverage of protein-sequence space with high-accuracy models. *Nucleic Acids Res* 50, D439–D444 (2021).

102. F. G. van der Goot, M.-E. Zaballa, The molecular era of protein S-acylation: spotlight on structure, mechanisms, and dynamics. *Critical Reviews in Biochemistry and Molecular Biology* 53, 420–451 (2018).

103. F. S. Mesquita, *et al.*, S-acylation controls SARS-Cov-2 membrane lipid organization and enhances infectivity. *Biorxiv*, 2021.03.14.435299 (2021).

104. M.-E. Zaballa, F. G. van der Goot, The molecular era of protein S-acylation: spotlight on structure, mechanisms, and dynamics. *Crit. Rev. Biochem. Mol. Biol.* 53, 420–451 (2018).

105. H. Hou, A. T. J. Peter, C. Meiringer, K. Subramanian, C. Ungermann, Analysis of DHHC Acyltransferases Implies Overlapping Substrate Specificity and a Two-Step Reaction Mechanism. *Traffic* 10, 1061–1073 (2009).

106. K. Lemonidis, M. C. Sanchez-Perez, L. H. Chamberlain, Identification of a Novel Sequence Motif Recognized by the Ankyrin Repeat Domain of zDHHC17/13 S-Acyltransferases*. *J Biol Chem* 290, 21939–21950 (2015).

107. G. M. Thomas, T. Hayashi, S.-L. Chiu, C.-M. Chen, R. L. Huganir, Palmitoylation by DHHC5/8 Targets GRIP1 to Dendritic Endosomes to Regulate AMPA-R Trafficking. *Neuron* 73, 482–496 (2012).

108. G. J. Fredericks, *et al.*, Stable expression and function of the inositol 1,4,5-triphosphate receptor requires palmitoylation by a DHHC6/selenoprotein K complex. *Proc. Natl. Acad. Sci.* 111, 16478–16483 (2014).

109. L. Abrami, *et al.*, Identification and dynamics of the human ZDHHC16-ZDHHC6 palmitoylation cascade. *Elife* 6, e27826 (2017).

110. R. Verardi, J.-S. Kim, R. Ghirlando, A. Banerjee, Structural Basis for Substrate Recognition by the Ankyrin Repeat Domain of Human DHHC17 Palmitoyltransferase. *Structure* 25, 1337-1347.e6 (2017).

111. K. Lemonidis, *et al.*, Substrate selectivity in the zDHHC family of S -acyltransferases. *Biochem Soc T* 45, 751–758 (2017).

112. J. M. Philippe, P. M. Jenkins, Spatial organization of palmitoyl acyl transferases governs substrate localization and function. *Mol. Membr. Biol.* 35, 60–75 (2020).

113. J. Howie, *et al.*, Substrate recognition by the cell surface palmitoyl transferase DHHC5. *Proc. Natl. Acad. Sci.* 111, 17534–17539 (2014).

114. Y.-H. Lin, *et al.*, Host Cell-catalyzed S-Palmitoylation Mediates Golgi Targeting of the Legionella Ubiquitin Ligase GobX*. *J. Biol. Chem.* 290, 25766–25781 (2015).

115. T. M. McMichael, *et al.*, The palmitoyltransferase ZDHHC20 enhances interferon-induced transmembrane protein 3 (IFITM3) palmitoylation and antiviral activity. *J. Biol. Chem.* 292, 21517–21526 (2017).

116. F. Plain, *et al.*, An amphipathic α-helix directs palmitoylation of the large intracellular loop of the sodium/calcium exchanger. *J Biol Chem* 292, 10745–10752 (2017).

117. J. D. Hull, R. Gilmore, R. A. Lamb, Integration of a small integral membrane protein, M2, of influenza virus into the endoplasmic reticulum: analysis of the internal signal- anchor domain of a protein with an ectoplasmic NH2 terminus. *J Cell Biology* 106, 1489–1498 (1988).

118. R. A. Lamb, S. L. Zebedee, C. D. Richardson, Influenza virus M2 protein is an integral membrane protein expressed on the infected-cell surface. *Cell* 40, 627–633 (1985).

119. C. Hammond, I. Braakman, A. Helenius, Role of N-linked oligosaccharide recognition, glucose trimming, and calnexin in glycoprotein folding and quality control. *Proc National Acad Sci* 91, 913–917 (1994).

120. K. Lemonidis, O. A. Gorleku, M. C. Sanchez-Perez, C. Grefen, L. H. Chamberlain, The Golgi S-acylation machinery comprises zDHHC enzymes with major differences in substrate affinity and S-acylation activity. *Mol Biol Cell* 25, 3870–3883 (2014).

121. I. Panina, *et al.*, Molecular Dynamics of DHHC20 Acyltransferase Suggests Principles of Lipid and Protein Substrate Selectivity. *Int J Mol Sci* 23, 5091 (2022).

122. M. Veit, *et al.*, Site-specific mutagenesis identifies three cysteine residues in the cytoplasmic tail as acylation sites of influenza virus hemagglutinin. *J Virol* 65, 2491–500 (1991).

123. R. D. Klausner, J. G. Donaldson, J. Lippincott-Schwartz, Brefeldin A: insights into the control of membrane traffic and organelle structure. *J Cell Biology* 116, 1071–1080 (1992).

124. J. Lippincott-Schwartz, *et al.*, Microtubule-dependent retrograde transport of proteins into the ER in the presence of brefeldin a suggests an ER recycling pathway. *Cell* 60, 821–836 (1990).

125. A. Harbig, *et al.*, Transcriptome profiling and protease inhibition experiments identify proteases that activate H3N2 influenza A and influenza B viruses in murine airways. *J Biol Chem* 295, 11388–11407 (2020).

126. H. Limburg, *et al.*, TMPRSS2 Is the Major Activating Protease of Influenza A Virus in Primary Human Airway Cells and Influenza B Virus in Human Type II Pneumocytes. *J Virol* 93 (2019).

127. V. Y. Lugovtsev, D. Melnyk, J. P. Weir, Heterogeneity of the MDCK Cell Line and Its Applicability for Influenza Virus Research. *Plos One* 8, e75014 (2013).

128. F. LeBouder, B. Lina, G. F. Rimmelzwaan, B. Riteau, Plasminogen promotes influenza A virus replication through an annexin 2-dependent pathway in the absence of neuraminidase. *J Gen Virol* 91, 2753–2761 (2010).

129. S. G. Lazarowitz, A. R. Goldberg, P. W. Choppin, Proteolytic cleavage by plasmin of the HA polypeptide of influenza virus: Host cell activation of serum plasminogen. *Virology* 56, 172–180 (1973).

130. L. V. Tse, V. C. Marcano, W. Huang, M. S. Pocwierz, G. R. Whittaker, Plasmin-Mediated Activation of Pandemic H1N1 Influenza Virus Hemagglutinin Is Independent of the Viral Neuraminidase. *J Virol* 87, 5161–5169 (2013).

131. M. Veit, M. F. G. Schmidt, Timing of palmitoylation of influenza virus hemagglutinin. *Febs Lett* 336, 243–247 (1993).

132. C. Salaun, L. Ritchie, J. Greaves, T. J. Bushell, L. H. Chamberlain, The C-terminal domain of zDHHC2 contains distinct sorting signals that regulate intracellular localisation in neurons and neuroendocrine cells. *Mol Cell Neurosci* 85, 235–246 (2017).

133. R. Zeidman, *et al.*, DHHC2 is a protein S-acyltransferase for Lck. *Mol Membr Biol* 28, 473–486 (2011).

134. A. R. Wild, *et al.*, CellPalmSeq: A curated RNAseq database of palmitoylating and de-palmitoylating enzyme expression in human cell types and laboratory cell lines. *Front Physiol* 14, 1110550 (2023).

135. D. J. Benton, *et al.*, Influenza hemagglutinin membrane anchor. *Proc. Natl. Acad. Sci.* 115, 10112–10117 (2018).

136. K. Tunyasuvunakool, *et al.*, Highly accurate protein structure prediction for the human proteome. *Nature* 596, 590–596 (2021).

137. R. Evans, *et al.*, Protein complex prediction with AlphaFold-Multimer. *bioRxiv*, 2021.10.04.463034 (2022).

138. K. S. Mineev, *et al.*, Structural investigation of influenza virus hemagglutinin membrane-anchoring peptide. *Protein Eng., Des. Sel.* 26, 547–552 (2013).

139. B. Thaa, I. Levental, A. Herrmann, M. Veit, Intrinsic membrane association of the cytoplasmic tail of influenza virus M2 protein and lateral membrane sorting regulated by cholesterol binding and palmitoylation. *Biochem J* 437, 389–397 (2011).

140. K. Tobler, M. L. Kelly, L. H. Pinto, R. A. Lamb, Effect of cytoplasmic tail truncations on the activity of the M(2) ion channel of influenza A virus. *J Virol* 73, 9695–701 (1999).

141. C. W. Naeve, D. Williams, Fatty acids on the A/Japan/305/57 influenza virus hemagglutinin have a role in membrane fusion. *Embo J* 9, 3857–3866 (1990).

142. T. Sakai, R. Ohuchi, M. Ohuchi, Fatty Acids on the A/USSR/77 Influenza Virus Hemagglutinin Facilitate the Transition from Hemifusion to Fusion Pore Formation. *J Virol* 76, 4603–4611 (2002).

143. K. Brett, *et al.*, Site-specific S-Acylation of Influenza Virus Hemagglutinin THE LOCATION OF THE ACYLATION SITE RELATIVE TO THE MEMBRANE BORDER IS THE DECISIVE FACTOR FOR ATTACHMENT OF STEARATE*. *J Biol Chem* 289, 34978–34989 (2014).

144. M. Zhang, X. Han, K. Osterrieder, M. Veit, Palmitoylation of the envelope membrane proteins GP5 and M of porcine reproductive and respiratory syndrome virus is essential for virus growth. *Plos Pathog* 17, e1009554 (2021).

145. C. Salaun, C. Locatelli, F. Zmuda, J. C. González, L. H. Chamberlain, Accessory proteins of the zDHHC family of S-acylation enzymes. *J Cell Sci* 133, jcs251819 (2020).

146. Q. Zhou, *et al.*, The ER-Associated Protein ZDHHC1 Is a Positive Regulator of DNA Virus-Triggered, MITA/STING-Dependent Innate Immune Signaling. *Cell Host Microbe* 16, 450–461 (2014).

147. M. Ujike, K. Nakajima, E. Nobusawa, Influence of Additional Acylation Site(s) of Influenza B Virus Hemagglutinin on Syncytium Formation. *Microbiol. Immunol.* 49, 355–359 (2005).

148. M. Ujike, K. Nakajima, E. Nobusawa, A point mutation at the C terminus of the cytoplasmic domain of influenza B virus haemagglutinin inhibits syncytium formation. *J. Gen. Virol.* 87, 1669–1676 (2006).

149. J. Greaves, *et al.*, Molecular basis of fatty acid selectivity in the zDHHC family of S-acyltransferases revealed by click chemistry. *Proc National Acad Sci* 114, E1365–E1374 (2017).

150. B. C. Jennings, M. E. Linder, DHHC Protein S-Acyltransferases Use Similar Ping-Pong Kinetic Mechanisms but Display Different Acyl-CoA Specificities*. *J Biol Chem* 287, 7236–7245 (2012).

151. M. Islinger, *et al.*, The diversity of ACBD proteins – From lipid binding to protein modulators and organelle tethers. *Biochimica Et Biophysica Acta Bba - Mol Cell Res* 1867, 118675 (2020).

152. E. Soupene, *et al.*, Association of NMT2 with the acyl-CoA carrier ACBD6 protects the N-myristoyltransferase reaction from palmitoyl-CoA. *J Lipid Res* 57, 288–98 (2015).

153. R. Puthenveetil, N. Gómez-Navarro, A. Banerjee, Access and utilization of long chain fatty acyl-CoA by zDHHC protein acyltransferases. *Curr Opin Struc Biol* 77, 102463 (2022).

This thesis is based on the following manuscripts:

Xiaorong Meng, Clark Templeton, Cecilia Clementi, Michael Veit, The role of an amphiphilic helix and transmembrane region in the efficient acylation of M2 from Influenza virus**, (In revision).**

Xiaorong Meng, Michael Veit, Palmitoylation of the Hemagglutinin of Influenza B virus by ER-localized DHHC enzymes 1, 2, 4 and 6 is required for efficient virus replication**, Journal of Virology.**

Preprint at Biorxiv:

https://www.biorxiv.org/content/10.1101/2023.06.15.545201v1

9. List of publications

Scientific publications:

Xiaorong Meng, Clark Templeton, Cecilia Clementi, Michael Veit, The role of an amphiphilic helix and transmembrane region in the efficient acylation of M2 from Influenza virus**, (In revision)**

Xiaorong Meng, Michael Veit, Palmitoylation of the Hemagglutinin of Influenza B virus by ER-localized DHHC enzymes 1, 2, 4 and 6 is required for efficient virus replication**, Journal of Virology.**

Dina A Abdulrahman†, **Xiaorong Meng**†, Michael Veit, S-Acylation of Proteins of Coronavirus and Influenza Virus: Conservation of Acylation Sites in Animal Viruses and DHHC Acyltransferases in Their Animal Reservoirs, ***Pathogens*** *2021, 10(6), 669*. (**co-first author**)

Jin Tian, Jiumeng Sun, Dongyan Li, Ningning Wang, Lifang Wang, Chang Zhang, **Xiaorong Meng**, Xiang Ji, Marc A. Suchard, Xu Zhang, Alexander Lai, Shuo Su, Michael Veit, Emerging viruses: Cross-species transmission of coronaviruses, filoviruses, henipaviruses, and rotaviruses from bats, ***Cell Reports*** *2022*,39(11).

Talks and poster presentations

Xiaorong Meng, Clark Templeton, Cecilia Clementi, Michael Veit. Poster: “Efficient acylation of the M2 protein of Influenza virus requires an amphiphilic helix, but the transmembrane region also plays a role” 03/2023, 32th Annual Meeting of the Society for Virology, Ulm.

10. Acknowledgments

Four years have gone in a blink. I consider myself lucky to have the opportunity to study at the Institute of Virology at the Free University of Berlin for my PhD. During this time, I have gained not only academic achievements and scientific experimental skills but also invaluable life lessons. The journey of a PhD is never easy, but the failures I encountered during my research taught me a lot. I would like to express my sincere gratitude to all the kind and supportive individuals who have helped me along the way.

Words cannot adequately express my appreciation for my supervisor, PD. Dr. Michael Veit. He provided me with the chance to study in his lab and pursue new topics in virology. As a responsible supervisor, he always motivates me to try new ideas and encourages me to explore science to its fullest potential. Whenever I faced challenges in my project, he was always there to provide me with timely suggestions and advice. During every presentation, he offered valuable feedback and suggestions to improve my performance. Without his guidance, support, and feedback, my PhD would not have been achievable.

I would like to thank Prof. Dr. Benedikt Kaufer and Prof. Dr. Klaus Osterrieder for valuable suggestions, insightful questions, and support during the institute seminars, which help a lot in my project.

I am extremely grateful to Prof. Dr. Klaus Osterrieder and Dr. Karsten Tedin for their invaluable guidance in my research. It's an honor to have them as members of my mentor committee.

I would also like to express my appreciation to Dr. Clark Templeton for his assistance with the MD stimulation experiments. His expertise and collaboration have greatly enhanced our ability to interpret and explain our results more effectively. Thanks to Dr. Andreas Nerlich from TZR for helping with the confocal microscope. Thanks to Ms. Christine Gaede from DRS for all the helps with the materials preparation and graduation process.

I would like to express my sincere appreciation to all the members of Veit's lab for their valuable assistance throughout my PhD journey. Dr. Minze Zhang, Dr. Mohamed Rasheed Gadalla, Dr. Xu Zhang, Dr. Xuejiao Han, Dr. Bodan Hu, Dr. Susanne Kaufer, Atika Hadiati. PhD students Dina Abdulrahman and Bang Qian. I am grateful for the collaborative and stimulating environment of the lab, which allowed me to learn from my colleagues and to grow both professionally and personally.

I would also like to extend my deep appreciation to all the members at the Institute of Virology for their support and help. Dr. Dusan Kunec, Dr. Jakob Trimpert, Dr. Ahmed Kheimar, Dr. Ludwig Krabben, Dr. Luca bertzbach, Dr. Azza Abdelgawad, Dr. Amr Aswad, Dr. Yu You, Dr. Na Xing, Dr. Nicole Groenke, Dr. Ibrahim Haggag, Dr. Tereza Faflikova, Dr. Pavulraj, Selvaraj, Dr. Andele Conradie, Dr. Sabrina Halecker. PhD students Thomas Höfler, Jana Reich, Giulia Aimola, Julia Maria Adler, Mariana Nascimento, Ricardo Vidal, Yingnan Cheng, Lisa Kossak, Sabsabi Mohammad, Dilan Serdar, Daria Vladimirova, Yulin Cong, Louis Cairn. I will always cherish the memories and experiences I shared with them. My sincere thanks to our technicians in the institute, Ann Reum, Annett Neubert, Angelika Thomele, Michaela Zeitlow, Sebastian Bischofberger, Elke Dyrks, Axel Teigeler and Constantin Rudolph for their great assist during the work and for making lab life easier. Thanks to our secretary Katharina Malik for her help during the work.

Thanks to China Scholarship Council (CSC) for the funding support. Without their support, I could not pursue my Ph.D in Germany.

Finally, I would like to express my deep love and appreciation to my parents and my sister Xiaodie for their support throughout my PhD journey. Their love has been my constant motivation and I am forever grateful for their encouragement.

In addition, I extend my gratitude to all of my family and friends who have provided me with their support and encouragement during this challenging yet rewarding journey. I would also like to thank Yoongi because his music has helped me through many difficult times.

In summary, I am immensely grateful for the past four years and the invaluable support that I have received from my supervisor and colleagues. I will always treasure this experience and the lessons I have learned along the way.

11. Funding sources

I received funding from the China Scholarship Council (CSC).

This work was supported by the German research foundation [grant no: Ve 141/18-1] to Michael Veit.

12. Conflict of interests

There are no conflicts of interests.

13. Selbständigkeitserklärung

Selbständigkeitserklärung Hiermit bestätige ich, dass ich die vorliegende Arbeit selbständig angefertigt habe. Ich versichere, dass ich ausschließlich die angegebenen Quellen und Hilfen Anspruch genommen habe.

Berlin, am 21.09.2023 Xiaorong Meng